DETECTING URBAN 3D STRUCTURE AND ITS IMPACT ON LAND SURFACE TEMPERATURE USING OPEN-SOURCE SATELLITE DATA

オープンソースの衛星データによる都市の立体構造検出と地表面温度に与える影響

July 2022

DIBYANTI DANNISWARI

Environmental Science and Landscape Architecture Course

Department of Environmental Horticulture

Graduate School of Horticulture

CHIBA UNIVERSITY

(千葉大学審査学位論文)

DETECTING URBAN 3D STRUCTURE AND ITS IMPACT ON LAND SURFACE TEMPERATURE USING OPEN-SOURCE SATELLITE DATA

オープンソースの衛星データによる都市の立体構造検出と地表面温度に与える影響

July 2022

DIBYANTI DANNISWARI

Environmental Science and Landscape Architecture Course

Department of Environmental Horticulture

Graduate School of Horticulture

CHIBA UNIVERSITY

ABSTRACT

Urban structure elements, such as the arrangement of land use/land cover and buildings, specifically its height, have been associated with land surface temperature that is affecting people and environment. This research examines how land cover and building height impacting the land surface temperature. However, building height data are difficult to obtain due to high operational cost and high computational complexity. Therefore, a method to obtain building height data simply is needed.

To address the issue caused by the arrangement of land use/land cover and buildings, and the limitation of obtaining building height data, this research aims to (1) analyze the land cover change and its impact on land surface temperature, (2) to examine a simpler alternative method to extract building height information, and (3) to analyze the relationship between building height and land surface temperature. The research is divided into three separate studies.

In the first study, the land cover changes in Jakarta and its three satellite cities of two different periods (approximately 25 years apart) are examined. The results show that the majority land cover change is from vegetation to built-up area, and it is followed by a significant land surface temperature increase in all cities.

In the second study, a simple building height estimation method from two open-source satellite products, AW3D30 (ALOS World 3D 30 m) and SRTM (Shuttle Radar Topographic Mission), is evaluated in Tokyo. The result showed that there is a good agreement between the estimated building height model and the reference data, although it does not produce accurate building height.

In the third study, the building height data obtained from the second study is utilized to analyze the relationship between building height impact and land surface temperature. The study areas include Tokyo, Beijing, Jakarta, New York, Los Angeles, and Chicago.

Building height is found to have a negative relationship with land surface temperature regardless of the analyzed urban area.

In summary, this research examined the land cover change and its impact on land surface temperature in Jakarta that is narrowly studied in existing studies, then attempted to extract building height with a simple method that is barely explored. No other study has applied the extracted building height to urban climate research, which is the originality of this study. The results of the third study add an insight to the contradictory findings in exiting studies and found that higher buildings tend to have lower land surface temperature. Practically, the findings could add some consideration for urban planner and policy makers.

TABLE OF CONTENTS

LIST OF TABLES

LIST OF FIGURES

CHAPTER 1: Introduction

1.1 Problem Statement and Researchable Question

Urban structure elements, such as the arrangement of land use/land cover and buildings, specifically its height, have been associated with ecological aspects and human well-being in cities (Larondelle et al. 2014). Urban structure elements serve as a framework to guide the development of well-functioning space, infrastructure, and buildings. The development of each element contributes to the convenience and the health of urban residents. It is important to consider these elements in urban planning and design to accommodate residents' needs.

Urbanization refers to a transition from rural to urban in terms of land use, economic and cultural activity, or population. The term is frequently used to refer to land cover and land use change on the outer edge of urban centers, usually developed for urban use such as housing or office buildings (Mcgranahan and Satterthwaite 2014). Urbanization is a complex process that affects economic, social, and environmental aspects. The increase of urban area is most likely coupled with the decrease of green open space, which causes the effect of urban heat island (UHI) in the urban center. UHI occurs when an urban region has higher temperature compared to its surrounding area (Voogt and Oke 2003). UHI is produced in cities regardless of size and location, though the intensity is found to increase as the city size and its compactness increase (Estoque, Murayama, and Myint 2017).

Indonesia's capital city, Jakarta, has very fast urbanization at a rate of 4.1% per year. With this level of urbanization, 68% of Indonesia population is expected to live in cities by 2025 (The World Bank 2016a). Jakarta has grown spatially into a larger region called Jabodetabek (Jakarta Metropolitan area). The name 'Jabodetabek' is an abbreviation

formed from the first syllables of Jakarta and its surrounding cities and regencies: Jakarta, Bogor, Depok, Tangerang, and Bekasi. These cities become the buffer of Jakarta to support people's needs of a residence, tourism, etc. The urban built-up area has been expanding widely, not only inside, but also beyond the capital city. As a result, rapid development also occurs in its surrounding/satellite cities.

The development in Jabodetabek results in changes in the landscape. Extensive housing and shopping mall development is seen in the outskirt of Jakarta, which expectedly leads to the intensification of UHI. The existence of UHI would affect the population that lives in the city as it may decrease the comfort of the city and increase energy consumption, which is bad for the environment. To avoid the worsening of UHI, urban monitoring is necessary so urban planners can take needed actions to control the urban development, especially in regard to policy making. Multitemporal analysis of land use/land cover change is important in understanding the urban expansion in the area. And land surface temperature (LST) is a significant indicator in monitoring the existence of UHI. Based on these problems, the first research question of this study is **"how does land cover change affect the land surface temperature in fast-growing cities such as Jabodetabek?"**.

Urban development results in the expansion of built-up area, horizontally (two-dimensional 2D) and vertically (three-dimensional 3D). Horizontally, the coverage of built-up area increases, and vertically, the height of built-up objects increases. Urban 3D structures referred to objects such as buildings, bridges, and other man-made structures, with buildings as the most prominent category. Information on urban 3D structure is important for the application in architecture, urban planning (R. Chen 2011), urban monitoring (Zhao, Weng, and Hersperger 2020), urban climate (Kouklis and Yiannakou 2021), disaster assessment (Jojene R. Santillan et al. 2015), and many others.

As a significant parameter of urban 3D structure, building height has been discussed regarding its influence on energy consumption (Güneralp et al. 2017), gas emission (Borck 2016), and urban heat island effects (Berger et al. 2017). Despite its significances, retrieving building height information is still difficult.

Building height can be extracted using various data sources and through various remote sensing-based approaches. Remotely sensed data are extracted from airborne light detection and ranging (LiDAR) (Zhang, Yan, and Chen 2006), optical stereo images (Tian, Cui, and Reinartz 2014), and synthetic aperture radar (SAR) (Gamba, Houshmand, and Saccani 2000). Data obtained from airborne LiDAR are favorable for extracting height information because of its high accuracy. However, these data are difficult to obtain due to high operational costs or they are only available under the authority of local government (Alobeid, Jacobsen, and Heipke 2010). As a result, they are unavailable for many areas in the world. A remote sensing-based methodology to obtain building height that can be applied globally is necessary.

To overcome this issue, there are a number of attempts to extract building height information from open-source digital surface model (DSM) that have global coverage. Global DSM data only provide the surface height information, but to extract building height, information on terrain or digital terrain model (DTM) is also needed. Therefore, the DTM must be extracted from DSM prior to calculating the building height. Misra et al. (Misra, Avtar, and Takeuchi 2018) compared the building height models extracted from four different DSMs over Yangon City and they used a multi-directional processing and slope-dependent filtering technique to extract the DTMs. Ren et al. (Ren et al. 2020) extracted building height in Hongkong and they used using the block minimum filtering method to extract the DTM. Li et al. (Li et al. 2020) proposed a method for obtaining the building height using backscatter coefficient from Sentinel-1

data. These methods show promising results but have high computational complexity, especially if applied to extensive areas. Easily applicable methods using open-source data are insufficiently explored.

Building height information is important, but it is difficult to obtain because the accurate data is expensive or classified. Existing studies that tried to extract building height from freely available data requires complex calculations, and easily applicable methods is not explored enough. Based on these problems, the first research question of this study is **"is there any simpler method to obtain building height information from open DSM?"**.

Further, the existence of a large number of buildings in urban areas is usually linked with environmental problems, such as urban heat island (UHI). Large cities worldwide have always been dealing with UHI issues (Peng et al. 2012) and how to mitigate it. To accommodate the ever increasing population in the city, coupled with the high cost and scarcity of land, high-rise buildings are considered a solution (Wong, 2004; Ibrahim, 2007). While the construction of high-rise buildings seems to solve the limited land issue, it also raises arguments on how it affects the urban environment.

Urban thermal condition is often presented with land surface temperature (LST) in UHI studies. LST has been extensively used due to its high availability, temporally and spatially. LST is reported to be strongly related with near surface air temperature (Good et al. 2017) and LST's mean value at the city scale has good fittings with air temperature (T. Sun, Sun, and Chen 2020). Studies have examined the relationship between LST and high-rise buildings. However, available studies show mixed results on how high-rise buildings were affecting LST. Some studies found that high-rise buildings tend to increase LST because of high anthropogenic heat (Guo et al. 2016; Rahman et al. 2020) and extensive impervious surface (Cai et al. 2018). Meanwhile, other studies found that

high-rise buildings tend to decreases LST because of large building shadows (Nichol 1996), reflective surface materials (Honjo et al. 2017), vegetation cover near the building (Zheng et al. 2019), and wind flow around the building (Wang and Xu 2021). Some studies with contradictive results are listed in Table 1. These findings raised another research question, which is **"what is the relationship between building height and land surface temperature?"**. It is worth to be investigated further whether high-rise buildings are affecting LST positively or negatively.

Table 1. Studies that examined relationship between building height and land surface temperature and have contradicting results

Studies that show building height increases land surface temperature	Studies that show building height decreases land surface temperature
Guo et al. 2016	Nichol 1996
Cai et al. 2018	Honjo et al. 2017
Rahman et al. 2020	Zheng et al. 2019
Alexander 2021	Wang and Xu 2021

Due to data availability constraints, existing building height studies using satellite data are limited in terms of study locations. Available building height studies used building height data from closed, limited access sources (Guo et al. 2016; Zheng et al. 2019; Wang and Xu 2021) or used simulated building models (Rad, Rafieian, and Sozer 2017; Yang and Li 2015). There are very few available studies that used an open access dataset to estimate building height in regard to building height and UHI study. The applicability of open dataset for such studies requires more examinations. This study introduces the application of extracted building height model in urban climate related study.

There are three main issues stated above that are not sufficiently explained by current studies. First, monitoring the urban development and its impact on LST in a metropolitan area with Jakarta as the case. Second, obtaining building height data with open DSM data with a simple method. Third, analyzing the relationship between building height and LST using building height data in areas with no LiDAR data.

1.2 Objectives

To address the UHI issue caused by urban development, the complexity of deriving building height from open-source satellite data and the contradicting results of building height's influence on land surface temperature, the objectives of this study are divided into the following points.

1) Analyzing the land cover change and its impact on land surface temperature,
2) Examining an alternative method to extract building height information from open-sources data that has lower computational complexity,
3) Analyzing the relationship between building height and land surface temperature.

Mainly, this study examines the main factors that influences land surface temperature in urban settings, such as horizontal urban development (Objective 1/Study 1) and vertical urban development (Objective 3/Study 3). Objective 2/Study 2 bridges the limitation in achieving Objective 3, which is difficulty in obtaining building height data for analysis. Therefore, in achieving Objective 3, the output of building height model from Objective 2 is used. This study also examines the applicability of derived building height model in the analysis of land surface temperature. Each objective belongs to different chapters. Objective 1 to 3 is discussed in Chapter 3 to 5, respectively.

1.3 Study Significance

This study analyzes the land cover change and its impact on land surface temperature in fast-growing cities such as Jakarta and its satellite cities. This study aims to examine how much the urban development in the city core of Jakarta expands to the satellite cities and how it influences the land surface temperature. The analysis is done city by city to see the development pattern, which was not done in existing studies.

This study attempts to solve the problem of limited access to building height data by using free global data and simple method based on two satellite products. Previous research mainly used high-cost data that only cover relatively small area, or global data that requires complex process to obtain. The result of this study has a global coverage and is easy to obtain, which should be an advantage for future research.

The derived building height is then used for analyzing the relationship between building height and land surface temperature in global cities, something that is narrowly investigated and show contradictory findings in existing studies. This study clarifies the relationship while exhibiting the applicability of extracted building height data, which make this study is the first to do that.

1.4 Thesis Structure

The structure of the thesis is shown in Figure 1. The thesis is divided into six chapters. Chapter 1 is the introduction part that describes the background and objectives of the research. Chapter 2 is the literature review that describes the basic knowledge of related terms in this study. Chapter 3 to 5 contains the research to achieve Objective 1 to 3, respectively. Chapter 3 to Chapter 5 contains standalone studies (Study 1 to Study 3), although the results of Chapter 4 is utilized in Chapter 5. Finally, Chapter 6 describes

the conclusion of this study, including the summary of findings, contributions and implications, and the limitations and future research. Overview of the research chapters are shown in Table 2.

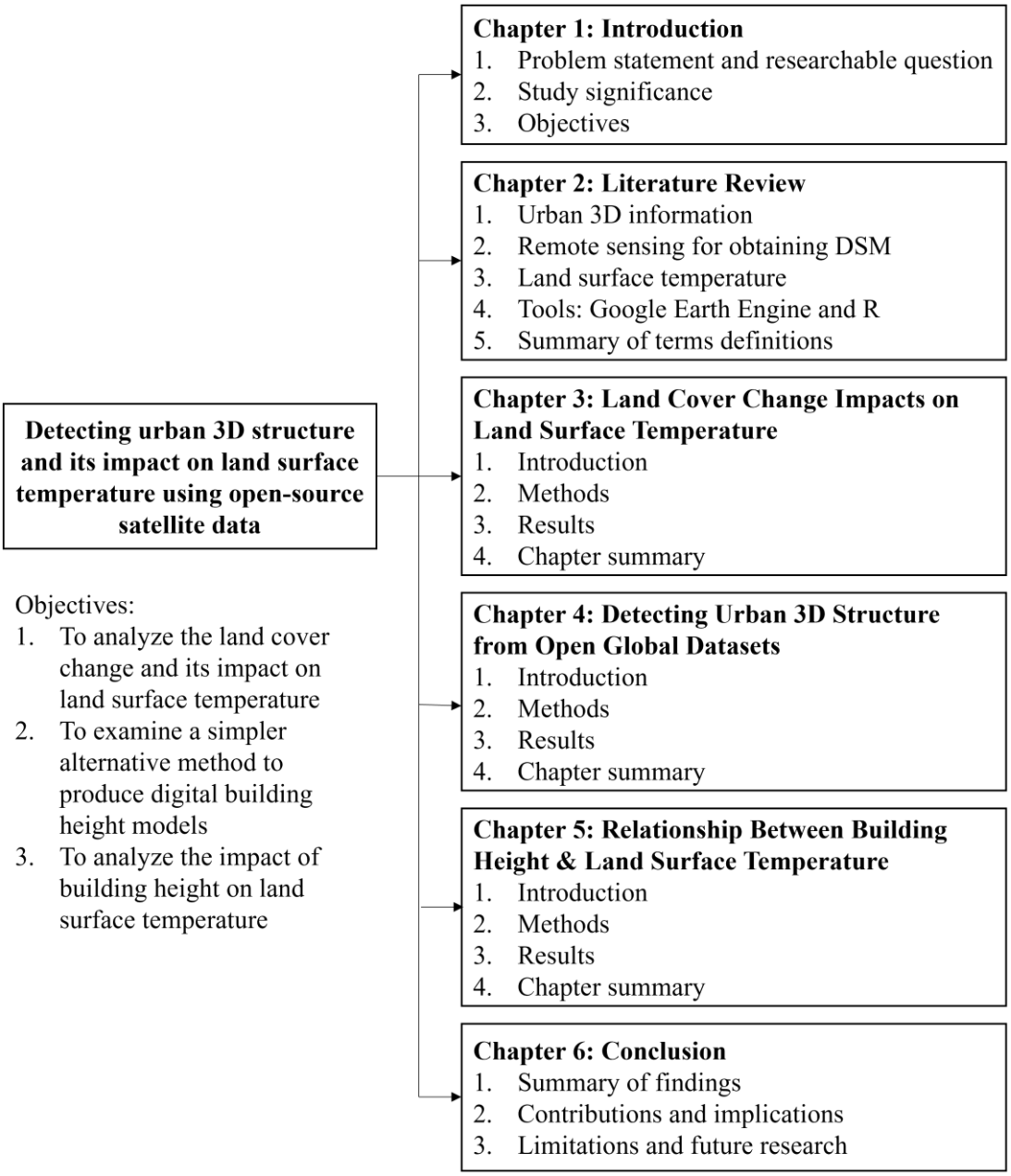

Figure 1. Thesis structure

Table 2. Overview of research chapters

	Chapter 3 (Study 1)	**Chapter 4 (Study 2)**	**Chapter 5 (Study 3)**	
			Study case: 6 cities	**Study case: 2 cities**
Goal	Monitoring land cover change and LST change in Jakarta and its satellite cities	Deriving building height with a simple method (AW3D30 - SRTM)	Analyzing relationship between building height and land surface temperature (closer observation in Tokyo and Jakarta)	
Study area	Jakarta, Bogor, Depok, Tangerang, Bekasi	Tokyo	Tokyo, Beijing, Jakarta, New York, Chicago, Los Angeles	Tokyo, Jakarta
Data collection	Land cover: 1. Landsat 5 visual band 2. Landsat 8 visual band Surface temperature: 1. Landsat 5 thermal band 2. Landsat 8 thermal band	Satellite DCHM: 1. AW3D30 2. SRTM LiDAR DCHM: 1. LiDAR DSM 2. LiDAR DTM	Building height: 1. AW3D30 2. SRTM Surface temperature: 1. Landsat 8 LST Veg. & water mask: 1. Landsat 8 NDVI 2. Landsat 8 NDWI	Building height: 1. AW3D30 2. SRTM Surface temperature: 1. Landsat 5 LST Veg. & water mask: 1. Landsat 5 NDVI 2. Landsat 5 NDWI
Data analysis	1. Land cover classification 2. Accuracy assessment 3. Comparison between LST of different land covers	1. 2D and 3D visualization 2. Smoothing filter 3. Correlation and regression between Satellite DCHM and LiDAR DCHM	1. 2D and 3D visualization 2. Correlation and regression between Satellite DCHM and LST	1. 2D and 3D visualization 2. Smoothing filter 3. Correlation and regression between Satellite DCHM and LST
Tools	QGIS and ArcGIS	Data collection: Google Earth Engine (GEE) Data analysis: R		

CHAPTER 2: Literature Review

2.1 Land Cover and Land Use

Land cover refers to the surface components of land that are physically present (EPA 2022). Examples of land covers are vegetation (lawn/grass, bushes, trees), water, bare soil, built-up (streets, buildings), and water. Classifications may differ from each other depending on the purpose of the observation. Some other classes may include wetlands, snow/ice, rocks, etc. The building category may be divided into smaller classes, such as low buildings and high buildings. As long as it is defined based on objects that are observed on the surface, the classification is based on land cover.

Land use refers to the usage of the land. It represents economic and cultural activities (EPA 2021). Examples of land uses are residential, agricultural, industrial, commercial, etc. Sometimes the terms land cover and land use are used together, but there is a clear difference between the two. For instance, when there is a large area of buildings, land cover classification system classifies all those buildings into the same category, which is “built-up”, but land use classification system may separate them into several classes, such as “residential” when the buildings are mostly houses, and “industrial” when the buildings are industries. This study focuses more on the land cover, but also discussed the land use when it is necessary.

2.2 Land Surface Temperature

Land surface temperature (LST) is the skin temperature of the land surface, which can be estimated mainly from thermal infrared (TIR) sensor on a satellite. LST is an important parameter that affect regional climates, surface energy balances, and energy exchanges (Sekertekin and Bonafoni 2020). Further, LST has been used to identify and characterize urban heat island (UHI) (Jeevalakshmi, Narayana Reddy, and Manikiam

2017). LST data are commonly extracted from Landsat as they have large coverage, spatially and temporally. Landsat visual bands have a resolution of 30 m, but thermal bands have lower resolutions, 120 m in Landsat 4-5 Thematic Mapper (TM) and 100 m in Landsat 8 Operational Land Imager (OLI) / Thermal Infrared Sensor (TIRS) (U.S. Geological Survey 2019). However, the resolution is resampled to 30 m in the distributed Landsat products.

2.3 Urban 3D Structure Information

The information of urban 3D structure in this study is expressed as the Digital Canopy Height Model (DCHM), which includes the height information of buildings and vegetation. DCHM can be obtained by subtracting the digital terrain model (DTM) from the digital surface model (DSM) (Guth et al. 2021). The digital elevation model (DEM)

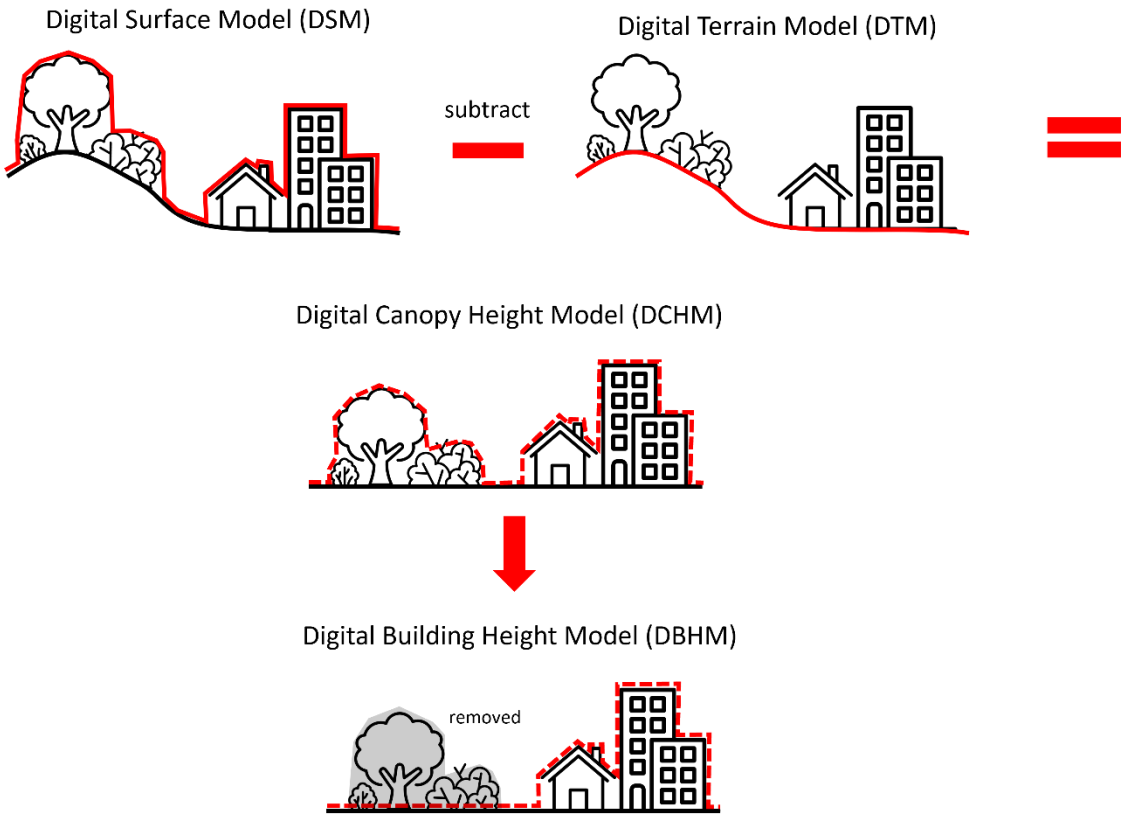

Figure 2. Illustration of DSM, DTM, DCHM, and DBHM

is sometimes synonymously with DTM. DCHM is also referred to as normalized DSM (nDSM). The model of building height is called Digital Building Height Model (DBHM), which can be obtained by excluding vegetation from DCHM. Figure 2 illustrates the explanations of these terms.

2.4 Remote Sensing Methods for Obtaining Digital Surface Model (DSM)

There are several methods to obtain DSM using remote sensing. Generally, they are classified into three categories, which are airborne light detection and ranging (Zhang, Yan, and Chen 2006), optical stereo images (Tian, Cui, and Reinartz 2014), and synthetic aperture radar (SAR) (Gamba, Houshmand, and Saccani 2000). This part of the literature review explains those methods in related to used datasets in this study.

The first method is measuring DSM using light detection and ranging (LiDAR) sensor on an aerial platform, or also referred to as Airborne Laser Scanning (ALS) (Căţeanu and Ciubotaru 2020). Light pulses are emitted from a laser scanner, and when the pulse hits an object, a portion of its photons are reflected back to the scanner. The collected LiDAR data is a data structure called point cloud, which have 3D location (XYZ coordinates) and it can be used to estimate the 3D structure of the target area (Melin, Shapiro, and Glover-Kapfer 2017). The illustration of airborne LiDAR system is shown in Figure 3. LiDAR method is popular within the surveying communities because they can produce extremely high accuracies and point densities, thus allowing precise, realistic, and three-dimensional representations of on-surface objects, including roadways, bridges, buildings, and other structures at high spatial resolutions (NOAA Coastal Services Center 2012).

LiDAR provides high precision and can collect data rapidly, but there are some disadvantages of it, such as difficulties in processing LiDAR data (Hummel et al. 2011),

high operational cost of data collection (Bi et al. 2021), and easily affected by the medium (light pulses). For example, moisture in the atmosphere affects the performance of a LiDAR system, therefore it cannot perform well in bad weather, such as rain (Jia, Zhu, and Ao 2006), fog, and snowstorm (Kim, McArthur, and Korevaar 2001). LiDAR is a method used to acquire the reference DSM and DTM in this study.

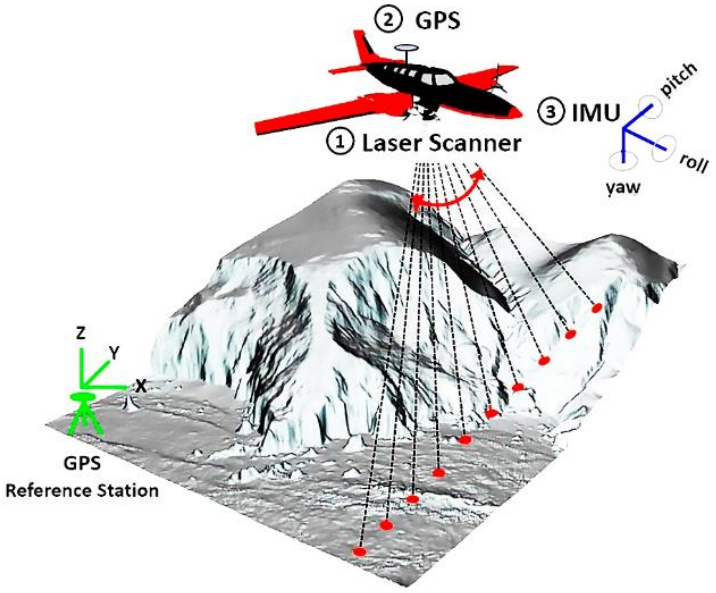

Figure 3. Illustration of airborne LiDAR system

(retrieved from (Tomljenovic et al. 2015))

The second method is measuring DSM from optical stereo image. In this method, along track stereo cameras are mounted on a satellite specially built for stereo acquisition. These camera systems use two or three CCD lines for along track stereo viewing. The key of generating DSM from optical images is the stereo image matching process. A high redundancy in the image is desirable for robust matching (Reinartz D'Angelo, P., Krauss, T., Chaabouni-Chouayakh, H. 2010). Advanced Land Observing Satellite (ALOS) World 3D 30 m (AW3D30) DSM dataset used in this study was generated from stereo or triplet pair images acquired by the Panchromatic Remote-

sensing Instrument for Stereo Mapping (PRISM) sensor aboard ALOS (Tadono et al. 2016). Figure 4 illustrates the observation of PRISM triplet and stereo observing mode.

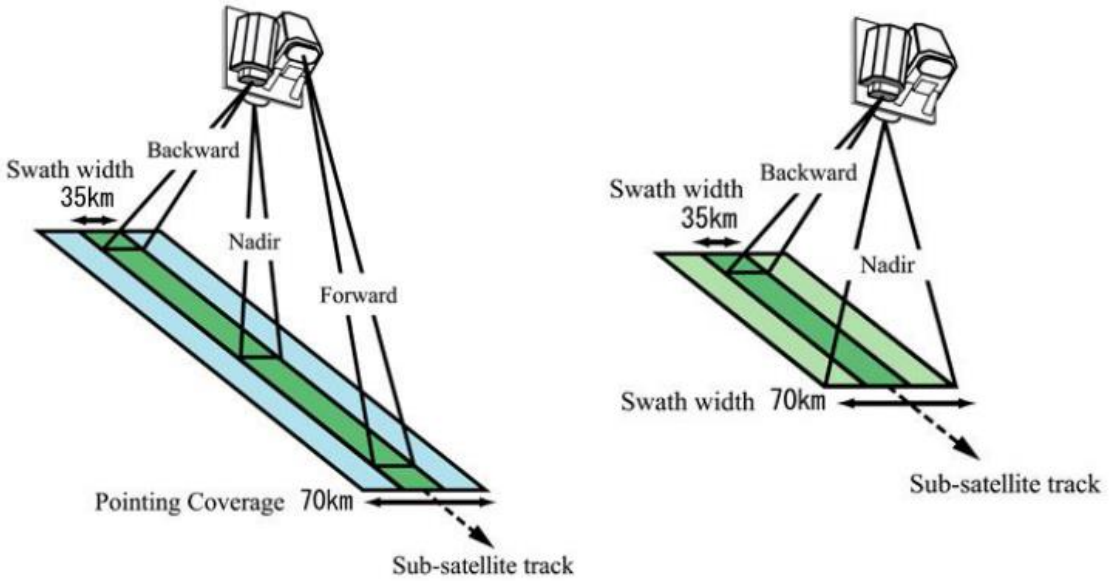

Figure 4. Observation geometries of PRISM triplet observing mode (left) and stereo observing mode (right) (retrieved from (Tadono et al. 2016))

The third method is using synthetic aperture radar. Radar stands for radio detection and ranging. Principally, it works almost identical to LiDAR, but it uses electromagnetic radio waves instead of lasers (Bhatta and Geethapriya 2017). In radar technology, there is an imaging technique called interferometric synthetic aperture radar (InSAR). SAR imagery is produced by reflecting radar signals off a target area and recording the two-way travel time back to the satellite, while InSAR technique uses two SAR images of the same area acquired at different times (USGS, 2018). If the distance between the ground and satellite changes between the two acquisitions, a phase shift will occur (Figure 5) (Geoscience Australia). InSAR is a technique used to acquire SRTM (Shuttle Radar Topography Mission) DEM used in this study.

Each explained method has its advantages and disadvantages. Table 3 summarizes the advantages and disadvantages of three different methods in obtaining DSM. In this

study, LiDAR point cloud data are used as the reference data, meanwhile the optical stereo images and radar measurement data are used as the materials for proposed method.

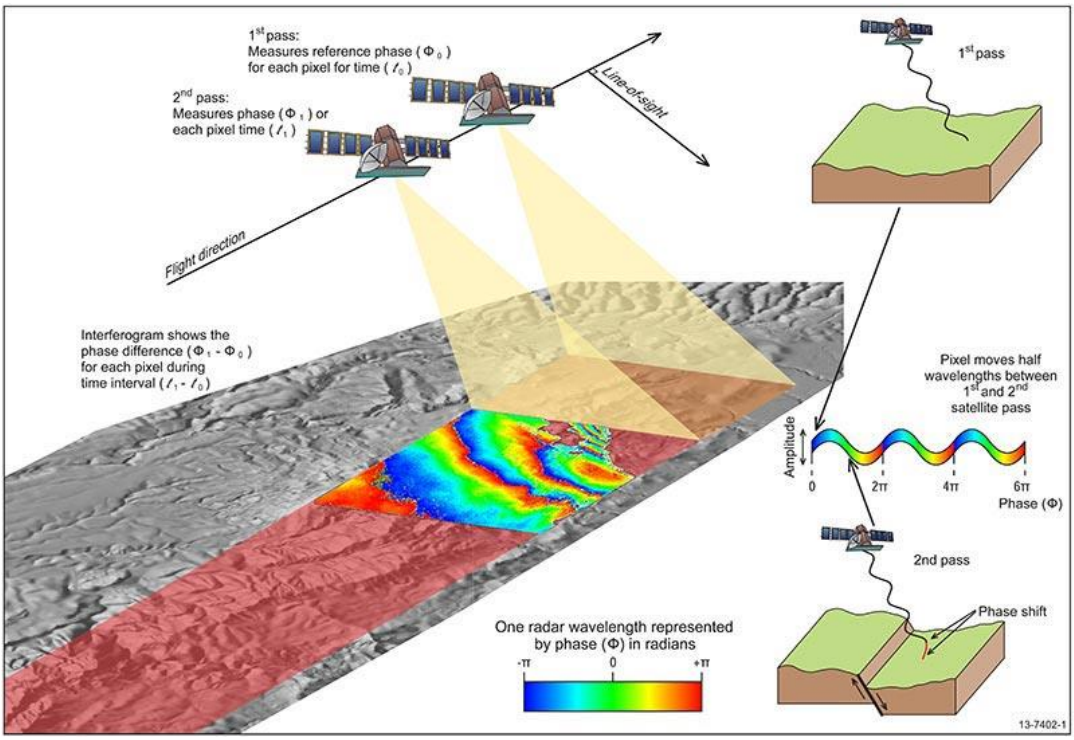

Figure 5. Two SAR images of the same area acquired at different times (retrieved from https://www.ga.gov.au/scientific-topics/positioning-navigation/geodesy/geodetic-techniques/interferometric-synthetic-aperture-radar)

Table 3. Advantages and disadvantages of different methods in obtaining DSM

Method	Advantage	Disadvantage
LiDAR	Very high-precision, very high spatial resolution	Expensive, relatively narrow coverage
Optical stereo image	Less inexpensive compared to LiDAR, large coverage, quite high spatial resolution	High spatial resolution is only available commercially
Synthetic aperture radar	Inexpensive, large coverage	Low resolution

2.5 Tools: Google Earth Engine and R

In this study, there are two tools or software used for data collection and data analysis, namely Google Earth Engine and R.

Google Earth Engine (GEE) is a cloud-based platform for planetary-scale geospatial analysis (Gorelick et al. 2017). GEE offers high performance computation service that is accessed and controlled through an internet-accessible application programming interface. GEE is also equipped with web-based interactive development environment that allows rapid visualization of results. Users can access and analyze data from a catalog that contains a large repository of publicly available geospatial datasets or their own private data.

GEE can be accessed free of charge by anyone who has a Google account and granted the permission after registration. Users are required to sign into their Google account (or sign up if possesses none), fill out an application, and wait until they receive a welcome email from GEE. The workspace for GEE can be accessed from https://code.earthengine.google.com/. GEE uses the programming language JavaScript. Google offers supports of pre-made analysis code, and tutorials can be easily searched online. With basic knowledge of JavaScript, users can analyze data in GEE. In this study, GEE is mainly used to collect satellite datasets before analyzed using programs written in R.

R is a language and free software environment for statistical computing and graphics (R Core Team 2020). R can be used to calculate a wide variety of statistical and graphical technique. Originally, R was not designed for spatial data analysis, but it has been long used in the geospatial developer community as a powerful Geographic Information System (GIS) platform. R relatively does not use much central processing unit (CPU) usage, compared to other geospatial analysis tools such as Geographic

Information System (GIS) desktop applications (ArcGIS, QGIS, etc.). In this study, RStudio is used to write the R program because of its convenient environment. RStudio is a free integrated development environment for R that includes a console, tools for plotting, etc. for easier management of our workspace (RStudio Team 2020).

2.6 Summary of Terms Definitions and Abbreviations

The following is a list of terms used in this dissertation. There may be slight differences in the definitions of the terms, but these are the ones applied in this study.

1) DTM: Digital Terrain Model. A representation of the bare earth topographic surface without vegetation, buildings, and any other surface objects.
2) DSM: Digital Surface Model. A representation of surface elevation that captures the natural and built feature on earth's surface, including vegetation, buildings, etc.
3) DEM: Digital Elevation Model.
4) LiDAR DTM: Reference DTM data from airborne LiDAR used in this study.
5) LiDAR DSM: Reference DSM data from airborne LiDAR used in this study.
6) DCHM: Digital Canopy Height Model. The net canopy height after subtracting the terrain elevation, includes the height of buildings and vegetation.
7) DBHM: Digital Building Height Model. The net building height after subtracting the terrain elevation, includes only the building height, without vegetation.
8) AW3D30: ALOS World 3D – 30m. A global DSM dataset from ALOS (Advanced Land Observing Satellite) at 30-m spatial resolution. Acquired by Japan Aerospace Exploration Agency.
9) SRTM: Shuttle Radar Topography Mission. A global DSM dataset from the space shuttle radar. Acquired by the National Aeronautics and Space Administration and the National Geospatial-Intelligence Agency.

10) LST: Land Surface Temperature. The radiative skin temperature of the surface of the earth.
11) NDVI: Normalized Difference Vegetation Index.
12) NDWI: Normalized Difference Water Index.
13) GEE: Google Earth Engine. A cloud-based platform for geospatial analysis.
14) High-rise buildings: buildings that have ten or more stories (>25m).
15) Medium-rise buildings: buildings that have 3-9 stories (10-25m).
16) Low-rise buildings: buildings that have 1-3 stories (3-10m).

CHAPTER 3: Land cover change impacts on land surface temperature in Jakarta and its satellite cities

3.1 Introduction

Cities in developing countries grow rapidly within the past few decades. Asian countries are the most rapidly growing regions and among them, Indonesia has the highest urbanization rate of 4.1% per year. With this level of urbanization, 68% of the Indonesia population is expected to live in cities by 2025 (The World Bank 2016b). Indonesia's capital city, Jakarta, is a megacity that has more than 10 million people. In 2016, the population of Jakarta was 10,277,628 people, which increased as much as 0.98% from the previous year (BPS - Statistics of DKI Jakarta Province 2017). Urbanization in Jakarta started to accelerate in the early 1980s when Jakarta began shifting its economic growth into a new mode of export-oriented industrialization (Douglass 2010).

Jakarta has grown spatially into a larger region called Jabodetabek (Jakarta Metropolitan area). The name 'Jabodetabek' is an abbreviation formed from the first syllables of Jakarta and its surrounding cities and regencies: Jakarta, Bogor, Depok, Tangerang, and Bekasi. These cities become the buffer of Jakarta to support people's needs of a residence, tourism, etc. The built-up area has been expanding widely, not only inside, but also beyond the capital city. As a result, rapid development also occurs in its surrounding/satellite cities. It is expected that the development in these areas in recent years might be even faster than in Jakarta that is almost fully occupied.

The urban development in the satellite cities of Jakarta mostly aims to meet the increasing needs of the residential area and its residents' services, including housings and shopping malls. These projects consumed a large area of land, specifically

agricultural land (Fitriani and Harris 2011). This results in unpredicted replacements of existing agricultural land and green space into buildings, roads, and other infrastructures. This type of unpredicted development makes it important to investigate the urbanization process because there may be some opportunities we could utilize and some challenges we could tackle to improve the city development planning. Therefore, this study aimed to analyze the built-up area expansion pattern of Jakarta and its satellite cities.

Some similar studies have investigated the built-up area expansion in the Jakarta Metropolitan Area (Estoque, Murayama, and Myint 2017; Nurwanda and Honjo 2018). These studies focused on individual cities or the Jakarta Metropolitan Area as a whole; however, no available study has compared the built-up area expansion patterns among Jakarta and its satellite cities. Additionally, no existing study has done a city-by-city analysis. Working with big spatial data all at once is challenging and could result in slightly lower accuracy due to the large heterogeneity in the study area. Nevertheless, by investigating the large area, as has been done for some smaller areas, this study aimed to fill gaps and provide an updated and more accurate overall result.

The increase of urban area and the decrease of green space in Jabodetabek intensify the effect of urban heat island (UHI) in the city. UHI occurs when an urban region has a higher temperature compared to its surrounding area (Voogt and Oke 2003). This study focuses on surface UHI, where the identification method is measured indirectly by remote sensing. Therefore, the land surface temperature (LST) of the study area was monitored to detect the existence of UHI.

Analyzing the land-use/land-cover change is the most important part of understanding the built-up area expansion and the impact it may cause to LST. Therefore, the objectives of this chapter were (1) to analyze the land cover changes in Jakarta and

its satellite cities and (2) to analyze the impact of these changes on LST using GIS-based analysis.

3.2 Methods

3.2.1 Study Area and Materials

The study area (Figure 6) includes Jakarta and its directly connected satellite cities: Depok, Tangerang, and Bekasi. The wet season in the study area lasts from October to May, while the dry season lasts from June to September.

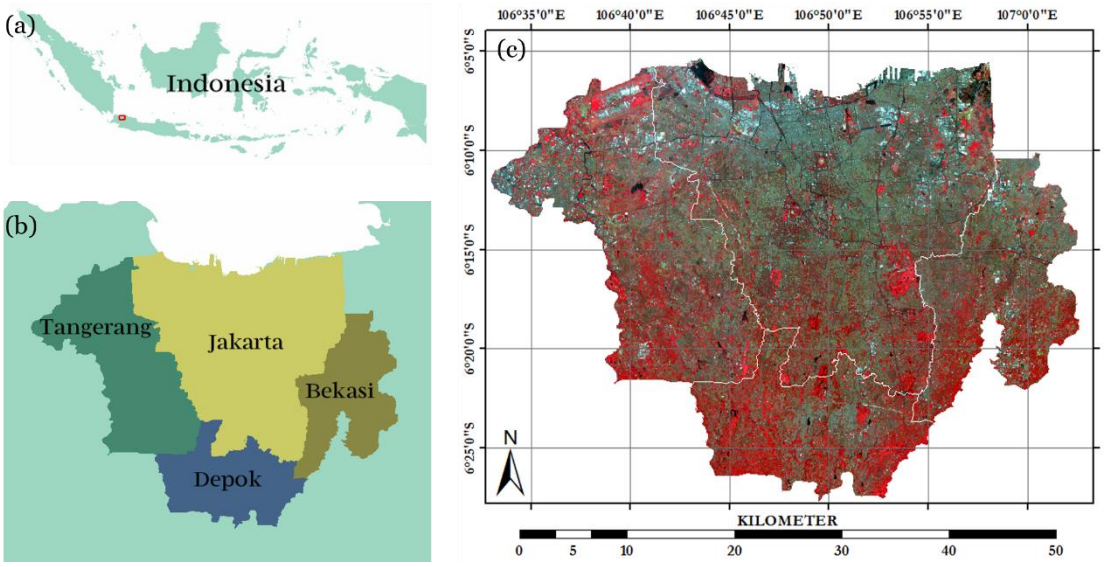

Figure 6. Map of the analyzed area. (a) The location in Indonesia, (b) Jakarta and its satellite cities, (c) Landsat satellite image of the study area in false color.

We used Landsat-5 Thematic Mapper (TM) and Landsat-8 Operational Land Imager and Thermal Infrared Sensor (OLI/TIRS) imagery with 30-m spatial resolution downloaded from the Earth Explorer United States Geological Survey (USGS) website. We analyzed two sets of different timeframe satellite imagery for each city (Table 4). Patching was needed when the main image is cloudy. All the maps were first re-projected into UTM Zone 48S, WGS84 datum.

Table 4. Descriptions of the Landsat Imagery used

City	Image Acquisition Date				Sensor	Bands
	Main Imagery		Patch			
	Year	Date	Year	Date		
Jakarta	1990	9 Jul	1990	6 Jun	Landsat-5	1-5 & 7
	2015	31 Aug	2014	13 Sep	Landsat-8	2-7
Depok	1989	6 Jul	*No cloud*		Landsat-5	1-5 & 7
	2018	1 Apr	*No cloud*		Landsat-8	2-7
Tangerang	1989	6 Jul	1989	12 Jun	Landsat-5	1-5 & 7
	2015	31 Aug	2014	13 Sep	Landsat-8	2-7
Bekasi	1989	6 Jul	*No cloud*		Landsat-5	1-5 & 7
	2015	31 Aug	*No cloud*		Landsat-8	2-7

3.2.2 Cloud patching

As the cloud is often a problem when working with satellite images of a tropical area, the cloud coverage was masked using the Fmask function developed by Zhu & Woodcock (Zhu and Woodcock 2012). If the Fmask algorithm could not detect the cloud, the cloud masking process was performed manually by drawing a shapefile over it. The area covered by the cloud mask was removed and then patched by another set of Landsat images from the closest time possible.

3.2.3 Land cover classification

We classified the land cover of the study area into five categories: water, grass, trees, built-up, and bare land. The water category includes rivers, canals, lakes, ponds, and flooded paddy fields in the early stage of planting. The grass category includes natural grasslands, golf courses, grass fields, and low plant crops in agricultural areas. The tree category includes natural woodlands, urban forests, and urban trees; the built-up category includes residential, commercial, and industrial areas and transportation

infrastructures; and bare land includes open soil and unplanted farmland. The images were classified by a supervised classification in QGIS using the Semi-Automatic Classification Plug-in and maximum likelihood algorithm.

3.2.4 Accuracy assessment

We created a layer of random points in Arc GIS. The number of the random points for each class ranged from 50 to 70 points, it exceeded the recommended minimum of $n\ (n + 1)$ where n is the number of classes (El-Hattab 2016). Every point was assigned to a class value (1: water, 2: grass, 3: trees, 4: built-up, 5: bare soil). This layer was then exported into a KML format to be displayed on Google Earth and compared to the higher resolution map displayed in Google Earth's historical imagery. The ground truth data obtained from the comparison then inputted to create an error matrix in Arc GIS and Ms. Excel.

3.2.5 Land cover change detection analysis

The land cover change was detected by a post-classification comparison that involved an independently produced classification result. The raster value of the maps was reclassified and then multiplied using the raster calculator function in Arc GIS. The advantages of this method are it reduces atmospheric, sensor, and environmental impact, it produces complete matrices of change, and it also minimizes the impact of using multi-sensor images (Hussain et al. 2013).

3.2.6 LST retrieval

The LST values were estimated from the conversion of digital number (DN) values of thermal infrared bands. The bands used were band 6 and band 10 for images acquired by Landsat-5 and Landsat-8, respectively. The retrieval of LST involved the following steps (USGS 2016).

1) Converting the DN values to spectral radiance. The conversion followed Eq. (1) in the case of Landsat-5 TM and Eq. 2 in the case of Landsat-8 OLI/TIRS.

$$L_\lambda = L_{min} + \left(\frac{L_{max} - L_{min}}{255}\right) \times DN \quad (1)$$

$$L_\lambda = M_L * DN + A_L \quad (2)$$

where:

L_λ = Spectral radiance (Watts / (m^2 * srad * μm)); L_{min} = Band minimum radiance value; L_{max} = Band maximum radiance value; M_L = Radiance multiplicative scaling factor for the band; A_L = Radiance additive scaling factor for the band

2) Converting the spectral radiance to surface temperature using Eq. (3).

$$T = \frac{K2}{\ln\left(\frac{K1}{L_\lambda} + 1\right)} \quad (3)$$

where:

T = Surface temperature; K1 = Thermal conversion constant for the band; K2 = Thermal conversion constant for the band

3.3 Results & Discussions

3.3.1 Accuracy assessment of land cover maps

A minimum of 250 random points was placed dispersedly throughout the map with each land cover type is covered by at least 50 points. The overall classification accuracy is shown in Table 5. These accuracy levels are considered reliable enough because they exceed the target overall accuracy of 85% with no class less than 70% accurate (Thomlinson, Bolstad, and Cohen 1999). When there was any data that did not reach this level, reclassification was mandatory.

Table 5. Accuracy assessment for the classified images

City	Reference Year	Overall Classification Accuracy	Overall Kappa Statistics
Jakarta	1990	91.48%	0.89
	2015	93.60%	0.92
Depok	1989	85.97%	0.82
	2018	93.81%	0.92
Tangerang	1989	93.05%	0.91
	2015	89.60%	0.87
Bekasi	1989	92.38%	0.90
	2015	89.15%	0.86

3.3.2 Land cover change

The summary of combined land cover maps from the initial year (1989/1990) and the recent year (2015/2018) is shown in Figure 7. Jakarta is more developed in the initial year compared to the other cities, but in the recent year, the built-up area has expanded and occupied most parts of the cities. The detail of each class' total area is shown in Table 6. A graphic is created to compare the land cover class proportion between the initial and recent years (Figure 8).

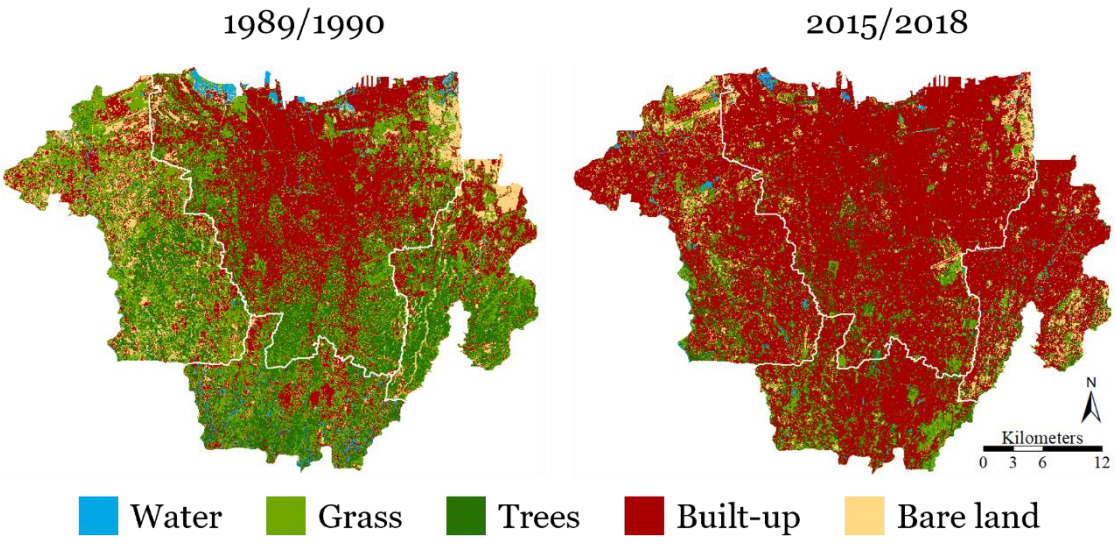

Figure 7. Land cover maps of the study area

Table 6. Land cover classification results of each city in hectares

Land cover	Jakarta		Depok		Tangerang		Bekasi	
	1990	2015	1989	2018	1989	2015	1989	2015
Water	1,381.14	606.15	1,076.40	150.84	341.28	650.07	119.52	279.36
Grass	13,262.13	4,058.46	7,141.77	3,483.09	14,150.43	5,002.92	6,417.81	1,342.35
Trees	12,375.36	4,271.94	6,463.35	3,161.07	6,722.91	2,816.37	6,496.83	1,983.15
Built-up	33,797.61	52,840.17	4,721.22	12,724.56	7,265.25	23,358.06	5,666.31	15,576.48
Bare land	4,449.06	3,488.58	701.46	584.64	6,333.57	2,986.02	2,742.21	2,261.34
Total	65,265.30	65,265.30	20,104.20	20,104.20	34,813.44	34,813.44	21,442.68	21,442.68

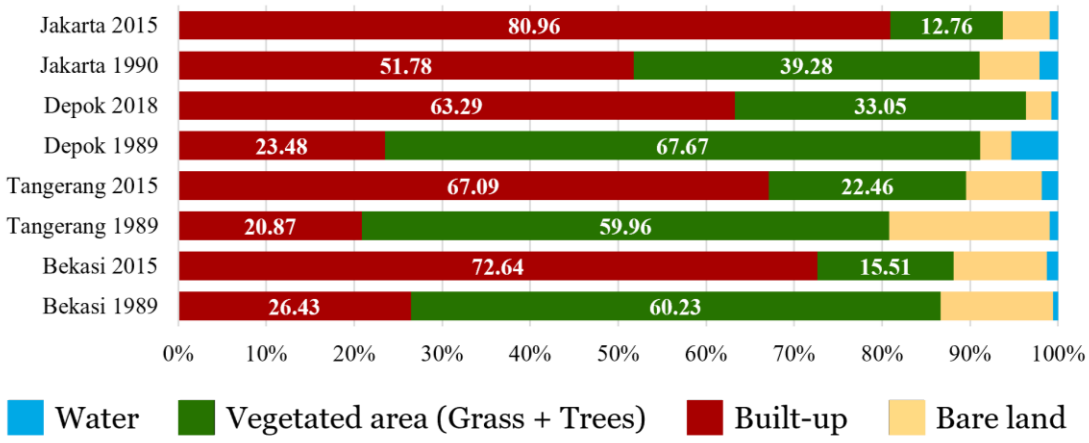

Figure 8. Study area's land cover change proportion (100% = the total area of each city)

The difference between the built-up area in the recent year and the initial year shows the built-up area expansion. The built-up area expansion was 19,042.56 ha in Jakarta, 8,003.34 ha in Depok, 16,092.81 ha in Tangerang, and 9,910.17 ha in Bekasi. In terms of total area, Jakarta had the highest built-up area expansion, followed by Tangerang, Bekasi, and Depok; however, in terms of proportion, Jakarta had the lowest expansion. The highest belongs to Tangerang, followed by Bekasi with a slight difference, then Depok. This result occurred because Jakarta is much larger and was initially more developed than in other cities.

Table 7 is derived from the matrices of change that were produced by land cover change detection analysis. It shows the total area and proportion of each land cover type that is converted to the built-up area. The expansion of the built-up area seemed to

happen mostly by replacing the vegetated area. The proportion of grass and tree area loss is almost the same in each city, except in Tangerang which grass area loss is near twice the tree area loss. This is due to the larger proportion of grass/low plant class in the initial year in Tangerang.

Table 7. Land cover types in the initial year that are converted to the built-up area in the recent year (100% = the total area of each city)

Land cover	Jakarta (2015)		Depok (2018)		Tangerang (2015)		Bekasi (2015)	
	Hectares	%	Hectares	%	Hectares	%	Hectares	%
Water	836.19	1.28	452.88	2.25	73.80	0.21	63.90	0.30
Grass	8,950.32	13.71	4,394.79	21.86	8,703.99	25.00	4,253.76	19.84
Trees	8,595.90	13.17	4,069.26	20.24	4,736.52	13.61	4,366.08	20.36
Built-up (still)	31,548.06	48.34	3,349.08	16.66	5,975.19	17.16	4,998.51	23.31
Bare land	2,909.70	4.46	458.55	2.28	3,868.56	11.11	1,894.23	8.83
Total	52,840.17	80.96	12,724.56	63.29	23,358.06	67.09	15,576.48	72.64

3.3.3 Built-up area expansion

The built-up area expands towards the outer part of Jakarta (Figure 9). There are some unchanged vegetated areas that are located in the middle of Jakarta, such as golf courses, city parks, and landmarks. Agricultural land in the western and eastern part of Jakarta is converted to built-up, along with the forest area in the southern part of Jakarta.

The initial built-up area in Depok was relatively small. In 1989, there were only a few concentrated high-density residential areas in the middle and the northern part of the city that is directly bordering with Jakarta. The initial built-up area included a train station and a government office. Tangerang is located on the west of Jakarta, so the eastern part of Tangerang is expected to be more developed. The initial built-up area in 1989 is mostly located near Jakarta and in the northern part of the city which consisted of Soekarno-Hatta International Airport and some compact residential areas. The expansion in Tangerang is mostly for residential area and shopping mall area.

In Bekasi, the initial built-up area was only distributed in the center and northern parts of the city. The center of the initial built-up area is the location of Bekasi's mayor office and railway stations (Kranji station and Bekasi station). Besides the railway, this area is connected to Jakarta through a major traffic road. Road network is one of the major factors that affect built-up area expansion in a city (Shi et al. 2019). This is suspected to be one of the main factors why built-up area expansion occurred quickly in that area.

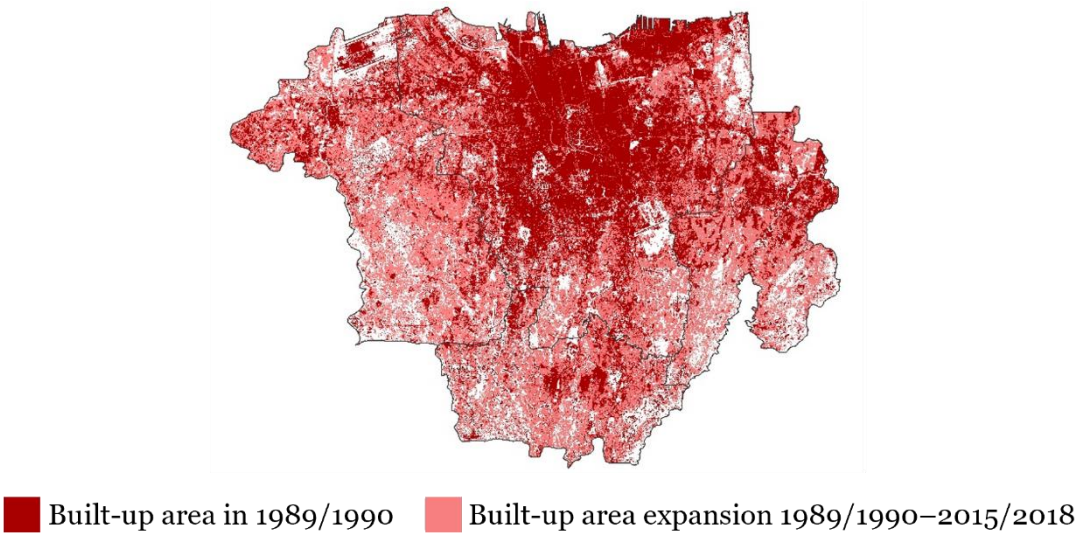

Figure 9. Built-up area expansion from the initial year to recent year

3.3.4 Impacts of land cover change on land surface temperature

LST distribution maps of the study area are shown in Figure 10. The LST pattern is highly related with the land cover distribution. In 1989/1990, the high LST area is mostly distributed in the center part of Jakarta where the built-up area is concentrated. The outer part of Jakarta had lower temperatures as that area was covered by more vegetation compared to the center part. Compared to Jakarta, other cities had a lower temperature. The high LST area continued to increase following the land conversion to

the built-up area. When the area is converted to built-up, the temperature increased which results in high LST distribution in 2015/2018.

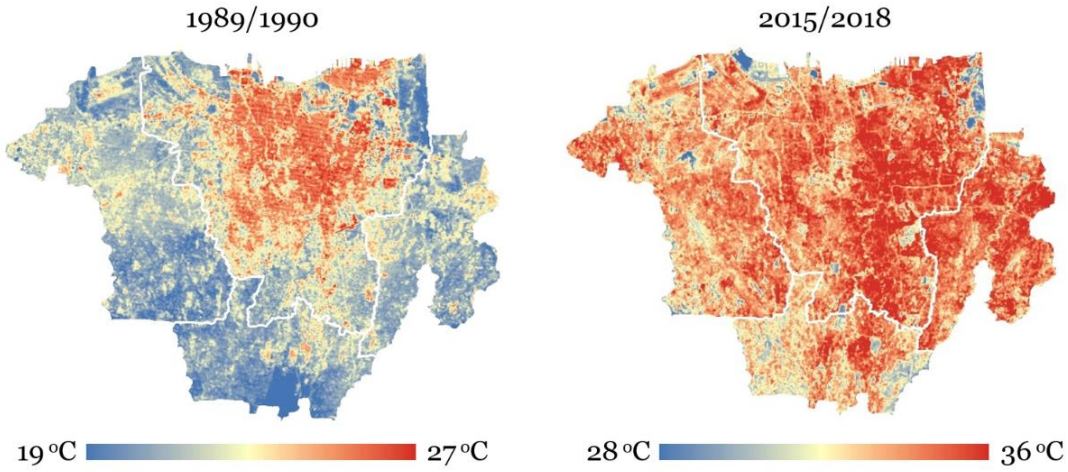

Figure 10. LST maps

Figure 11 illustrated the mean LST fluctuation by different land cover types and Table 8 shows the mean LST in numbers. In general, the LST of all land cover increases in during the two observed periods, indicating that the surface temperature gets warmer in the study area. However, the temperature of the built-up area was the highest among the land cover types, followed by bare land, trees, then grass with a slight difference, and finally water. In the initial year, Jakarta had the highest mean LST, followed by Bekasi, Tangerang, and Depok; however, in the recent year, Bekasi had the highest mean LST, followed by Jakarta, Tangerang, and Depok.

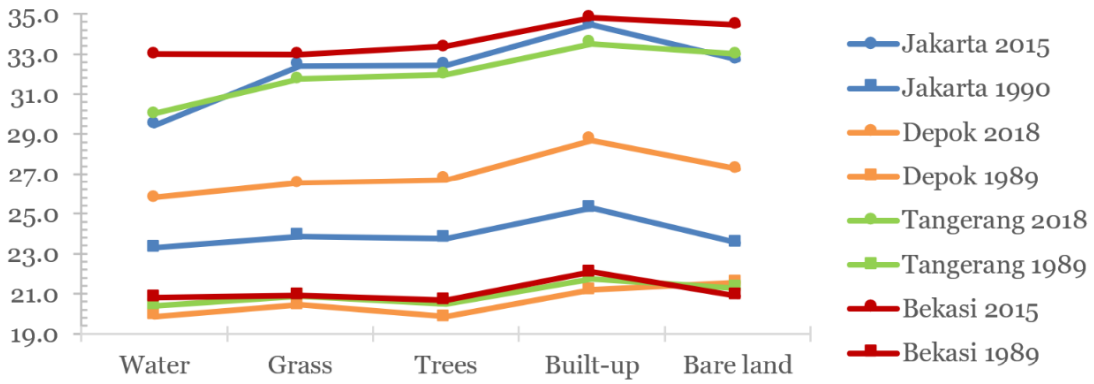

Figure 11. Mean LST by land cover type

Table 8. Means LST (°C) in different land cover types

Land cover	Jakarta		Depok		Tangerang		Bekasi	
	1990	2015	1989	2018	1989	2015	1989	2015
Water	23.29	29.44	19.86	25.81	20.40	30.03	20.79	33.00
Grass	23.85	32.41	20.44	26.55	20.89	31.76	20.91	32.98
Trees	23.76	32.43	19.85	26.70	20.49	31.96	20.68	33.38
Built-up	25.29	34.45	21.21	28.69	21.73	33.52	22.09	34.82
Bare land	23.53	32.72	21.55	27.27	21.27	33.01	20.88	34.46
Mean	23.95	32.29	20.58	27.01	20.96	32.05	21.07	33.73

The city that has the most significant difference between mean overall LST in the initial and the recent year is Bekasi with 12.66 °C, then followed by Tangerang (11.05°C), Jakarta (8.34 °C), and Depok (6.43 °C). There are large differences between the two periods. Although, it is certain that the overall LST increases, the difference may be enlarged by different satellite sensors that capture the temperatures. The initial year data is acquired from Landsat 5, meanwhile, the recent year data is acquired from Landsat 8. The sensors from Landsat 5 and Landsat 8 that are in charge for thermal mapping have slightly different wavelength, 10.40–12.50 in Landsat 5 and 10.60–11.19 in Landsat 8. This slight difference may impact the detected temperature. In addition, according to J. Sun and Ongsomwang (2021), even one pixel of LST at the same place may have great variability at different dates, especially if the time interval is large. Therefore, a reconstruction of LST values is recommended in multitemporal analysis to produce more accurate results, which is not performed in the present study. Future study should consider LST validation in the analysis to mitigate the fluctuation of LST values.

Bekasi shows the highest LST difference although the highest built-up expansion proportion belongs to Tangerang. It might be caused by higher proportion of built-up area combined with higher loss of vegetated area in Bekasi compared to Tangerang

(Figure 8). Bekasi and Tangerang underwent major developments between the initial and the recent year. There is a significant increase in family shopping malls in Bekasi to the point where the government's income from the shopping mall's taxes in 2014 doubled from 2011 (Emahlia and Baiquni 2017). These shopping malls are built in the center part of the city near the Bekasi railway station (initial built-up area in 1989). Further, there are more industrial area development in Bekasi compared to in other cities. This industrial land use is likely to have bigger influence in increasing LST compared to other type of land use, such as commercial, residential, and recreational areas.

3.4 Chapter Summary

The land cover change that occurred in Jakarta and its satellite cities are mostly vegetated area conversion to built-up area. The urbanization is started from Jakarta and then spread to the surrounding cities. According to the built-up expansion proportion of each city's total area, the expansion occurred most extensive in Tangerang, followed by Bekasi, with a slight difference, Depok, and lastly Jakarta. The main cause of built-up area expansion in every city was construction for residential purposes and shopping malls to accommodate the continuously growing population.

The land cover changes resulted in significantly higher mean LST of the analyzed cities. The mean LST difference ranged from 6.43 ^{o}C to 12.66 ^{o}C. These differences may be enlarged because the LST are derived from two different satellite sensors. The highest LST difference belongs to Bekasi, meanwhile, the lowest belongs to Depok. If observed by land cover types, a high LST area is mostly distributed in the built-up area. The increase of the high LST area is highly affected by the land conversion to the built-up area. Future study should consider calibrating and validating the LST data of different periods, especially if using different sensors, to produce more accurate results.

CHAPTER 4: Detecting Urban 3D Structure from Open Global Datasets

4.1 Introduction

Urban 3D structure is important information for the application in architecture, urban planning (R. Chen 2011), urban monitoring (Zhao, Weng, and Hersperger 2020), urban climate (Kouklis and Yiannakou 2021), disaster assessment (Jojene R. Santillan et al. 2015), and many others. As a significant parameter of urban 3D structure, building height has been discussed regarding its influence on energy consumption (Güneralp et al. 2017), gas emission (Borck 2016), and urban heat island effects (Berger et al. 2017; Danniswari et al. 2021). Furthermore, the building height is used in local climate zones (LCZ), a classification scheme to describe the urban characteristic by Stewart and Oke (Stewart and Oke 2012).

The characteristic of the urban 3D structure is expressed as the Digital Canopy Height Model (DCHM), which includes the height information of buildings and vegetation. DCHM can be obtained by subtracting the digital terrain model (DTM) from the digital surface model (DSM). The digital elevation model (DEM) is sometimes synonymously with DTM. DCHM is also referred to as normalized DSM (nDSM). The model of building height is called Digital Building Height Model (DBHM), which can be obtained by excluding vegetation from DCHM.

Many researchers have used remote sensing-based methods to obtain DCHM. Remotely sensed data are extracted from airborne light detection and ranging (LiDAR) (Zhang, Yan, and Chen 2006), optical stereo images (Tian, Cui, and Reinartz 2014), and synthetic aperture radar (SAR) (Gamba, Houshmand, and Saccani 2000). Data obtained from airborne LiDAR are favorable for extracting height information because of its high

accuracy. However, these data are difficult to obtain due to high operational costs or they are only available under the authority of local government. As a result, they are unavailable for many areas in the world (Alobeid, Jacobsen, and Heipke 2010). A remote sensing-based methodology to obtain DCHM that can be applied globally and easily is necessary.

There have been attempts to extract DCHM using globally available data. Global DSM data only provide the surface height information. Therefore, the DTM must be extracted from DSM prior to calculating the building height. Misra et al. (Misra, Avtar, and Takeuchi 2018) compared the building height models extracted from AW3D (Advanced Land Observation Satellite (ALOS) World 3D), SRTM (Shuttle Radar Topography Mission), TanDEM-X (TerraSAR-X Add-On for Digital Elevation Measurements), and ASTER (Advanced Spaceborne Thermal Emission and Resolution) DSMs over Yangon City using a multi-directional processing and slope-dependent filtering technique to extract the DTMs. Ren et al. (Ren et al. 2020) extracted building height in Hongkong from AW3D30 using the block minimum filtering method to extract the DTM from AW3D30. Li et al. (Li et al. 2020) developed a method for obtaining the building height using Sentinel-1 data. These methods show promising results but have high computational complexity, especially if applied to extensive areas. Easily applicable methods using open-source data are insufficiently explored. This study developed a simpler method to detect height information using open-source satellite data.

In analyzing urban 3D structure, we noticed that the difference between AW3D30 and SRTM has some similarities with DCHM, although AW3D30 and SRTM are DSM data based on the measurement of the surfaces. AW3D30 was made by stereo image of a visible band (Takaku, Tadono, and Tsutsui 2014), while SRTM was made of interferometric radar data (Farr et al. 2007). Almost no study has examined the

possibility of obtaining the urban 3D structure from the difference between AW3D30 and SRTM. Only (Li et al. 2020) used those data as a comparison to the derived building height model in that study. Therefore, in this study, we explored in more detail the potential of deriving height information from both satellite data.

We defined "Satellite DCHM" as the value derived by subtracting SRTM from AW3D30. If we obtain the information on urban 3D structure from the difference between AW3D30 and SRTM, the method only needs a very small calculation load, and we can get the global urban 3D structure instantly for various research topics. Satellite DCHM can be derived using Google Earth Engine (Gorelick et al. 2017). On a related note, many studies related to LCZ classification are based only on Landsat data which do not have stereo pair images (Ferreira and Duarte 2019; Nurwanda and Honjo 2018), (Demuzere, Kittner, and Bechtel 2021). Considering the LCZ classification is based on the building height information, Satellite DCHM would be a useful tool to support the validation of the classification.

This study aims to develop and evaluate the simple method of obtaining the urban 3D structure derived from the Satellite DCHM in the center of the Tokyo Metropolitan Area. The derived model of Satellite DCHM was evaluated by the comparison with LiDAR DCHM, which is defined as the value by subtracting DTM from DSM made from airborne LiDAR point cloud data. LiDAR DCHM is considered a reference DCHM.

4.2 Methods

The summary of methods in this chapter is shown in Figure 12. The input data are AW3D30 and SRTM. Then, it is validated with data derived from airborne LiDAR. The output of building height model in this chapter is used in the next chapter.

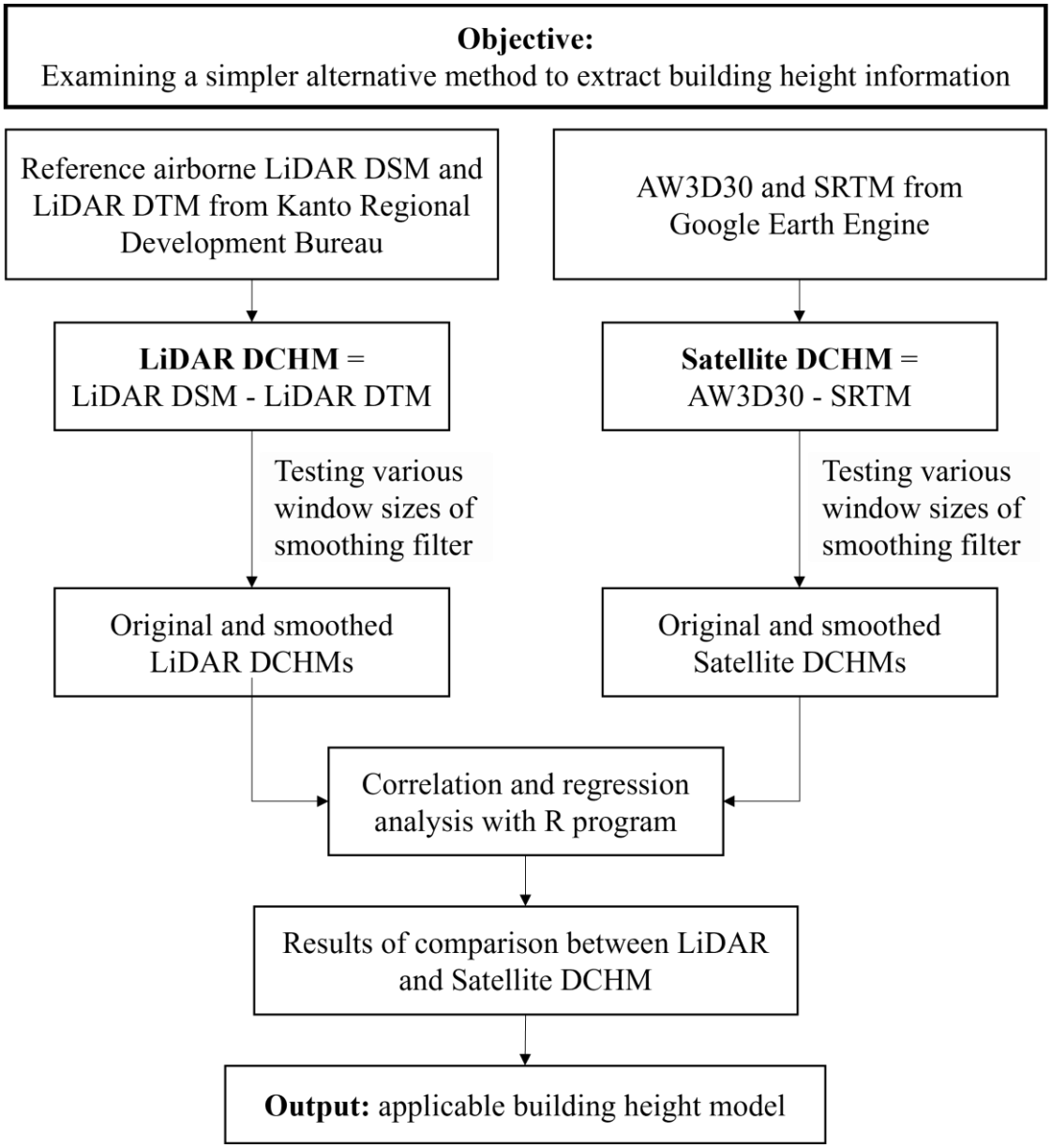

Figure 12. Methods overview

4.2.1 Study Area

The study area is the center part of Tokyo, the capital city of Japan. Reference data are crucial to examine the validity of the proposed method to derive building height. Considering the existence of numerous high-rise buildings and the availability of the reference data, Tokyo is selected as the study area.

The study area includes the Yamanote Line (a circular railway line in the center of the Tokyo Metropolitan Area) and Tokyo Bay in the southeast part of the area (Figure 13). It has a coverage of 20 km × 18 km. The majority of the area is covered by low-rise and mid-rise buildings. The high-rise building areas are concentrated inside and along the Yamanote Line and in the Tokyo Bay area. The categories of building height mentioned in this study follow the LCZ classification (Stewart and Oke 2012), where low-rise buildings range from 3 to 10 m, mid-rise buildings from 10 to 25 m, and high-rise buildings exceed 25 m.

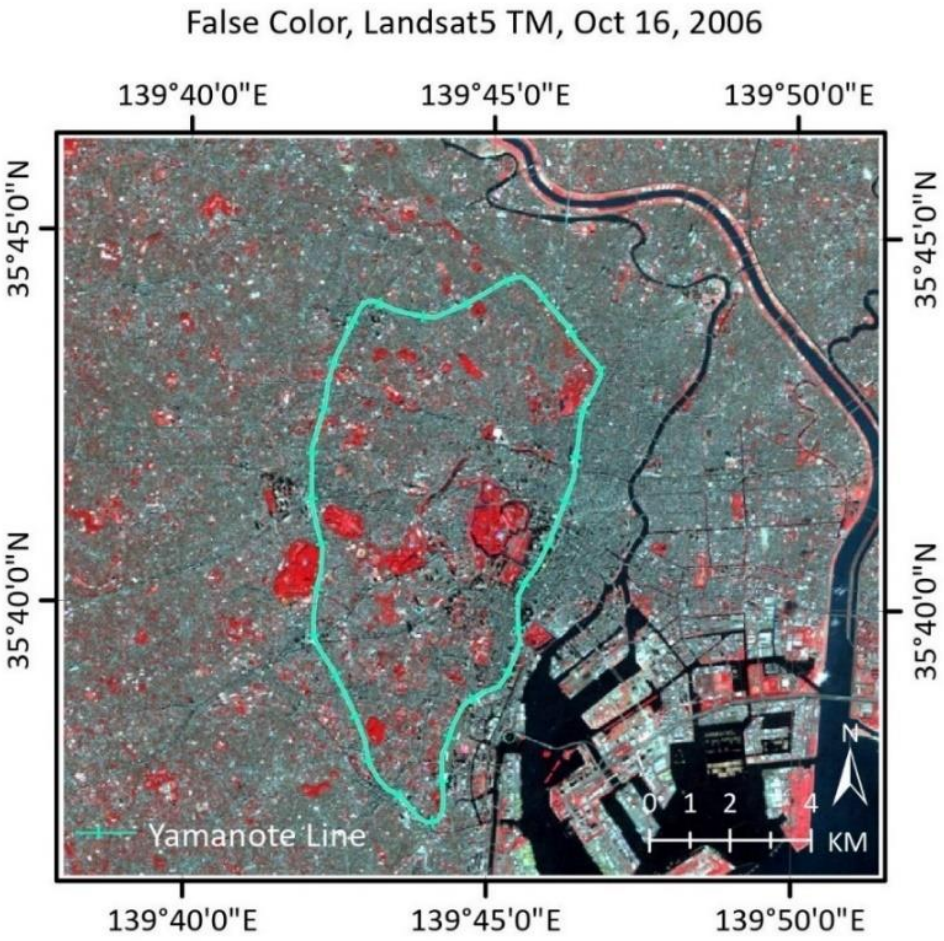

Figure 13. Study area

4.2.2 Used Data

The used data include the examined open satellite data, which are AW3D30 DSM (AW3D30) and SRTM DEM (SRTM), and the reference data, which are DSM and DTM derived from LiDAR (Table 9).

Table 9. Datasets for building height extraction

Name	Resolution	Acquisition Period	Source
Satellite data (examined)			
AW3D30	1 arcsec (≈30 m)	2006-2011	JAXA (open source), ver. 2.2
SRTM	1 arcsec (≈30 m)	2000	NASA (open source), ver. 3.0
Reference data			
LiDAR DSM	2 m	2006	Kanto Regional Development
LiDAR DTM	2 m	2006	Bureau (limited access)

AW3D30 DSM dataset was generated from stereo or triplet pair images acquired by the Panchromatic Remote-sensing Instrument for Stereo Mapping (PRISM) sensor aboard Advanced Land Observing Satellite (ALOS), operated by Japan Aerospace Exploration Agency (JAXA). Approximately 3 million scenes were acquired from 2006 to 2011 to create fine resolution DSM (5m resolution) and ortho-rectified image (2.5m resolution). The AW3D30 dataset was generated from the commercial AW3D 5 m mesh images, which was resampled to 30 m using the averaging method, where one pixel value on AW3D30 is calculated from an average value of 7 by 7 pixels on AW3D 5 m, except for masked out values (Tadono et al. 2016). The AW3D30 is reportedly to have height accuracy of 4.40m (root mean square error RMSE) globally (Tadono et al. 2016). Based on the landcover types, the RMSEs of AW3D30 range from 4.29m in built-up area to 6.75 m in dense vegetation area (J. R. Santillan and Makinano-Santillan 2016).

SRTM DSM data was produced from a joint project between NASA, the National Geospatial-Intelligence Agency, and the German and Italian Space Agencies. SRTM data was acquired in during 10-days of observation in 2000 using Synthetic Aperture Radar (SAR) (Farr et al. 2007). The SRTM 1 arc-second global dataset used in this research was resampled from an original resolution of 1 arcsecond (~30m) for US and 3 arcsecond (~90m) for regions outside the US (USGS 2020). The SRTM DSM has height accuracy of 9.73m (RMSE) globally (Mukul et al. 2017). Based on the landcover types, the RMSE ranges from 5.91m in built-up area to 10.42 m in bushland area (J. R. Santillan and Makinano-Santillan 2016). Both AW3D30 and SRTM data were downloaded from Google Earth Engine in 30 m-resolution.

For the reference data, we used DSM and DTM with 2 m-resolution acquired from airborne LiDAR point cloud data. The data were provided by the Kanto Regional Development Bureau and were measured in 2006. In this study, the reference data are referred to as LiDAR DSM and LiDAR DTM. They were used to produce LiDAR DCHM, the model representing the precise height of buildings and vegetation in the area. Both LiDAR DSM and DTM were resampled as 30 m-resolution to match the resolution of AWD3D30 and SRTM.

The LiDAR DSM, LiDAR DTM, and AW3D30 were made around the same period, while SRTM was made earlier. Building heights did not change dramatically in the analyzed area except for some urban development areas during this period. For this reason, we consider the produced LiDAR and Satellite DCHM are comparable. The data used in this study is shown in Figure 14.

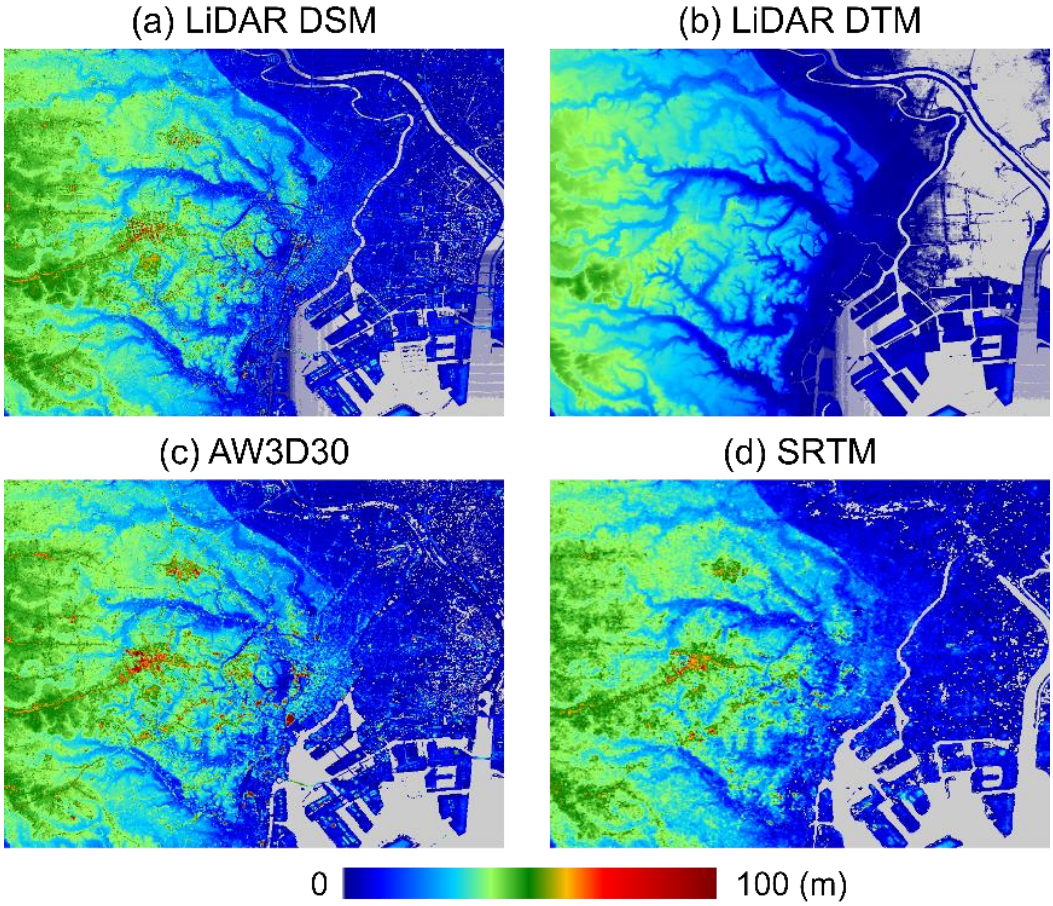

Figure 14. Data used for deriving building height with a simple method

The LiDAR DCHM is calculated following the Eq. (1), and Satellite DCHM is calculated following the Eq. (2). Theoretically, DCHM has positive values in the urban areas. In cases where the SRTM value is higher than AW3D30, the Satellite DCHM would result in a negative value. As it is unlikely to have negative values of building height in the field, the negative values of Satellite DCHM were set to 0.

$$LiDAR\ DCHM\ =\ LiDAR\ DSM\ -\ LiDAR\ DTM \quad (1)$$

$$Satellite\ DCHM\ =\ AW3D30\ -\ SRTM \quad (2)$$

Figure 15 compares the height values of LiDAR DSM, LiDAR DTM, AW3D30, and SRTM along an east-west cross-section (white horizontal line in Figure 15a). The values of DSM are higher than DTM, while the values of AW3D30 and SRTM overlap in some parts.

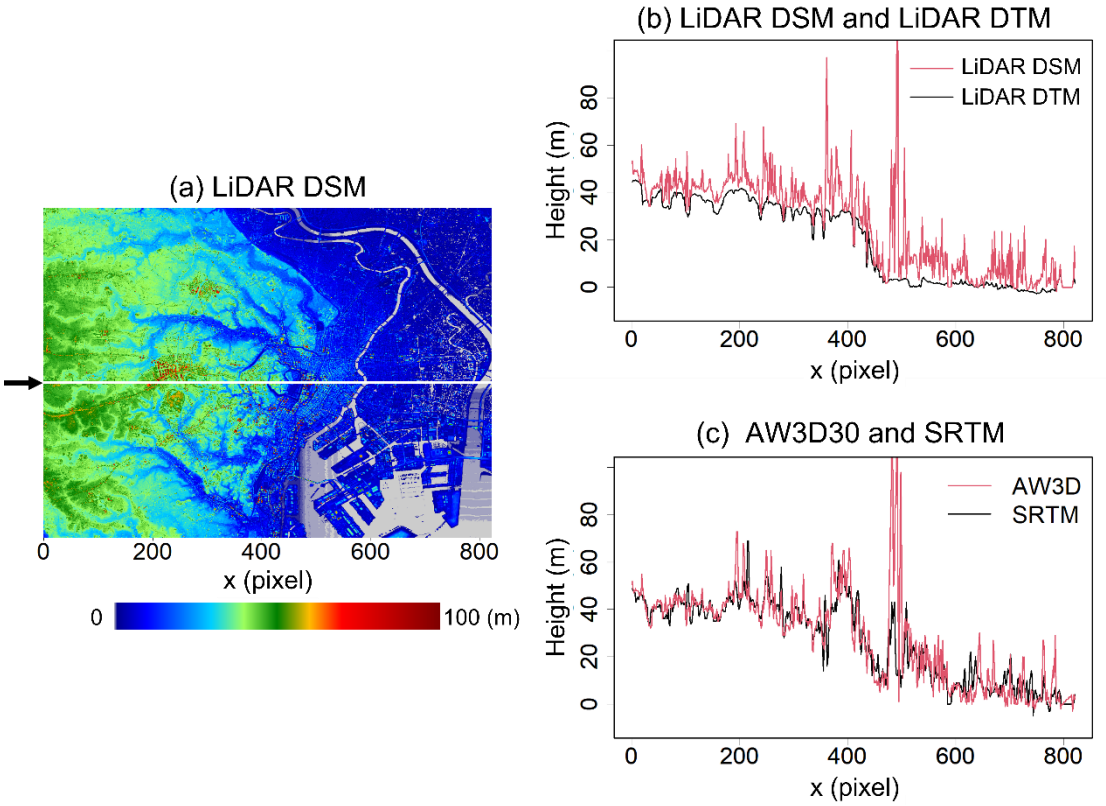

Figure 15. Cross-section comparison of LiDAR DSM, LiDAR DTM, AW3D30 and SRTM

4.2.3 Three-Dimensional Visualization

The 3D models are created for comparisons of Satellite DCHM and LiDAR DCHM, and for visualization of LST on DBHM. This method greatly helps when evaluating the spatial relationship between them. One-pixel shift significantly influences the value of correlation, but it does not affect the visual recognition of the 3D models. To visualize the 3D models, we used the RGL package, a 3D visualization system for R (Murdoch and Adler 2022). The 3D models are also created for LST and building height visualization.

In the case of LiDAR and Satellite DCHM comparison, the height was rendered as terrain, and colors in accordance with the height were mapped on the terrain. In the case of LST on DBHM visualization, the colors in accordance with LST were mapped on the

terrain. It provides a perspective view of the building height model for easier 3D recognition.

4.2.4 Evaluation of the Satellite DCHM

The result of Satellite DCHM was evaluated by comparing it with LiDAR DCHM. A direct pixel-by-pixel comparison is inappropriate to analyze the agreement of LiDAR and Satellite DCHMs because the exact coincidence of both locations between LiDAR and Satellite DCHM is not assured. To alleviate the error caused by a one-pixel difference in the location, we applied a smoothing filter to LiDAR and Satellite DCHM with an averaging window of which size is 2n+1 by 2n+1 pixels with *n* value ranges from 0 to 10 (0 means no smoothing). The smoothing process replaces each pixel's value with an average of its neighboring pixels without changing the pixel size. It is illustrated in Figure 16. The smoothing formula is shown in Eq. (5).

$$a'_{i,j} = \frac{\sum_{i=-n}^{n} \sum_{j=-n}^{n} a_{i,j}}{(2n+1)^2} \tag{5}$$

where a' is the output value, a is the original pixel value, i is the pixel number in x direction, j is the pixel number in y direction, and n is a number showing the window size. The value of n is changed from 0 to 10.

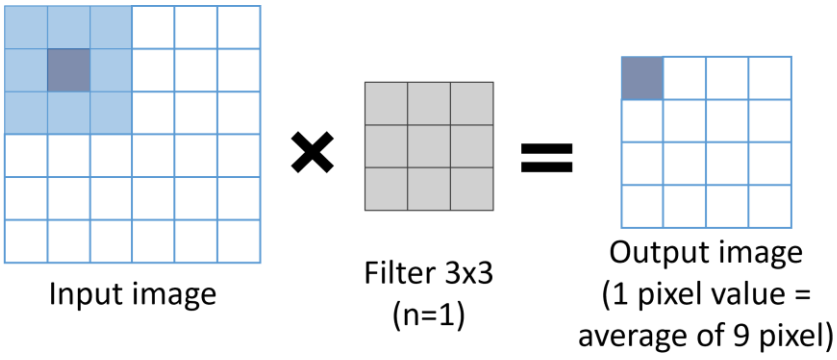

Figure 16. Illustration of smoothing filter application

We then apply Pearson correlation and regression analysis to measure the relationship between Satellite DCHM and LiDAR DCHM. The Pearson formula is expressed in Eq. (4), and the regression model is expressed in Eq. (6)

$$r = \frac{\sum(x_i - \bar{x})(y_i - \bar{y})}{\sqrt{\sum(x_i - \bar{x})(y_i - \bar{y})}} \quad (6)$$

where r is the correlation coefficient, x_i is the value of LiDAR DCHM, $\bar{x}$ is the mean value of the LiDAR DCHM, y_i is the value of Satellite DCHM, $\bar{y}$ is the mean value of Satellite DCHM, and i is the pixel number.

$$y = a \times x \quad (7)$$

where y is the Satellite DCHM, x is the LiDAR DCHM, and a is the slope line, the change rate in Satellite DCHM per unit change in LiDAR DCHM.

4.3 Results

4.3.1 Detected Information in Satellite DCHM and LiDAR DCHM

Figure 17 presents the comparison of LiDAR DCHM and Satellite DCHM. Generally, Satellite DCHM shows a lower value than LiDAR DCHM. There is similarity between the two, especially in the high-rise buildings. However, not all the buildings in LiDAR DCHM are clearly seen in the Satellite DCHM. Buildings along the roads, which are clearly seen in LiDAR DCHM, are less clear in Satellite DCHM. Bridges are well detected in both LiDAR and Satellite DCHM, but the highways are sometimes less visible in Satellite DCHM.

The height class distribution of LiDAR and Satellite DCHMs is shown in Table 10. A one-story building is assumed to have a minimum height of 3 m. Thus, a class lower than 3 m is not shown. For both DCHMs, the proportion of low-rise objects is the highest compared to the other classes. The ratio between the low classes in Satellite DCHM and

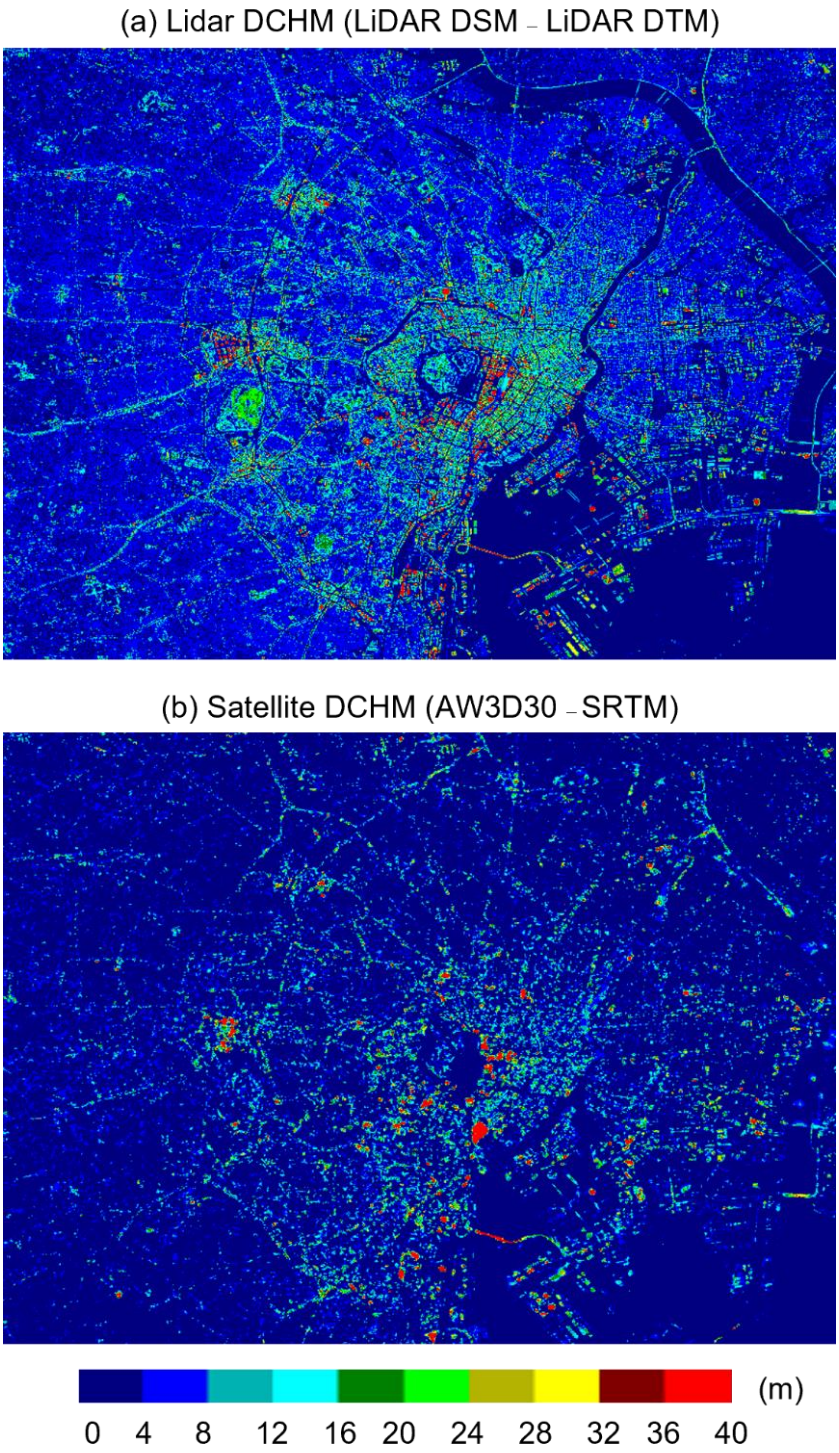

Figure 17. (a) LiDAR DCHM and (b) Satellite DCHM with a resolution of 30 m

LiDAR DCHM is closer to 3:1, but it is closer to 2:1 between the mid-rise and high-rise classes. Although the detection rate is not high, the information on the urban 3D structure can be obtained by the method in this study.

Table 10. Height class distribution of study area.

Height Class	LiDAR DCHM (%)	Satellite DCHM (%)	Ratio of DCHMs (LiDAR : Satellite)
Low-rise (3-10 m)	54.755	18.924	2.893 : 1
Mid-rise (10-25 m)	11.383	5.378	2.117 : 1
High-rise (>25 m)	1.884	0.985	1.913 : 1

Figure 18 shows the comparison of vegetation and the high-rise building area in LiDAR and Satellite DCHM. Imperial Palace is a large forest-like area surrounded by moats and contains some buildings. The red color areas in the Landsat 5 image of Figure 18a are vegetated. In LiDAR DCHM (Figure 18b), most trees are detected, while in Satellite DCHM (Figure 18c), many trees are missing. The high-rise building area in the east part of Imperial Palace (white rectangle in Figure 18) can be seen in both LiDAR and Satellite DCHM. The high-rise buildings in Satellite DCHM are well detected but seem more clumped, possibly due to the difference in sensor resolution between Satellite and LiDAR DCHM.

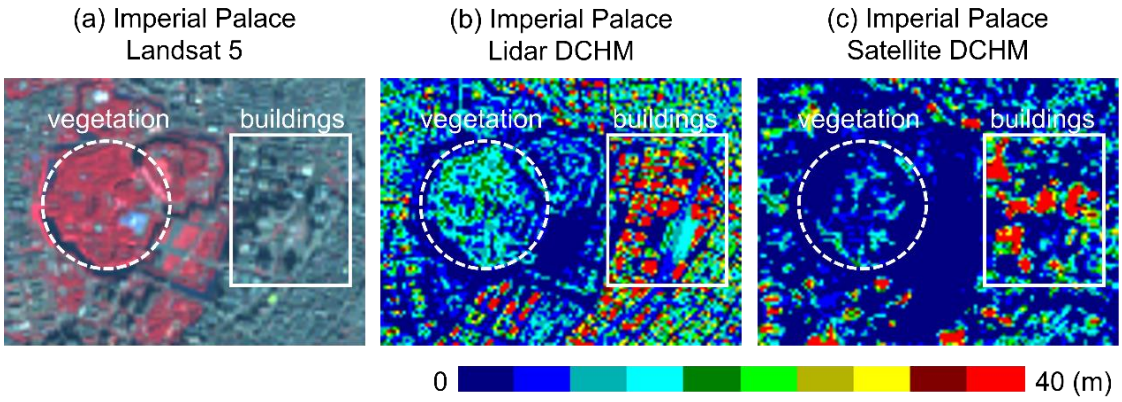

Figure 18. Comparison of Imperial Palace and the high-rise building area in (a) false color of Landsat 5, (b) LiDAR DCHM, and (c) Satellite DCHM.

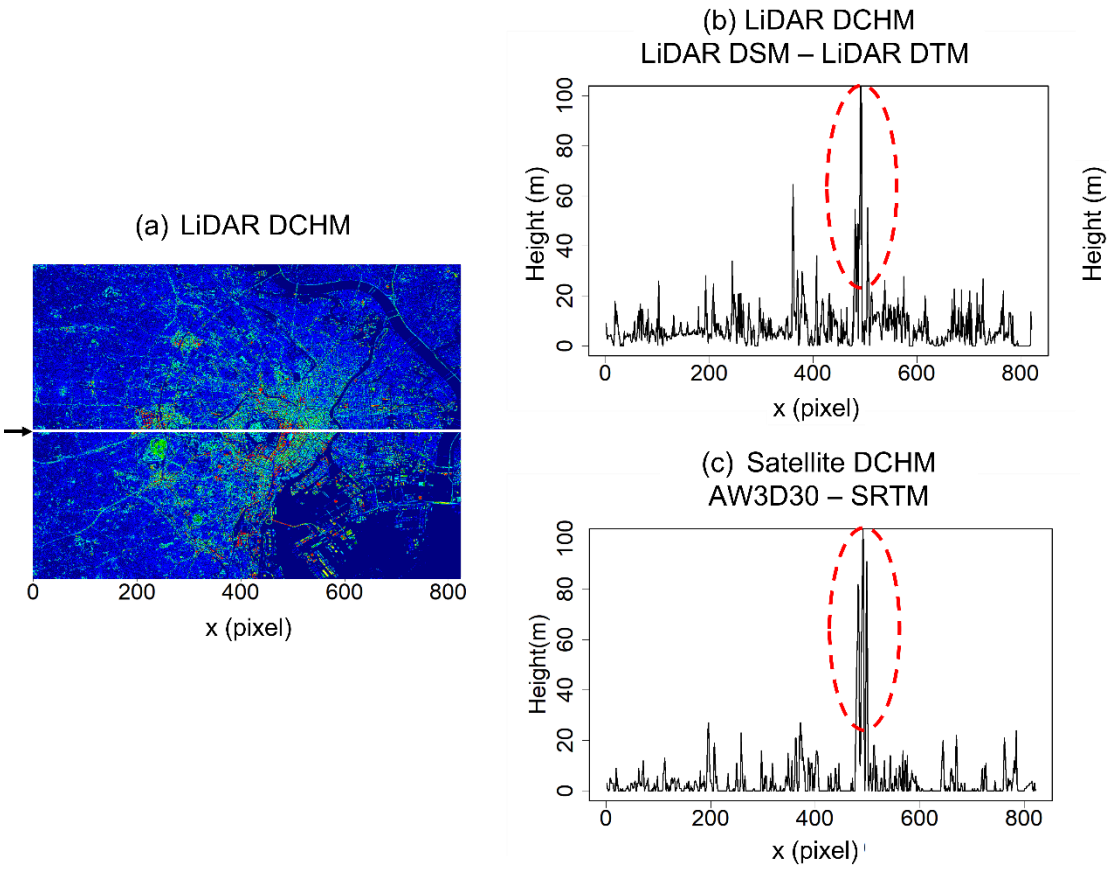

Figure 19. Cross-section comparison of LiDAR DCHM and Satellite DCHM

Figure 19 compared cross-section values of LiDAR DCHM and Satellite DCHM. In general, they show a similar pattern. Satellite DCHM mostly shows lower values than LiDAR DCHM. Consequently, low objects are not detected well in Satellite DCHM. There is a high part in both DCHMs (red circle), but in the other parts, the values are generally lower in Satellite DCHM.

4.3.2 Visualized 3D Model

The 3D version of LiDAR and Satellite DCHM shows the characteristics and similarities of both DCHMs (Figure 20). In the Satellite DCHM, the number of detected high buildings is smaller, but major high-rise building areas (Ikebukuro, Shinjuku, Otemachi, Shiodome, Shinagawa, and Osaki are well detected. Large vegetation areas,

such as Yoyogi Park and Imperial Palace, are not clearly detected in Satellite DCHM. The high buildings of Shiodome in LiDAR DCHM are shown as a massive high building in Satellite DCHM. Bridges like Arakawa Bridge and Rainbow Bridge are clearly seen in both DCHM.

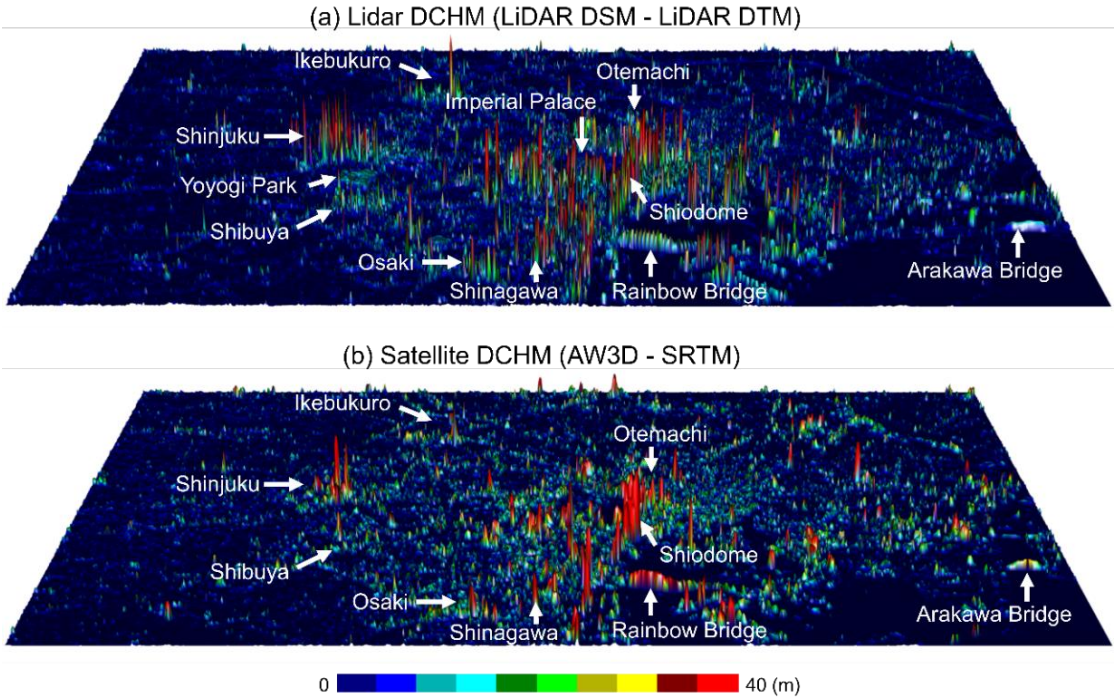

Figure 20. 3D visualization of LiDAR and Satellite DCHM

4.3.3 Comparison of Satellite DCHM and LiDAR DCHM

The correlation coefficient between LiDAR and Satellite DCHM was calculated with various smoothing window sizes ((2n+1)x(2n+1) pixel, from n = 0 to n = 10), and the result is shown in Figure 21. The correlation coefficient increases significantly from window size of 0 (no smoothing) to 3×3 pixel. The increase is slower as the n becomes bigger. The elbow point where the correlation change becomes slower is considered at a window size of 5×5 pixels.

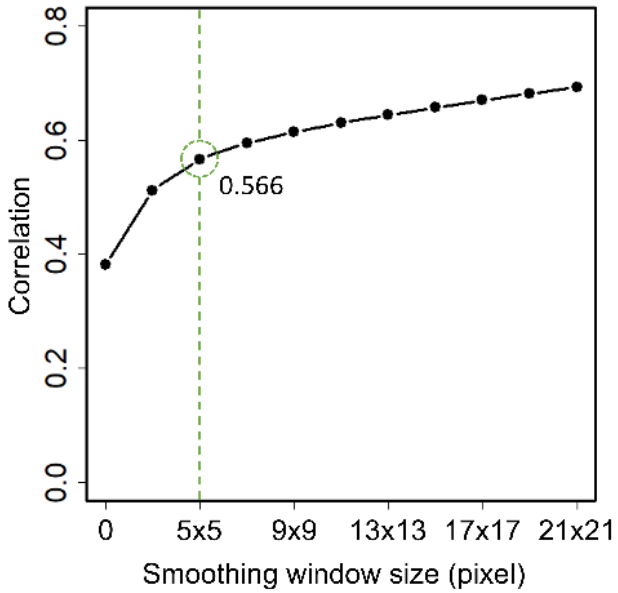

Figure 21. Correlation between LiDAR and Satellite DCHM in accordance with the smoothing window sizes (0 = no smoothing)

Relations between LiDAR and Satellite DCHM are shown in Figure 22. In the original resolution with no smoothing, the data are scattered, and it seems there is a weak correlation between Satellite and LiDAR DCHM despite their similarity in the visual comparison. After the smoothing filter is applied, the multiple R^2 values of the regression line in Figure 22 increases and the linear relationship between LiDAR and Satellite DCHM becomes clearer as the smoothing window size becomes bigger. As the result of the regression model, nearly all the values of Satellite DCHM are about half of LiDAR DCHM. In the Shiodome area, there are outliers where Satellite DCHM shows higher values than LiDAR DCHM (red marks in Figure 22**Error! Reference source not found.**).

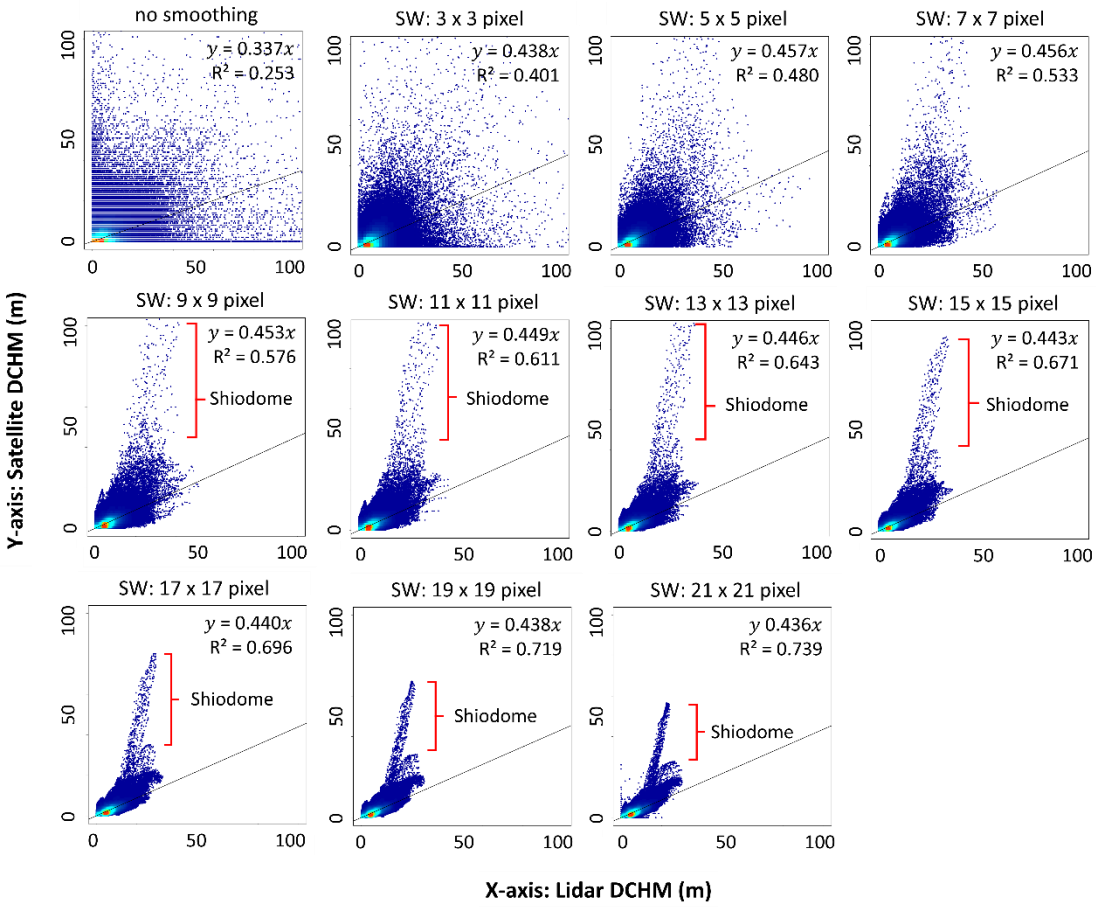

Figure 22. Relation between Satellite DCHM (Y-axis) and LiDAR DCHM (X-axis) in original value without smoothing and DCHM values after smoothing with increasing window size. The sizes of the smoothing window (SW) are (2n+1) by (2n+1) pixels with n = 0, 1, ..., 10.

As the elbow point of the correlation values belongs to a smoothing window size of 5x5, the smoothed images of the DCHMs of the window size are shown in Figure 23. The similarity of the high-rise building area in both LiDAR DCHM and Satellite DCHM can be recognized easier in the smoothed images. Satellite DCHM is suitable for detecting high-rise buildings, but not for low-rise buildings. If the color scale is shifted, the dark cyan of LiDAR DCHM corresponds well with the light blue area of Satellite DCHM.

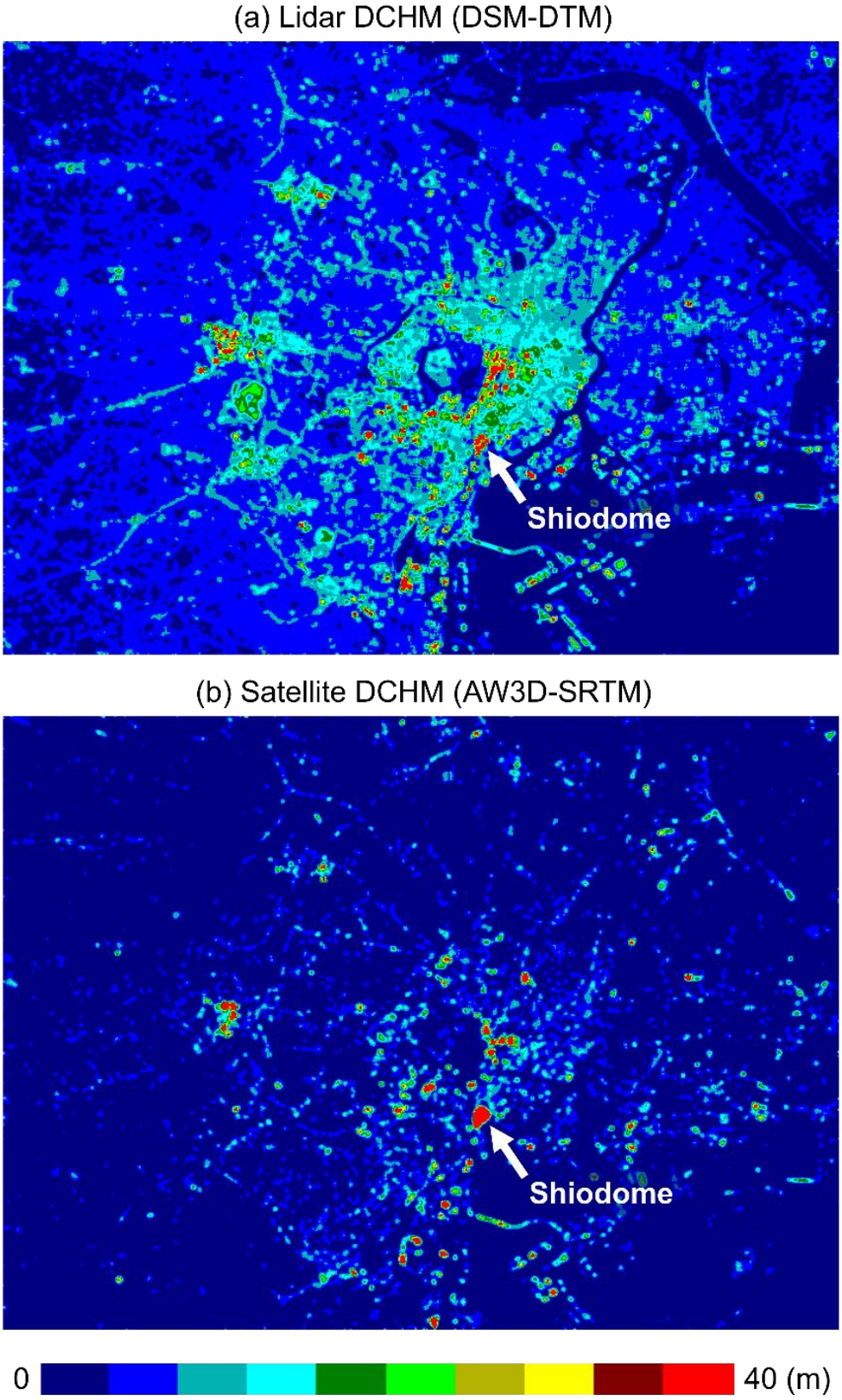

Figure 23. Comparison of smoothed (a) LiDAR DCHM and (b) satellite DCHM. The smoothing window size is 5x5 pixels.

4.4 Discussion

4.4.1 Similarity Between The Derived Urban 3D Model with The Reference

AW3D30 and SRTM measured the surface elevation of the earth, and both are categorized as DSM. However, based on the results of this study, the value difference between the two datasets detects building height. The possible reason why Satellite DCHM showed a similarity with LiDAR DCHM is that the building surface height can be well detected in AW3D30 but not in SRTM. AW3D30 and SRTM had different methods to calculate the surface elevation. AW3D30 was calculated using triplet stereo images (Takaku, Tadono, and Tsutsui 2014), while SRTM was measured by two interferometric radar images (Farr et al. 2007). The accuracy of different sensors could affect the derived values.

Table 11 presents the correlations between used datasets. When SRTM is compared to LiDAR DTM and LiDAR DSM, LiDAR DTM has a higher correlation. When AW3D30 is compared to LiDAR DTM and LiDAR DSM, LiDAR DSM has a higher correlation. Therefore, AW3D30 shows a more similar value to DSM, and SRTM shows relatively a more similar value to DTM. As a result, the value of subtracting SRTM from AW3D30 is similar to DCHM.

Table 11. Correlations matrix between used datasets

Dataset	LiDAR DTM	LiDAR DSM
SRTM	0.938	0.901
AW3D30	0.882	0.903

The results showed that vegetation is not well detected in Satellite DCHM. AW3D30 and SRTM can detect vegetation height well, and the difference is small. For that reason, the vegetation height cannot be obtained by subtracting SRTM from

AW3D30. Satellite DCHM can be considered as DBHM without vegetation height model. In urban morphological research, only the building height is often focused on, and the absence of vegetation height could be an advantage of Satellite DCHM.

4.4.2 Applicability and Limitation of Derived Urban 3D Structure Model

Through the results presented in this study, we showed that the Satellite DCHM has similar information to the LiDAR DCHM, except for vegetation height. The value is about half of the LiDAR DCHM based on the regression model. Information of some buildings is missing in the case of Satellite DCHM, which is a limitation of the method. But it is still possible to detect the urban 3D structure from Satellite DCHM.

The correlation between LiDAR and Satellite DCHM increases as the smoothing window size becomes bigger. The increase becomes less significant after surpassing 5x5 pixels (150x150 m) of a smoothing window. The urban 3D structure, i.e., dense urban areas and main roads are more recognizable in the smoothed image. Comparative analysis with 150 m resolution of Satellite DCHM with other spatial data like surface temperature would also be appropriate. Existing studies extracted building height information in relatively coarse grid sizes. i.e., 300 m (Ren et al. 2020), 500 m (Li et al. 2020). This 150 m resolution offers adequate information for applications in other fields, including the validation of LCZ classification.

The Satellite DCHM can be calculated in most urban areas in the world because both AW3D30 and SRTM are globally available. The simple calculation in deriving the Satellite DCHM is also an advantage. It can easily be calculated in Google Earth Engine and downloaded for applications. If the Satellite DCHM is calculated in the local environment of personal computers, the calculation load is very small.

4.4.3 Smoothing Filter in The Analysis

In this study, different window sizes of smoothing filter were applied, and the correlation value increases as the window size becomes bigger, or the image becomes smoother. This result indicates that the examined relationship is scale dependent (Rahimi, Barghjelveh, and Dong 2021). Similar tendency was found in the relationship between Satellite DCHM and LiDAR DCHM, and Satellite DBHM and LST. This is a common finding in other studies that examined the relationship between two factors at multi-scale as well. A study (Song et al. 2014) analyzed the correlation between LST and urban patterns and the correlation increased as the pixel size increases, they stated that 660 m and 720 m were the most suitable spatial resolution to measure the relationship between LST and landscape. Another study (Lu et al. 2020) analyzed the correlation between NDVI and LST with a pixel size of 210 to 240 m and stated that the increasing correlation as the increasing pixel size indicates that there is a threshold distance for the cooling effect of green spaces.

The increasing correlation as the pixel size becomes bigger (coarser resolution) or the smoothing window size becomes bigger (smoother image) can be observed in multi-scale analysis. The benefit of applying various smoothing window sizes is to provide a wider view to look at the same phenomenon. Each window size is looking at the same phenomenon at a different scale, which is an advantage since most studies examine the relationship at a single scale. The Satellite DCHM, LiDAR DCHM, and LST are all collected from different sensors with different scales. Although the coordinate is matched, each image may not be perfectly aligned spatially to one another. Smoothing is useful for constructing spatially correlated images.

4.5 Chapter Summary

This study evaluated the simple method of obtaining urban 3D structure derived from subtracting SRTM from AW3D30, Satellite DCHM, by comparing it with LiDAR DCHM made from high-resolution LiDAR measurement in the center of the Tokyo Metropolitan Area. Satellite DCHM generally has a lower value than LiDAR DCHM, but Satellite DCHM visually shows good similarity with LiDAR DCHM, and it helps to understand the urban 3D structure. Satellite DCHM shows better performance in detecting mid-rise and high-rise buildings than low-rise buildings. The similarity is presented better in the 3D visualization and the smoothed images. The linear relationship between LiDAR and Satellite DCHM becomes clear as the smoothing window size increases. About 150 meters of a smoothing window would be appropriate for comparative urban analysis. Considering the availability and its simple calculation, using the Satellite DCHM is an effective alternative method when the precise LiDAR DCHM cannot be obtained due to economic or technical reasons.

The analysis is executed only in the limited area in this study. It is necessary to validate the applicability of the Satellite DCHM in other regions in the world in further research.

CHAPTER 5: Relationship Between Building Height & Land Surface Temperature

5.1 Introduction

Urban development, particularly the modification of land surfaces, is known to be the main cause of UHI effect. Large cities worldwide have always been dealing with UHI issues (Peng et al. 2012) and how to mitigate it. To accommodate the ever-increasing population in the city, many developers build high-rise complexes and promote a compact city where people live, work, and recreate in a confined space. One of the concerns that comes with high-rise development is how it further affects the existing UHI issue.

Some studies found that high-rise buildings tend to increase LST because of high anthropogenic heat (Guo et al. 2016; Rahman et al. 2020) and extensive impervious surface (Cai et al. 2018). Meanwhile, other studies found that high-rise buildings tend to decreases LST because of large building shadows (Nichol 1996), reflective surface materials (Honjo et al. 2017), vegetation cover near the building (Zheng et al. 2019), and wind flow around the building (Wang and Xu 2021). More studies are needed to address these contradictive findings. Additionally, existing studies mostly only analyze a small region, such as one city, due to the limitation of available building height data.

For a general observation, six global cities including Tokyo, Beijing, Jakarta, Los Angeles, New York, and Chicago are selected. These cities have many high-rise buildings in the center part of the city and are major cities in different countries or states. For a closer observation, Tokyo and Jakarta are selected. Tokyo is the most populated city in the world with a population of about 37 million people (United Nations, Department of Economic and Social Affairs 2018). Jakarta has a population of about

over 10 million people in 2017, making it the largest megacity in Southeast Asia (Wandira and Jongwook 2017).

Tokyo and Jakarta have many high-rise building clusters formed in the center part of the city. In terms of climate, Tokyo is located in subtropical zone, while Jakarta is in tropical rainforest zone (Kottek et al. 2006; Richards et al. 2019). The importance of both large metropolitan cities, the existence of high-rise clusters with different level of high-rise development, along with contrasting climate condition, make these two cities intriguing to be investigated deeper.

In the general observation, we use LST from Landsat 8 that are more recent. In the closer observation, we use LST of Landsat 5 which acquisition period coincides with the acquisition period of AW3D30. We also sample areas of different height classes to observe the impact of building height more closely, which was not done in the existing study.

The objective of this chapter is to analyze the relationship between LST and building height, and to clarify whether high-rise buildings tend to increase or decrease LST. In order to achieve this, six urban areas in cities around the world were analyzed as study cases. As there are no airborne LiDAR data in these areas, we introduced the application of DBHM derived in the Chapter 4 in this analysis.

5.2 Methods

The method summary is shown in Figure 24. The main data inputs are building height model derived in the previous chapter and the land surface temperature images from Landsat. Normalized Difference Vegetation Index (NDVI) and Normalized Difference Water Index (NDWI) are also collected remove the vegetation and water coverages. More details are explained in the later subsections.

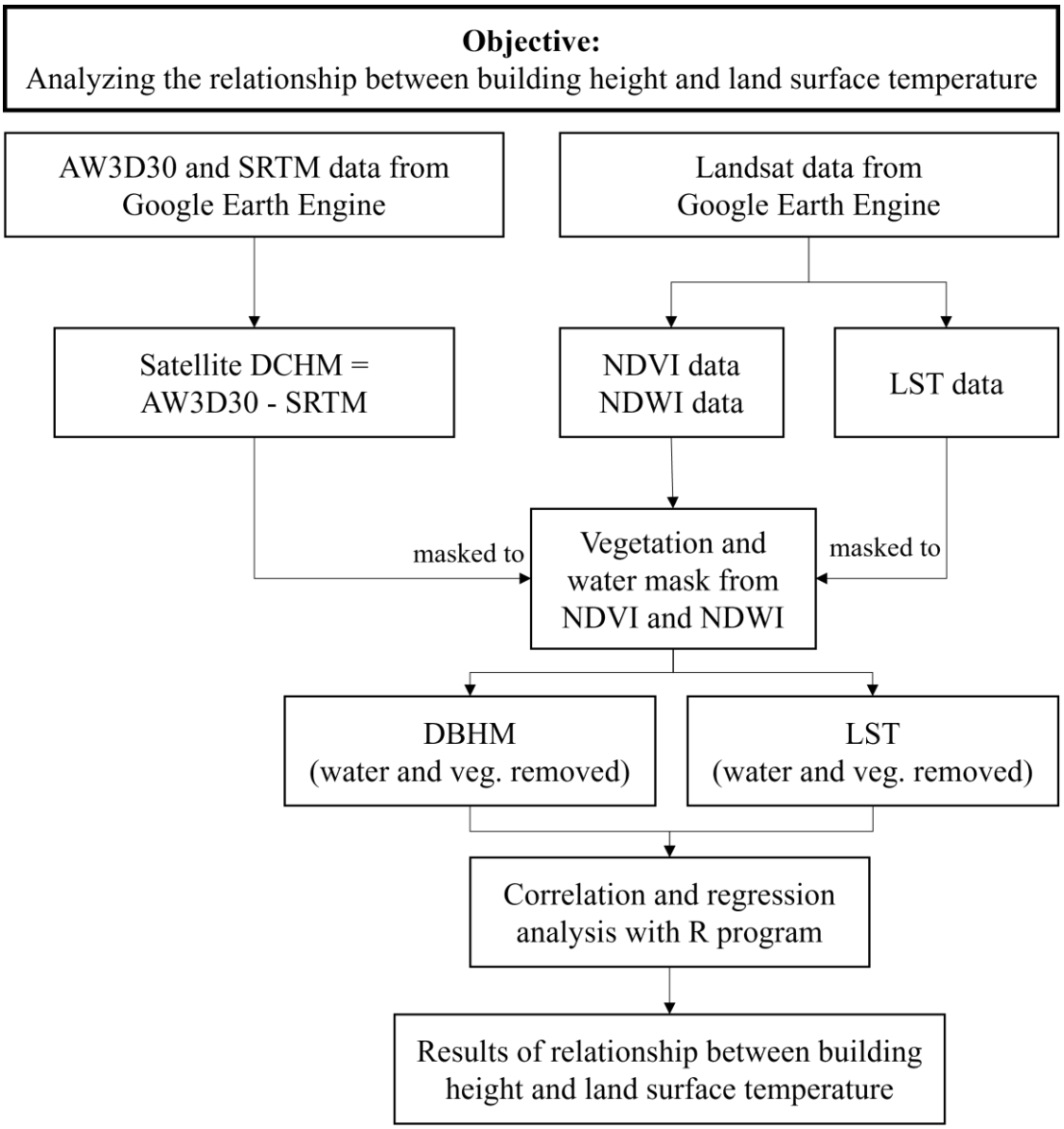

Figure 24. Methods overview

5.2.1 Study Areas

The study area consists of six urban areas, Tokyo, Beijing, Jakarta, Los Angeles, New York, and Chicago (Figure 25). The center coordinates are shown in Table 12. The areas were selected by considering the number of high buildings, the availability of cloud-free images, and the climatic conditions. Each urban area has a coverage size of 0.1 × 0.1 degrees in longitude and latitude.

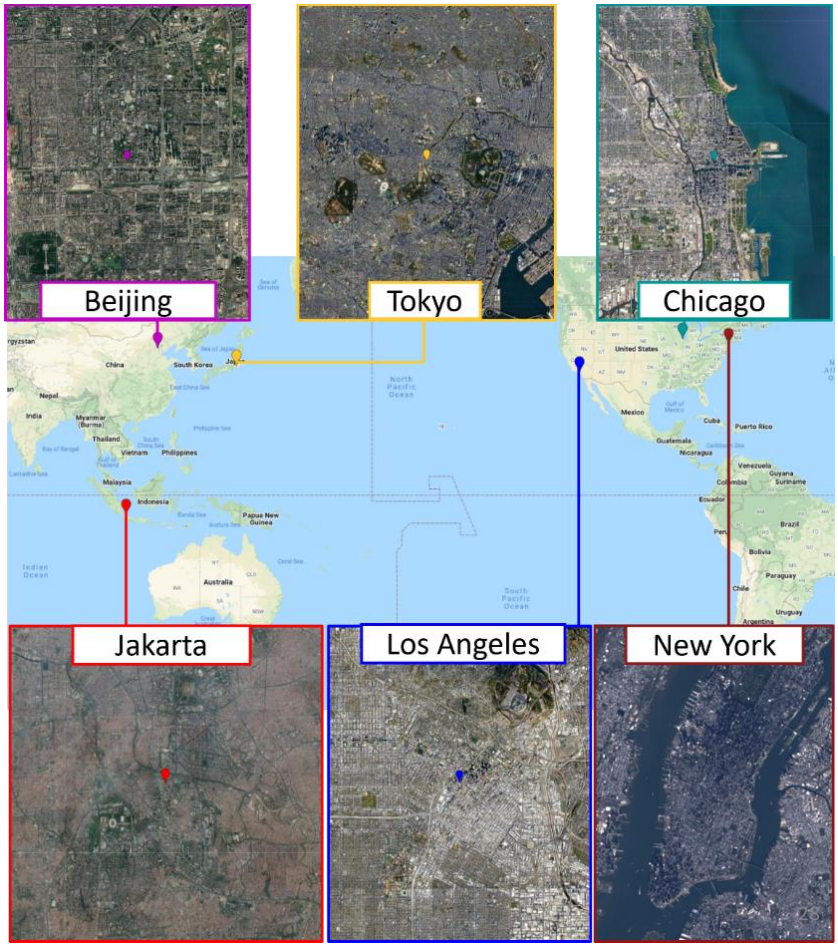

Figure 25. Study areas

Table 12. Study area's center point coordinates

Area	Center Point	
	Longitude	**Latitude**
Tokyo	139.7313	35.6857
Beijing	116.4407	39.9092
Jakarta	106.8196	-6.2058
Los Angeles	-118.2627	34.0480
New York	-73.9836	40.7591
Chicago	-87.6301	41.8897

According to Köppen-Geiger's climate classification (Kottek et al. 2006; Richards et al. 2019), Tokyo and New York belong to the same climate zone, Cfa, which is warm

temperate (subtropical), fully humid, and hot summer. Los Angeles belongs to Csa, which is warm temperate with dry and hot summer. Beijing belongs to Dwa (warm continental zone with dry winter and hot summer), and Chicago belongs to Dfa (warm continental zone with fully humid and hot summer). Jakarta is classified as Af or tropical rainforest zone.

5.2.2 Building Height Data

The same two open access datasets as Chapter 4 are used to extract the building height information, AW3D30 and SRTM (Table 13). We generate the building height by subtracting SRTM from AW3D30, as the formula shown in Equation (1). Figure 26 shows the DBHM result calculated from Equation (1).

$$Digital\ Building\ Height\ Model\ (DBHM) = AW3D30 - SRTM \quad (1)$$

Table 13. Datasets for building height extraction

Name	Band	Resolution	Acquisition Period	Version
AW3D30	AVE_DSM	1 arcsec (≈30 m)	2006-2011	Ver. 2.2, April 2019
SRTM	elevation	1 arcsec (≈30 m)	2000	Ver. 3, 2007

There are very few studies that regard the difference between AW3D30 and SRTM as building height. Li et al. (Li et al. 2020) used the building height obtained from AW3D30 and SRTM (defined as DBHM in this study) as a comparison to building height obtained from Sentinel-1 data. That study found that DBHM has a correlation value of 0.60 with the reference height data at 500 m resolution (Li et al. 2020). Honjo et al. (Honjo et al. 2022) applied moving averaging filters at DBHM then examined the correlation of DBHM with LiDAR data at multiple filter window sizes and found that the correlation increases as the DBHM becomes smoother (coarser resolution). Visually,

DBHM showed a good agreement with LiDAR data even before averaging, but the optimum correlation with LiDAR data was found after applying averaging filter of 5x5 pixels (150 x 150 m), which was 0.566 (Honjo et al. 2022). Considering the similarity of DBHM and reference building height data presented in existing studies, DBHM is used in this analysis. The AW3D30 and SRTM data of the defined study area are downloaded from Google Earth Engine (GEE) (Gorelick et al. 2017).

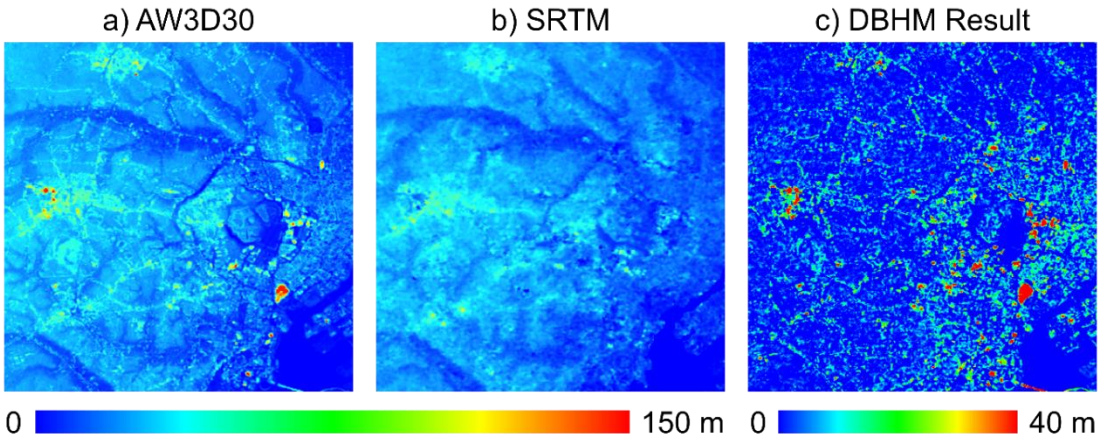

Figure 26. (a) AW3D30, (b) SRTM, and (c) DBHM result of Tokyo

5.2.3 Land Surface Temperature Data

For this chapter, the data used are the building height model derived from the results of the previous chapter (Satellite DCHM), and LST data derived from Landsat. The LST data used for analysis are composites of several cloud-free Landsat 8 data (Band 10 – Thermal Infrared 1) (Vermote et al. 2016) of the same scene for each urban area. We sort available Landsat data by their cloud coverage in GEE and pick the clearest dates. The Landsat data's digital numbers are converted to brightness temperature using the GEE algorithm, and then the converted value is subtracted by 273.15 to change the value from Kelvin to Celsius.

The data used to create the LST maps are presented in Table 14. The LST dates are in the warm season (from March to October) because the surface temperature difference

between land cover types is more apparent than in cool season. Composite LST was created to avoid the anomaly of single LST data. Considering the area with the fewest cloud-free images, the number of images to create each composite LST is six. The data were exported as GeoTIFF (Tag Image File) format from GEE and then the mean values of the six images were calculated into a new composite image.

Table 14. Landsat 8 data

Area / Time*	**Dates used (March –Oct)**
Tokyo 10:15	2013/09/17, 2014/05/31, 2015/03/31, 2015/10/09, 2017/03/20, 2018/10/01
Beijing 10:55	2013/10/03, 2014/09/04, 2017/05/07, 2017/07/10, 2017/09/12, 2017/09/28
Jakarta 10:00	2019/09/11, 2018/07/06, 2019/07/25, 2014/09/13, 2020/04/22, 2015/08/31
Los Angeles 10:30	2016/09/26, 2018/08/31, 2019/07/01, 2014/06/01, 2018/09/16, 2015/06/20,
New York 10:40	2017/07/30, 2013/06/01, 2016/06/09, 2015/06/07, 2017/06/12, 2014/07/06
Chicago 10:30	2014/09/23, 2014/07/21, 2017/09/15, 2020/07/05, 2014/05/18, 2016/05/23

*) local acquisition time of the satellite image. The time may differ slightly (less than 5 minutes).

Analysis using Landsat 5 data is also done for Jakarta and Tokyo to test if the tendency can also be observed in different period. Composites of Landsat-5 Thematic Mapper (TM) images courtesy of the U.S. Geological Survey in the period of 2006 to 2011 were used. This period is the same as the operational period of AW3D30. Author would like to see if there is a different tendency. The images were sorted by the clearest

cloud coverage, six images were picked for Tokyo and five images for Jakarta, due to fewer clear days in Jakarta. Jakarta is often cloudy, only fewer images could be chosen. The image dates used to create the LST maps are presented in Table 15. The selected dates fall within April and October since it is warm season in both cities, thus the surface temperature between different land cover types is more distinguishable.

Table 15. Landsat 5 data

Area	Dates (March to October)
Tokyo Time: Around 10:15	2006/10/16, 2007/05/12, 2008/10/21, 2010/10/11, 2011/04/05, 2011/07/10
Jakarta Time: Around 10:00	2006/05/18, 2006/06/19, 2006/08/06, 2007/09/26, 2009/07/29

5.2.4 Vegetation and Water Coverage Removal

Vegetation and water coverage removal is done only in the analysis of relationship between building height and LST to minimize the bias in the value of LST. Vegetation and water coverages were removed using masks from binarized images of Normalized Difference Vegetation Index (NDVI) and Normalized Difference Water Index (NDWI), respectively. The thresholds were decided for each area by comparing the binarized NDVI and NDWI images with Google Earth image. Mostly, the threshold is 0.4 for NDVI and 0.1 for NDWI. To make the precise masks, manual corrections were also made in the final step. The images used for creating mean composite NDVI and NDWI are from the same dates used for LST. The two masks were then combined to create the complete vegetation and water mask. The process is illustrated in Figure 27.

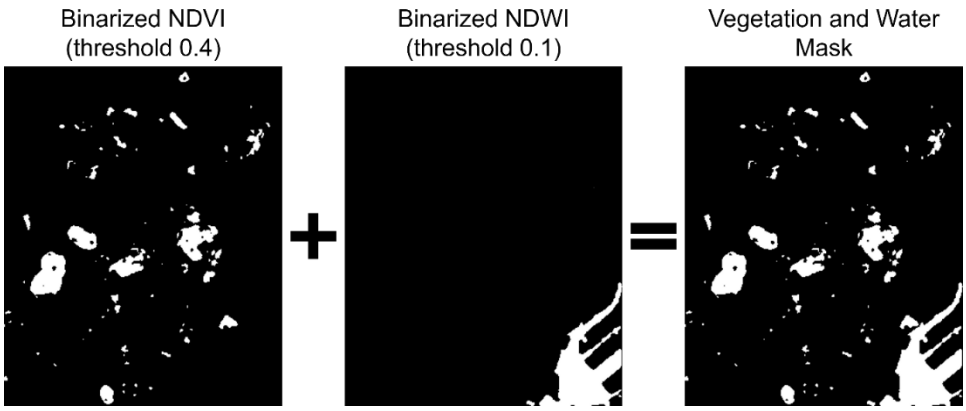

Figure 27. The creation of vegetation and water mask in the case of Tokyo

The following formulas were used to calculate the NDVI and NDWI (McFeeters 1996) values.

$$\mathrm{NDVI} = \frac{\mathrm{NIR} - \mathrm{Red}}{\mathrm{NIR} + \mathrm{Red}} \qquad (1)$$

$$\mathrm{NDWI} = \frac{\mathrm{Green} - \mathrm{NIR}}{\mathrm{Green} + \mathrm{NIR}} \qquad (2)$$

where NIR (Near-Infrared reflectance) is Band 5 for Landsat 8 and Band 4 for Landsat 5, Red (top of atmosphere (TOA) red light reflectance) is Band 4 for Landsat 8 and Band 3 for Landsat 5, and Green (TOA green light reflectance) is Band 3 for Landsat 8 and Band 2 for Landsat 5.

5.2.5 Statistical Analysis

After retrieving the LST maps and DBHM maps, the relation of both factors in each city was examined with Pearson's correlation and regression analysis. The Pearson's correlation coefficient is calculated following the equation:

$$r = \frac{\sum(x_i - \bar{x})(y_i - \bar{y})}{\sqrt{\sum(x_i - \bar{x})(y_i - \bar{y})}} \qquad (8)$$

where r is the correlation coefficient, x_i is the value of the DBHM, $\bar{x}$ is the mean value of the DBHM, y_i is the value of the LST, $\bar{y}$ is the mean of the values of the LST, and i is the pixel number.

The regression model is following the equation:

$$Y = a + bX \qquad (9)$$

where a is the intercept, the value of when $X = 0$, and b is the slope of the line, the change rate in Y per unit change in X. In this study, Y is the LST, and X is the DBHM.

5.3 Results

5.3.1 LST and DBHM Comparison

In the following part of the study of relationship between building height and LST, the vegetation and water coverage are removed from the DCHM, therefore the building height model is referred as DBHM. Figure 28 shows the comparison of LST and DBHM in Tokyo. The 3D visualization shows the mapped LST on the 3D DBHM model. The grey color is the masked vegetation and water area, the same area as the white color in the 2D visualization.

From general visual observation, the low LST area corresponds well with the high DBHM area in Tokyo (Figure 28). The right part of the image (Circle A) noticeably has quite a large high buildings area with low temperature. In the middle of the high building's area, there is a removed white part, Imperial Palace, covered by vegetation and surrounded by a water canal. There is also the Marunouchi business district that has many high buildings. At the lower part of Circle A, there are Shiodome and Shibaura districts. Shiodome and Shibaura are business districts near Tokyo Bay with many high-rise hotels and office towers. On the left part of the Tokyo map, there are also noticeable low LST areas with high DBHM, Shinjuku (Circle B), Ikebukuro (Circle C), and Shibuya (Circle D).

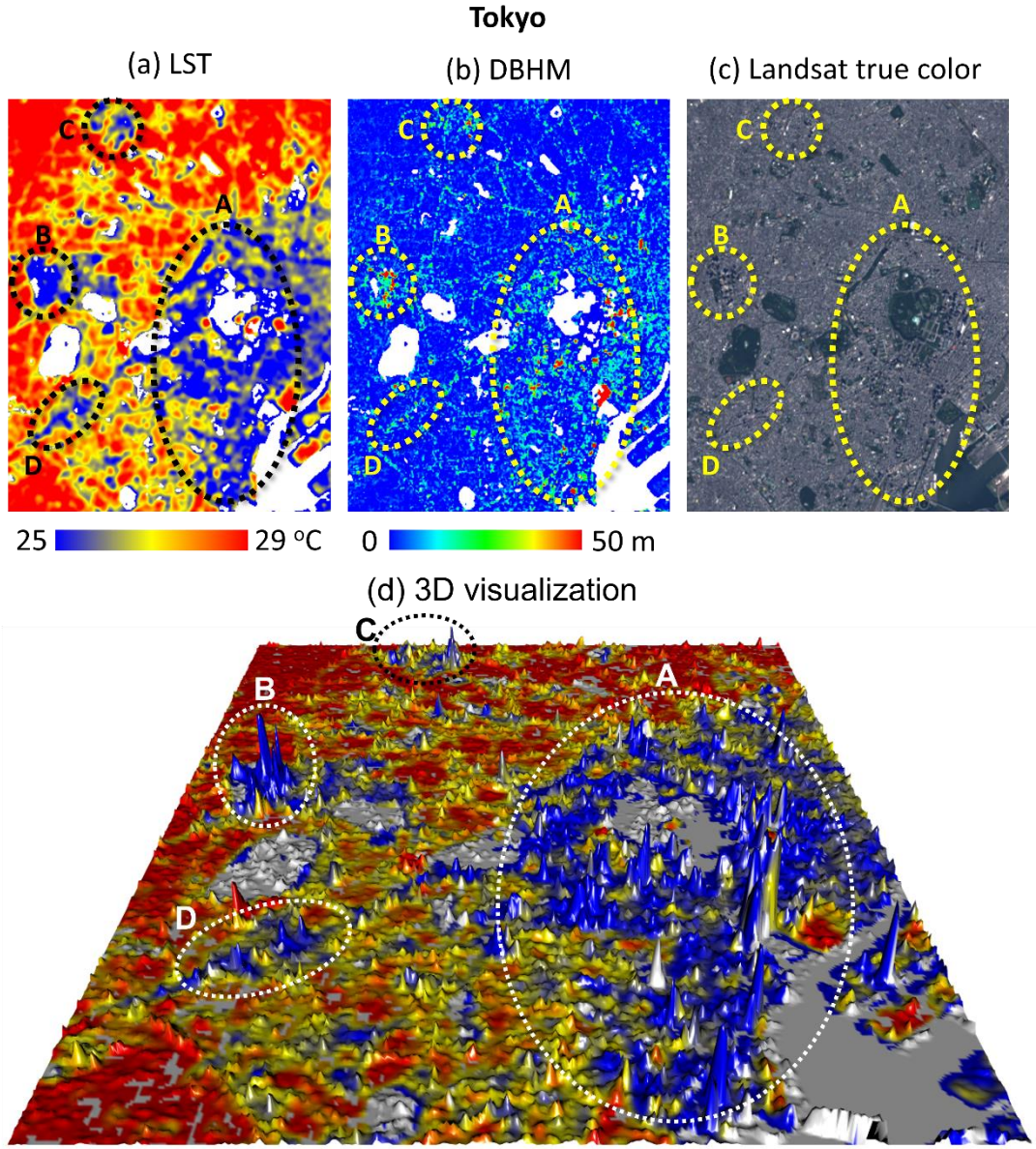

Figure 28. (a) Land Surface Temperature, (b) Digital Building Height Model, (c) Landsat true color, and (d) 3D visualization of Tokyo

In Beijing (Figure 29), there are numerous low LST areas with high DBHM. Circle E is Dongzhimen area, part of Dongcheng Districts that has many high buildings. The high DBHM area inside Circle E is the buildings built along the East 2nd Ring Road, the innermost ring road highway that encircles Beijing's city center. The largest and the most apparent low LST area is Jianguomen Outside area (Circle F). There are many

high buildings in this area, including Beijing World Financial Center, The China World Trade Center I, and Beijing Yintai Centre Tower 2. In the south part of the area (Circle G), there are Beijing's central business district (CBD) and Jinsong area.

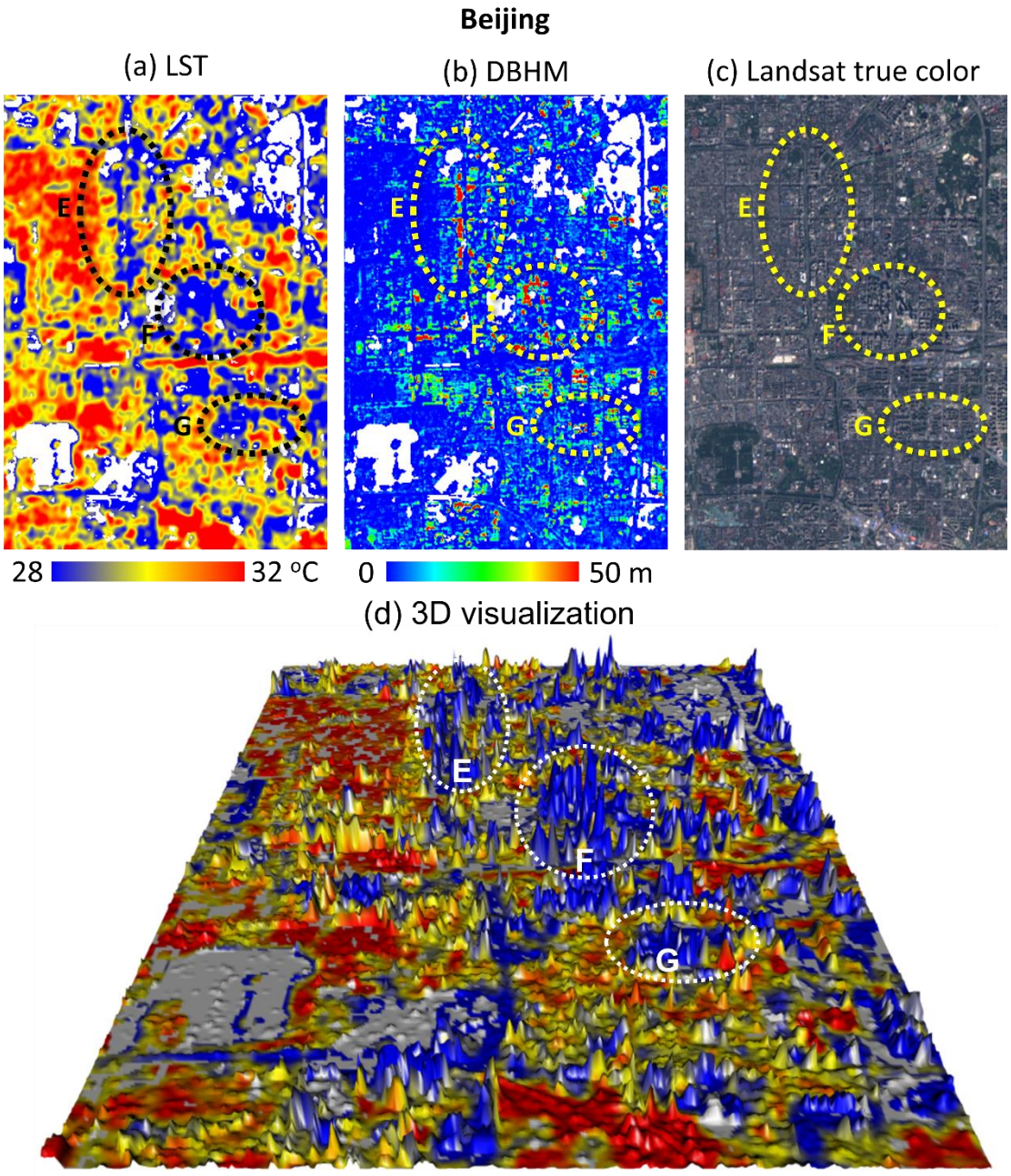

Figure 29. (a) Land Surface Temperature, (b) Digital Building Height Model, (c) Landsat true color, and (d) 3D visualization of Beijing

In Jakarta, the high buildings complexes and the areas of the low building are clearly detected and separated from each other (Figure 30). The high building areas obviously have lower LST compared to the low buildings. There are several high building complexes with low LST, such as Central Park mixed-use buildings complex (Circle H), The Bellezza Shopping Arcade and Sommerset Berlian Hotel in Permata Hijau area (Circle I), and Pakubuwono apartment complex (Circle J). Larger business districts, such as Senayan (Circle K), Sudirman (Circle L), and Kuningan (Circle M), form broad low LST coverages in their respective areas.

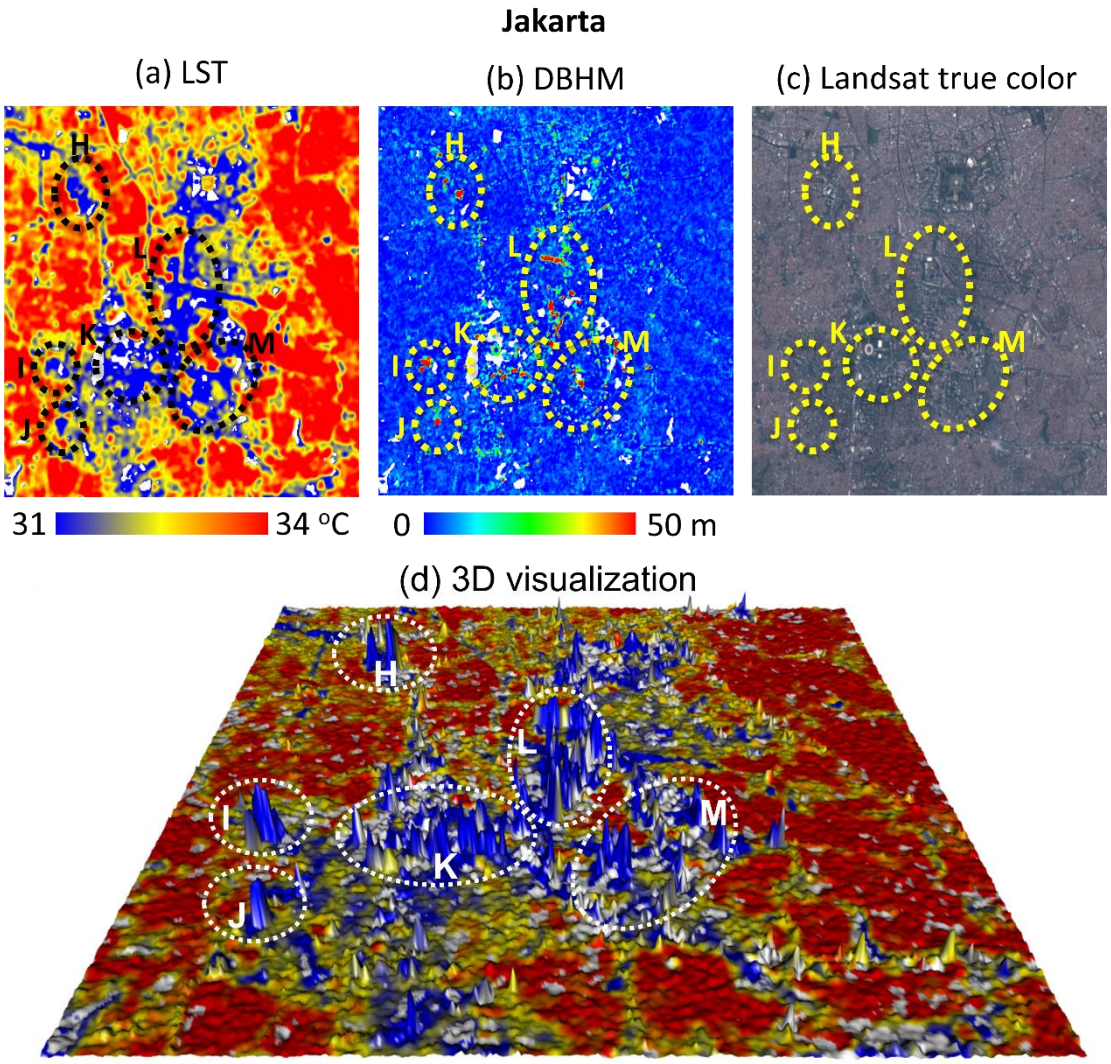

Figure 30. (a) Land Surface Temperature, (b) Digital Building Height Model, (c) Landsat true color, and (d) 3D visualization of Jakarta

In Los Angeles, there are several low LST areas visible (Figure 31). The area labeled with Circle N is Wilshire Center, with high-rise apartment buildings, hotels, commercial and office buildings. The largest low LST area is Circle O, the Downtown Los Angeles, including Financial District with many high-rise buildings.

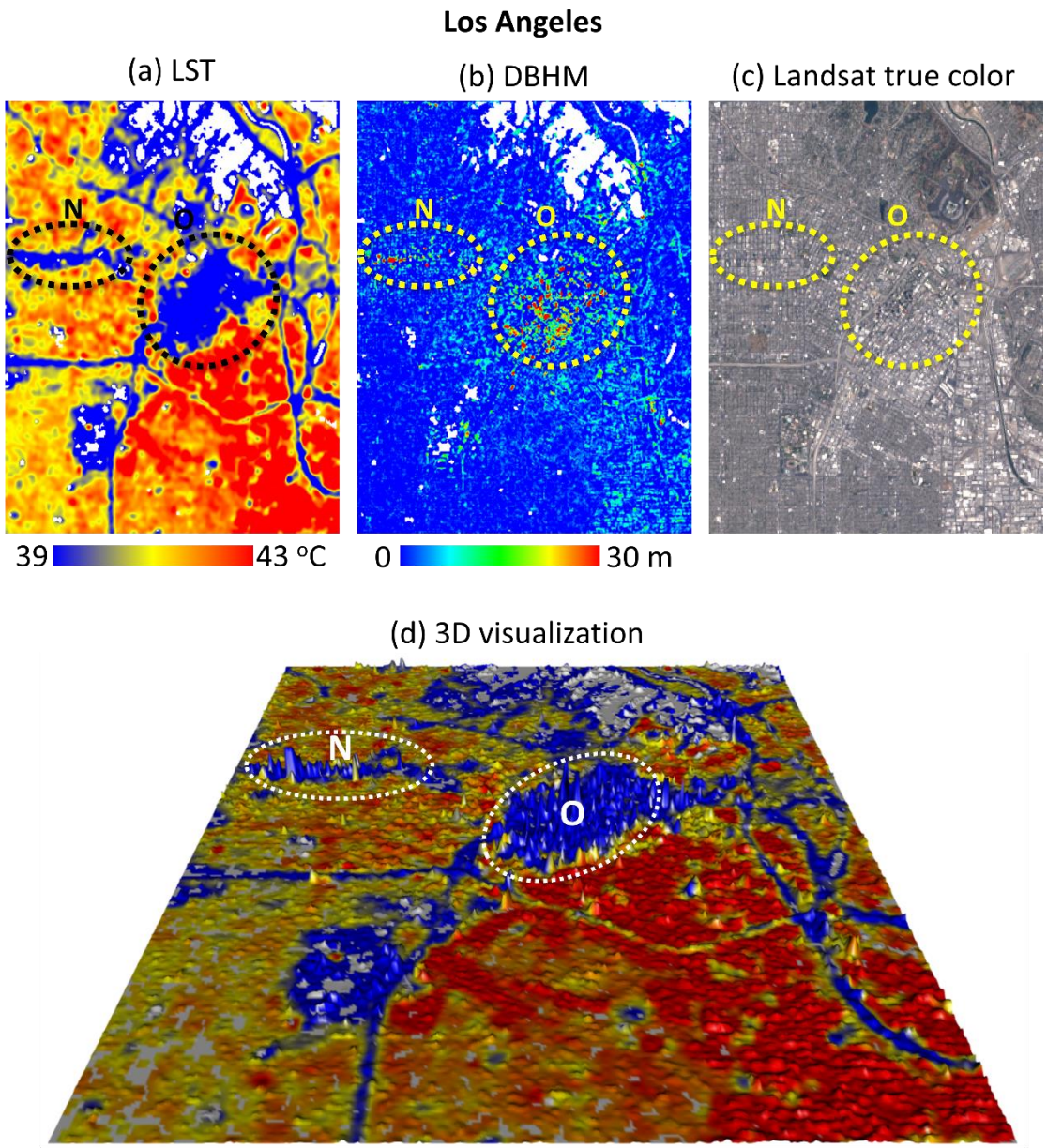

Figure 31. (a) Land Surface Temperature, (b) Digital Building Height Model, (c) Landsat true color, and (d) 3D visualization of Los Angeles

Figure 32 illustrates the models of the New York area. The study focused on the Manhattan area, and it is mainly made up of high-rise buildings. Circle P is building complexes in Midtown Manhattan, the south part of Central Park. Circle Q is Financial District in Lower Manhattan. Circle Q appears to have a higher building density than Circle P, and it also has uniformly low LST.

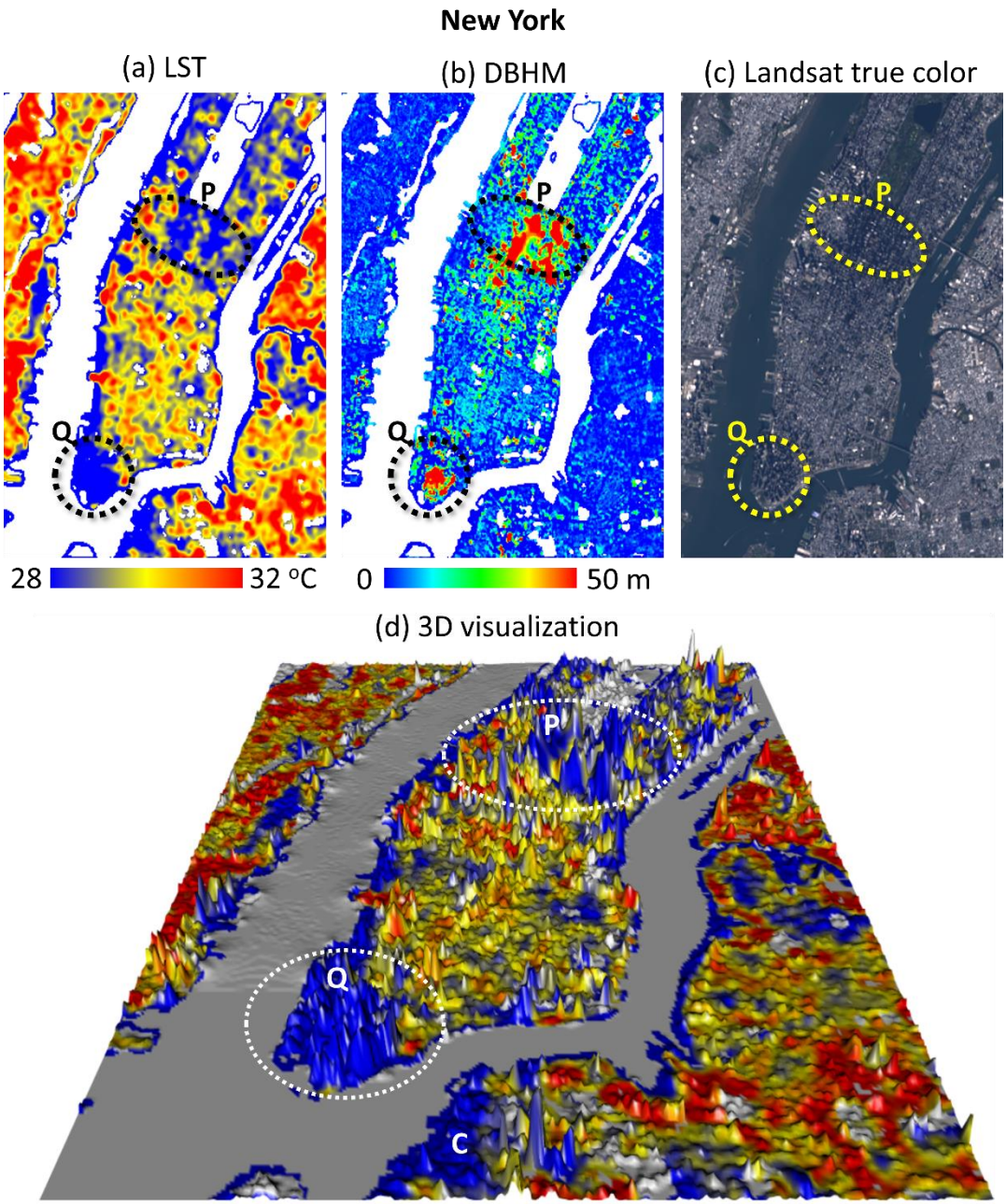

Figure 32. (a) Land Surface Temperature, (b) Digital Building Height Model, (c) Landsat true color, and (d) 3D visualization of New York

In Chicago (Figure 33), there are two noticeable low LST and high-rise buildings areas. Circle R is where a high-rise residential area is located. Circle S includes The Loop, the central business district in Chicago's downtown, that is comprised of high-rise buildings.

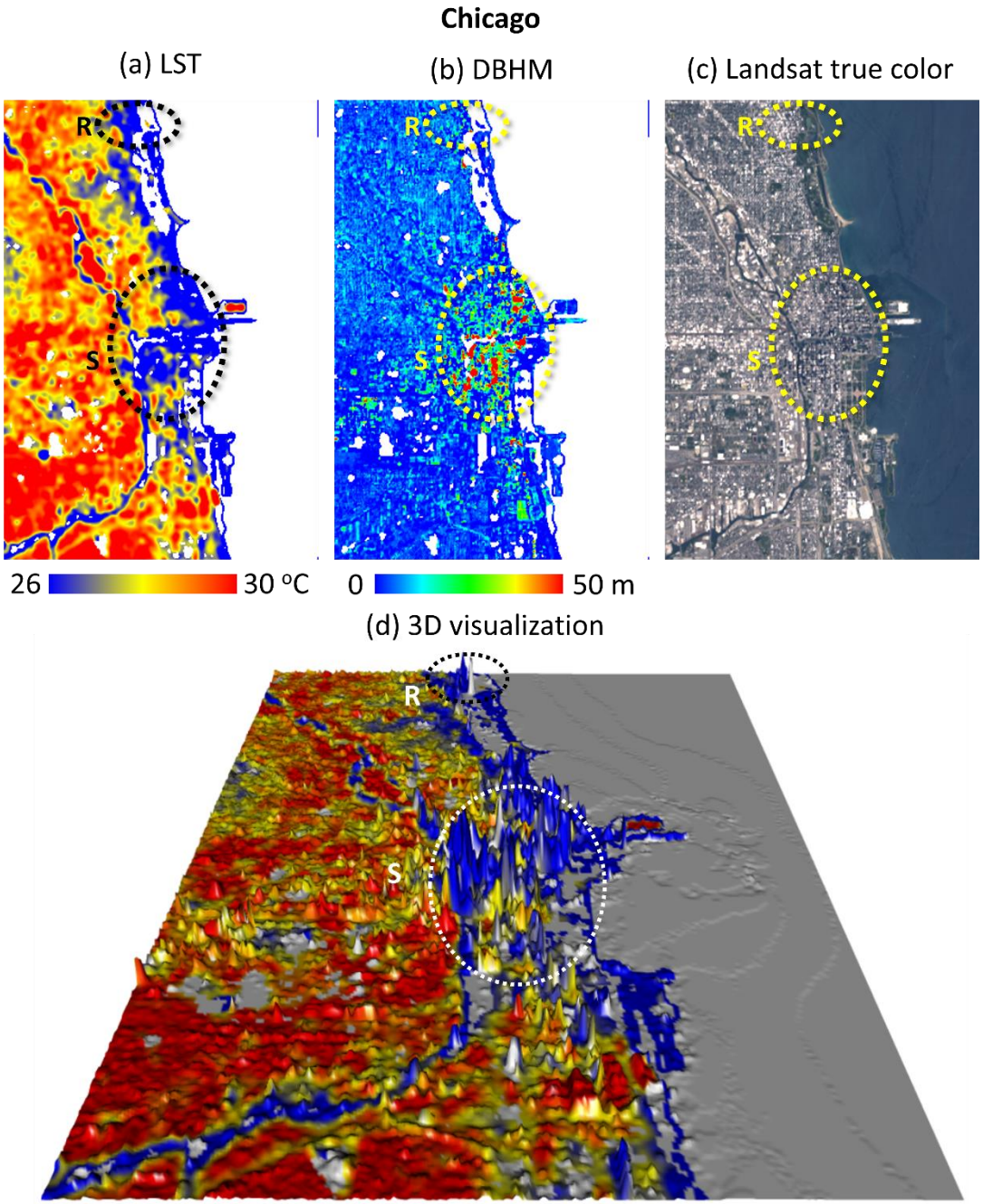

Figure 33. (a) Land Surface Temperature, (b) Digital Building Height Model, (c) Landsat true color, and (d) 3D visualization of Chicago

Through the comparison between the LST and DBHM, we confirm that high-rise buildings areas mainly have low LST. Some low-rise buildings have low LST due to the vegetation coverage. However, it does not change the overall tendency of low LST in high-rise buildings area.

5.3.2 Relationship Between DBHM and LST

The coefficients displayed in Table 16 are Pearson's correlation coefficient, r in Equation 3 that measures the relationship between the real values of LST and DBHM maps. Jakarta has the highest correlation coefficient, and New York has the lowest among the areas. The results of regression analysis between LST and DBHM are presented in Table 17. These results are statistically significant at the 0.05 level. According to Pearson's correlation and regression analysis, each study area shows a negative relationship between LST and DBHM, indicating that LST decreases as DBHM increases.

Table 16. Pearson's correlation coefficient, *r*, between LST and DBHM

Area	*r*	Number of analyzed pixels
Tokyo	-0.2474	114,818
Beijing	-0.2282	107,797
Jakarta	-0.2973	137,641
Los Angeles	-0.1535	117,750
New York	-0.0885	106,964
Chicago	-0.1667	104,813

Table 17. Relation between LST and DBHM (Equation: LST = a + b×DBHM)

Area	a	b
Tokyo	27.2938	-0.0456
Beijing	29.8596	-0.0331
Jakarta	33.1949	-0.0489
Los Angeles	41.1800	-0.0654
New York	29.4429	-0.0143
Chicago	28.3656	-0.0314

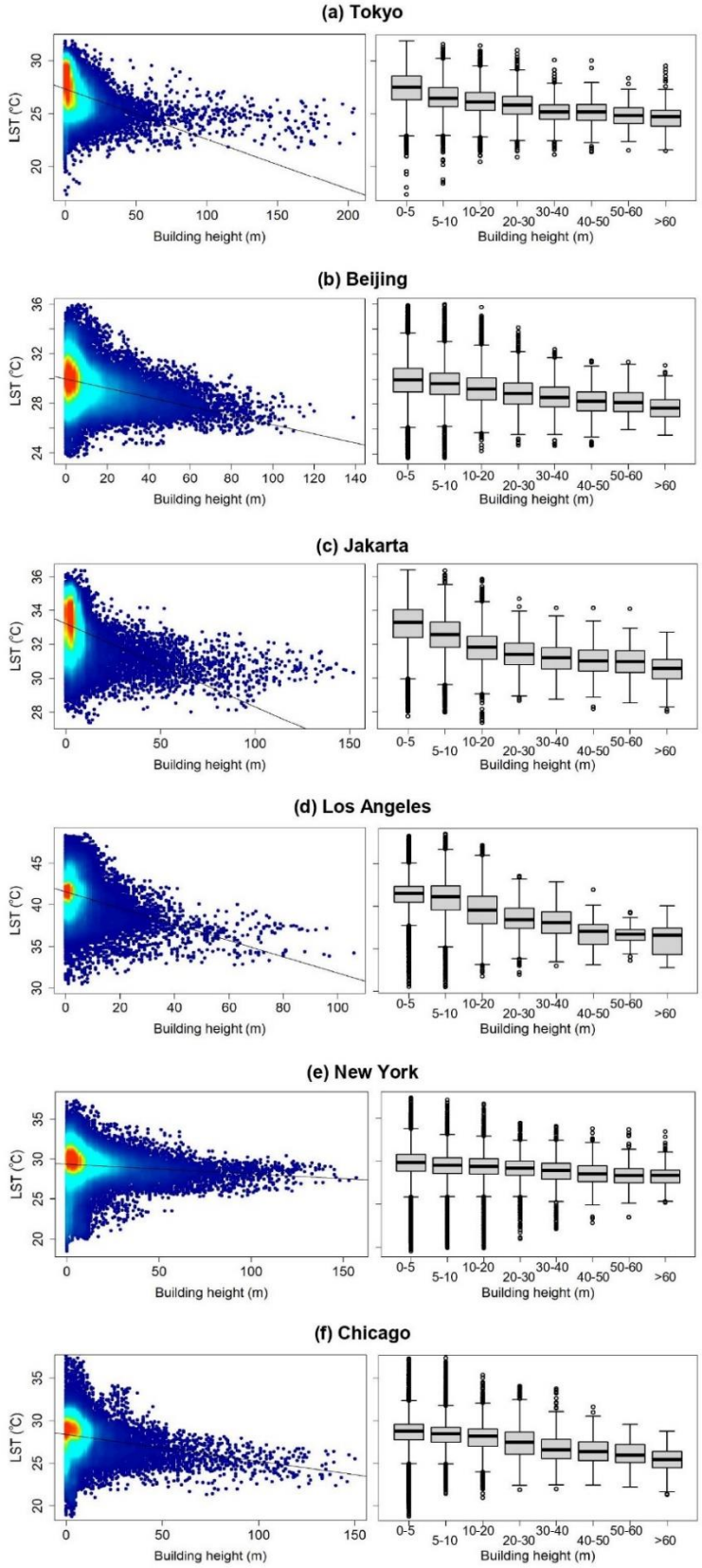

Figure 34. The scatterplots (left) and boxplots (right) of the relationship between land surface temperature and building height in each area

Figure 34 shows the scatterplot and boxplot diagrams between LST and building height. Generally, the scatterplots show a tendency that LST decreases as the building height increases. The lower heights data is more deviated. Then, all become less deviated as the height increases.

From the boxplot diagrams (Figure 34), the median values of LST also show a tendency to decrease as the building height increases. This tendency appears the weakest in New York's data. Generally, the decrease of LST's median values after the 30-40 m class is not as significant as the lower height classes. We observe that lower building height classes have more significant variability and more prominent outliers than higher building height classes in all areas.

5.3.3 Closer Observation: Study Case of Tokyo and Jakarta

A closer observation is done in Tokyo and Jakarta to support the results. In this sub-subsection, the data input for LST is different from the global city analysis. Here, the LST is from older period using Landsat 5 data, while global cities use newer data from Landsat 8. A different period is tested to examine if there is a different tendency in different period.

4.2.3.1 LST and DBHM

The spatial distributions of LST and DBHM in both cities are shown in Figure 35. From a visual observation, the low LST area corresponds well with high DBHM area. In Tokyo LST map (Figure 35b), there is a large low LST area at the right part of the image, and at the same part in Tokyo DBHM (Figure 35a), the area appears to have many high buildings. These areas are Otemachi and Marunouchi business districts and major stations like Shibuya, Shinjuku, and Ikebukuro. For comparison, we picked three samples that represent three height group areas, which are low-rise buildings, mixed-

height buildings, and high-rise buildings areas. Each sample area has size of 20×20 pixel (about 600×600 m) and marked with a square in Figure 35. Square H (high-rise) is located in Marunouchi business district, Square M (mixed-height) is in the commercial area of Shibuya, and Square L (low-rise) is in residential area in Toshima-ku.

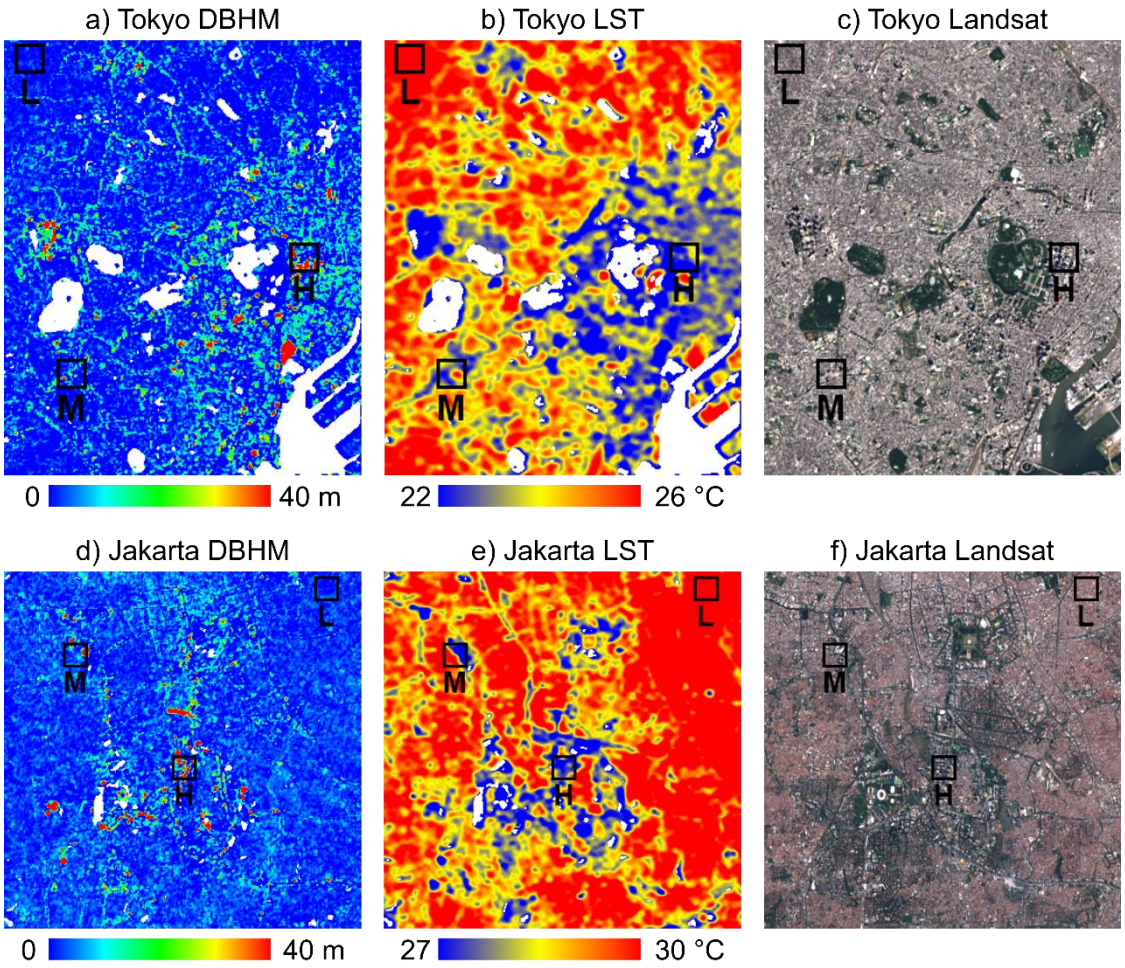

Figure 35. (a) Tokyo DBHM (Digital Building Height Model), (b) Tokyo LST map, (c) Tokyo Landsat Map, (d) Jakarta DBHM, (e) Jakarta LST map, (f) Jakarta Landsat map. Square H: high-rise building area sample, Square M: mixed height building area sample, Square L: low-rise building area sample

In Jakarta, the low LST and high DBHM area also match well (Figure 35d & Figure 35e). The low LST area belongs to the Sudirman Central Business District (SCBD) that has numerous high-rise buildings from National Monument area in the north to Senayan

business district in the south part. For the sample area in Jakarta, Square H is located inside SCBD, Square M is in Taman Aggrek area which is a complex of mixed-use high-rise buildings for shopping malls, apartments, and offices, and Square L is in residential area in Kemayoran.

Figure 36 presents the graphs of mean building height and mean LST in each sampled area in both cities. There is a similar trend in both cities where low-rise area has the highest mean LST, and high-rise area has the lowest. This further show the tendency of high buildings to have low LST. However, the LST decrease is steeper from low-rise to mixed-height, compared to mixed-height to high-rise. In Tokyo, the mean BH increase from low-rise to mixed-height is 6.69m and the LST decrease is 3.57 ^{o}C, meanwhile the mean BH increase from mixed-height to high-rise is 22.38m and the LST decrease is 1.21 ^{o}C. In Jakarta, the mean BH increase from low-rise to mixed-height is 7.20m and the LST decrease is 2.98 ^{o}C, meanwhile the mean BH increase from mixed-height to high-rise is 15.82m and the LST decrease is 0.82 ^{o}C.

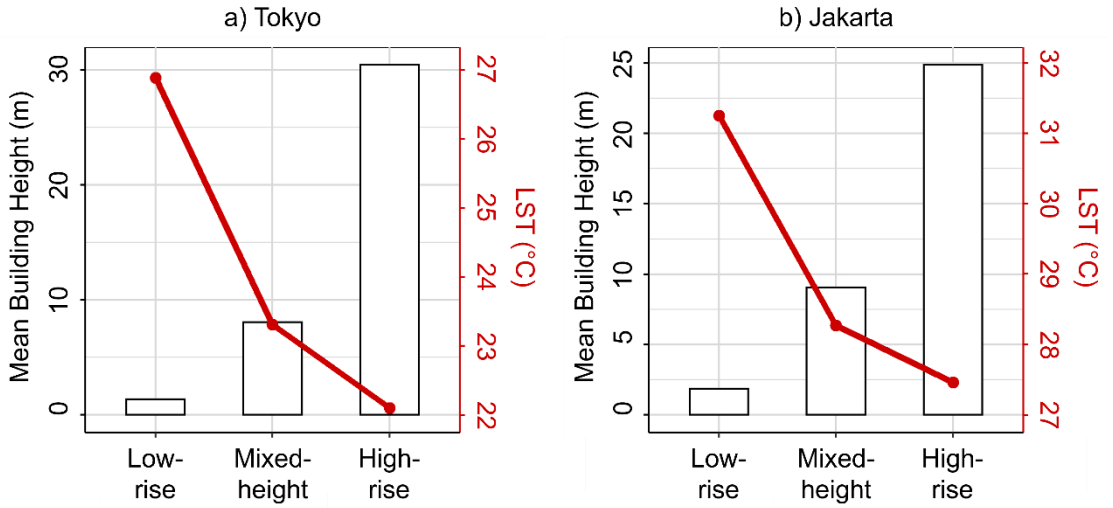

Figure 36. Mean building height and mean LST of different sample areas in Tokyo and Jakarta

4.2.3.3 Smoothed LST and DBHM

Smoothing filter is applied to improve the spatial alignment between DBHM and LST map before the statistical analyses. Figure 37 shows the results of DBHM and LST after smoothing with a window size of 5×5 pixel (150×150 m). The tendency of high-rise building area to have low LST can be observed clearer in the smoothed version of LST and DBHM maps. Areas that appear cooler are areas that have higher DBHM.

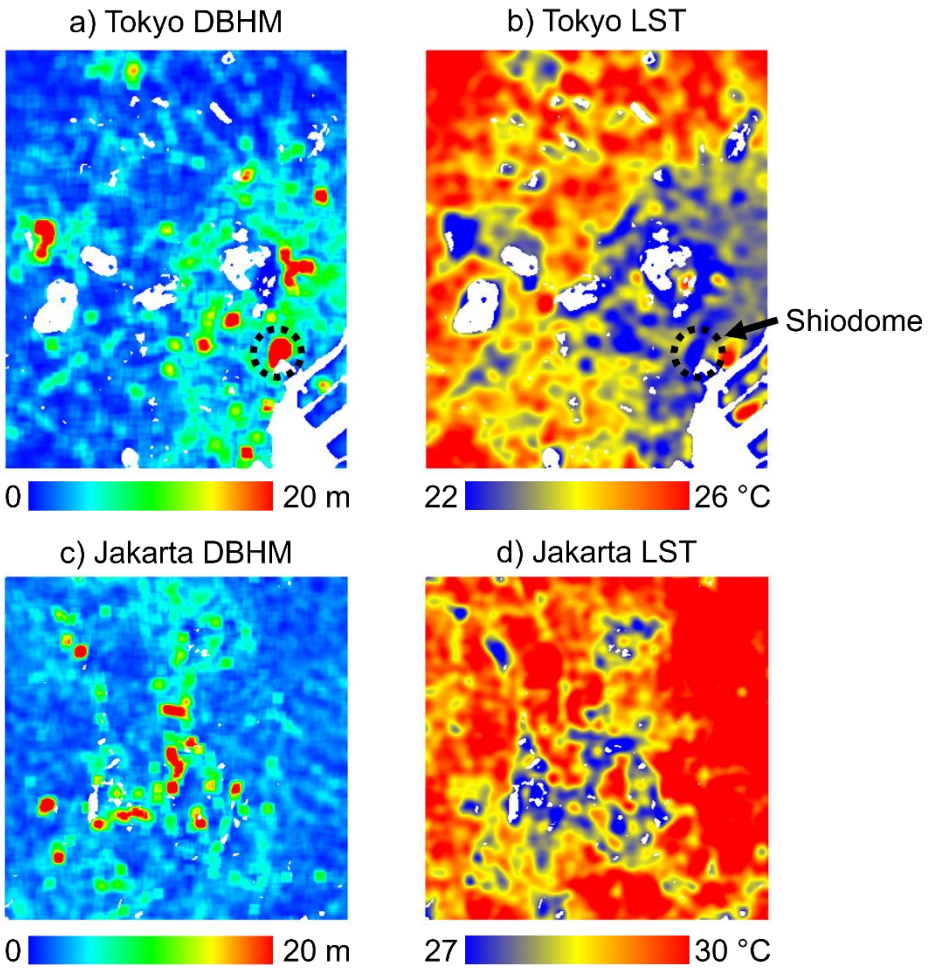

Figure 37. Smoothed LST and DBHM

The building height values decrease after the averaging process, but there is an area near Tokyo Bay, Shiodome, that exceedingly have very high values than other areas (marked in Figure 37). Shiodome is a redeveloped business and leisure city district near

Tokyo Bay that has many high-rise buildings. The present Shiodome was built after the year 2000.

4.2.3.4 Relationship Between Smoothed LST and DBHM

Correlation and regression analysis are done after the LST and DBHM are averaged. Based on the correlation analysis results, LST and DBHM have negative correlation coefficient values of -0.440 in Tokyo and -0.434 in Jakarta. Both cities show p-values below 0.05, indicating that LST and building height are significantly correlated. The negative values show that there is a decrease in LST when there is an increase in building height. Areas covered with high-rise buildings tend to have lower LST than areas covered with low-rise buildings, which shows that high-rise buildings have cooling effect to the local surface temperature.

The regression analysis results are presented in Table 18. The results show that building height significantly affects LST in Tokyo and Jakarta. From the scatterplot and boxplot diagrams in Figure 38, it is clearly seen that the LST tend to decrease as the building height increases. Lower building classes, especially 0-5 m, have wider range of LST. High-rise buildings seem to have significant cooling effect within the height range of 0-20 m in both areas. After surpassing the 20 m class, the mean LST does not decrease significantly. It is worth to note that the height value is the height after averaging process with window size of 150 x 150 m, which is lower than the actual building height. In the scatterplot of Jakarta, the highest value is about 50 m, meanwhile in Tokyo, although not many, there are points that surpassed 60 m and form a certain pattern. These values are detected in Shiodome where the values are unusually higher than other places.

Table 18. Relationship between averaged LST and averaged satellite DBHM

Area	Equation	Adjusted R^2
Tokyo	LST = -0.115×BH + 24.537	0.194**
Jakarta	LST = -0.135×BH + 29.864	0.188**

LST: averaged LST (°C) BH: averaged BH (m)

**: strongly significant with a *p*-value below 0.05

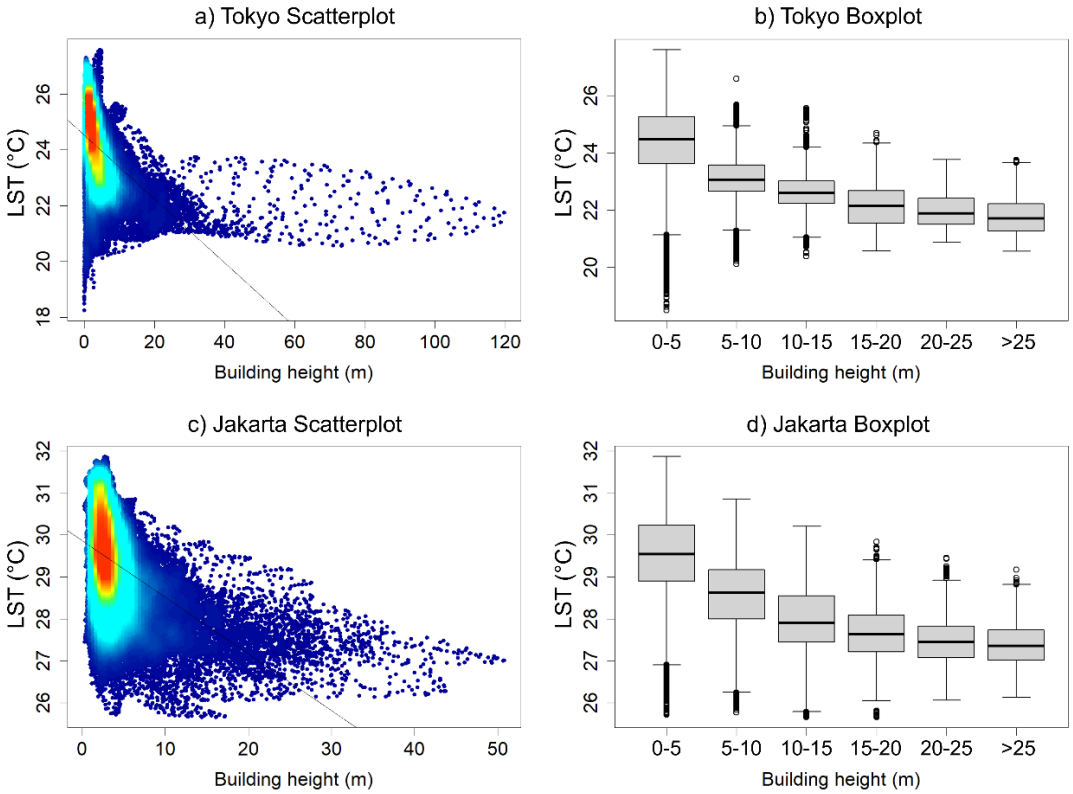

Figure 38. Scatterplots and boxplots of relationship between averaged LST and BH

The scatterplots presented in Figure 38 demonstrate the tendency of LST to decrease as the building height increases. Generally, the dots in lower heights are more scattered compared to dots in higher height. The boxplots in Figure 38 show the distribution of LST differences among different building height groups. Lower height groups (0-15 m) tend to have greater variability and larger outliers than higher groups (more than 15 m). In both cities, there is a steeply decrease in median LST of lower

height groups, but only a slight decrease in higher height groups, specifically after surpassing the 10-15m group.

5.4 Discussion

5.4.1 Causes of Low Land Surface Temperature in High-Rise Building Area

According to the results, high-rise buildings consistently have lower LST compared to low-rise buildings in all analyzed cities. There are several factors that may cause the phenomenon. First is the large vertical surface of buildings. Whether the high-rise buildings are clumped together, like in Los Angeles, or rather solitaire, like in Jakarta, they still exhibit lower LST than their surroundings. The vertical surface of high-rise buildings absorbs and reflects the solar radiation and preventing it from reaching the ground, which leads to lower land surface temperature as the satellite can only "see" the horizontal surface temperature. Then, the vertical surface of higher buildings also generates larger shadow than lower buildings. The shadow effect of high-rise buildings have been discussed in previous studies as well. Nichol (1996) pointed that smaller shadow by lower buildings is only a minor proportion even at 30-m satellite image resolution. Therefore, the shadow effect in low-rise buildings is almost negligible. Wang and Xu (2021) mapped the shadow of high-rise buildings and confirmed that the shaded area is cooler than the non-shaded area.

The ratio between horizontal surface versus vertical surfaces has also been discussed in a study by Yang and Li (2015) that found low-rise setting absorbs more solar radiation than high-rise because it is dominated by horizontal surface (roof or street surface) and the high-rise building blocks the solar radiation reaching the street. This phenomenon can be observed in Figure 39 that shows a 3D building model overlayed by averaged LST and BH map in Shinjuku, Tokyo. The LST difference between the

high-rise complex and its surrounding low-rise buildings is very distinguished. In low-rise buildings area, a large part of urban area is covered by street surface, meanwhile in high-rise buildings area, there are more coverage from wall and roof surfaces, and the street surfaces are covered by building shadows.

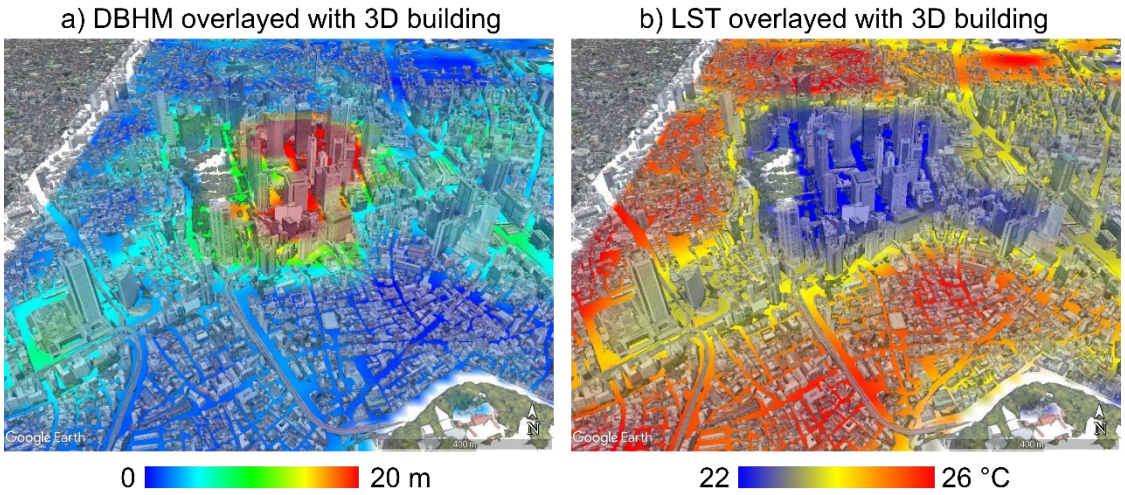

Figure 39. Overlayed averaged LST map and DBHM map to the 3D building model of Shinjuku, Tokyo

(Google Earth, Gray Buildings © 2008 ZENRIN)

Contrasting building height may also accentuate the cooling effect of high-rise buildings. Aside from Tokyo shown in Figure 39, this phenomenon is also observed in Jakarta and Los Angeles where the low-rise area has very contrasting height with the high-rise area. The low-rise area seems to be very hot than the high-rise area. On the contrary, at places like Beijing and New York that has many mid-rise/high-rise buildings with varying heights distributed throughout the area, the cooling effect of high-rise building does not appear as significant as in Tokyo, Jakarta, and Los Angeles. Large low-rise area with uniform height that are found in Tokyo, Jakarta, and Los Angeles have large horizontal surface to absorb the solar radiation that increase the LST. Meanwhile, when the building height in not uniform like in Beijing and New York, there

is a higher chance that the solar radiation is absorbed by the vertical surface and results in lower LST. Therefore, the LST difference appears more contrast in areas where the clump of high-rise buildings is surrounded by uniform-height low-rise buildings.

The coverage of green space might also have impact in lowering the LST in high-rise building area. High-rise buildings usually have a certain amount of green space coverage around them, which can also be found in Shinjuku (Figure 39). Although the influence of green space is not examined in this study, a prior study suggests that building height still has a greater impact on LST compared to building density and vegetation coverage (Zheng et al. 2019). In Figure 39a & Figure 39b, it is apparent that a large high-rise building complex in the middle forms a low LST area, but if observed closely, even only several adjacent high buildings also form a lower LST area. Inside the large building complex, there is a vegetation coverage that might contribute to the low LST, however, in other smaller complexes that has little to no vegetation coverage, the LST is also lower, suggesting that high building tend to have low LST regardless of the building density and vegetation coverage.

Vegetation coverage possibly have greater influence on LST in low-rise building area than in high-rise building area. This may partially explain the large LST variation in lower building height classes. Large vegetation coverage is removed by the mask created in this study, but small vegetation coverage is hard to exclude due to the satellite resolution. Figure 40 shows two spots in Los Angeles that have different compositions and different LST. Figure 40a is the hotter area (higher LST) and it is mostly covered by mid-rise commercial buildings. Figure 40b is the cooler area (lower LST) and it is covered by low-rise residentials with lawns and trees in front of most houses. Although the building height in Figure 40a is higher than Figure 40b, the LST is lower in Figure 40b. This is suspected to happen because the vegetation coverage around the residential

area in Figure 40b tends to decrease the LST. In addition, generally, the street width and the building size are larger in the hotter area than the cooler area, which may be related to the previously mentioned reason, ratio of horizontal versus vertical surfaces. Analyzing the interaction between factors, such as building height, building density, building size, street width, vegetation, etc., is required to explain the tendency of land surface temperature.

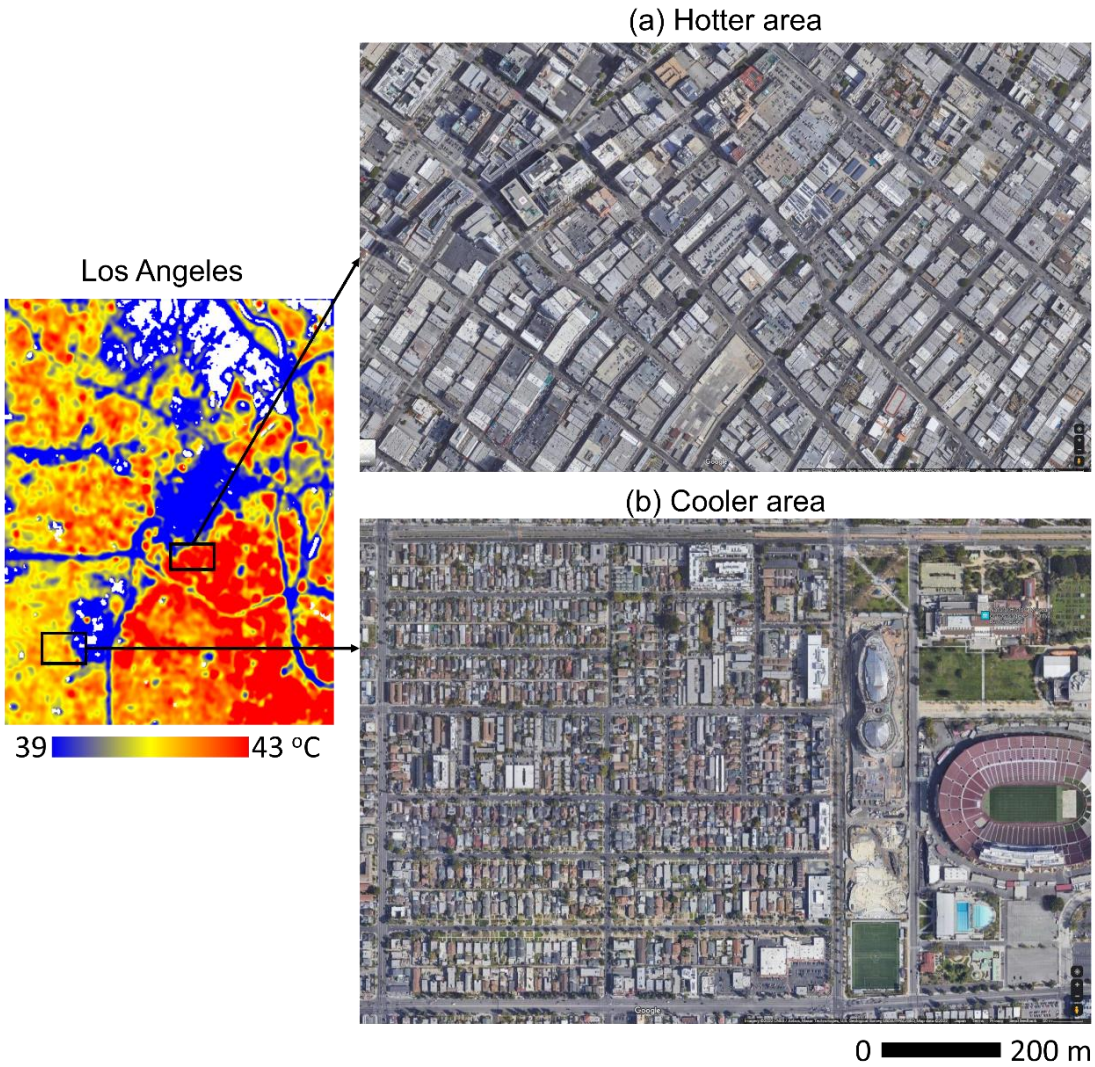

Figure 40. Spots of low-rise and mid-rise buildings in Los Angeles that have (a) hotter temperature and (b) cooler temperature

(Google Earth)

The building materials may also play a role in the varying temperature. High albedo materials significantly affect LST and can mitigate urban heat. We do not investigate the building materials for this study, but a study found that bricks absorb and store heat greater than concrete, granite, and white concrete tiles during daytime (Md Din 2012). The difference between materials that are commonly used for high-rise buildings and low-rise building may affect the LST difference between them.

Another possible factor is the formation of wind corridor between parallel buildings that encourage the wind speed. A corridor formed by parallel buildings may increase the wind speed by approximately 0.3 m/s (Jiang, Wu, and Teng 2020). As wind transports moisture and temperature to another place, the LST is expected to be lower when wind exists. Another study also suggests that there is a wind cooling effect between buildings (W. Chen et al. 2020).

The factors discussed above is based on the findings of this study and other studies that observed the phenomenon during daytime (around 10:00 to 11:00). A similar phenomenon may not be found during nighttime, which is the limitation that cannot be explained by this study. Yang et al. (2017) stated that the cooling effect of high-rise buildings, defined as "urban cool island", can be found almost in an entire year, but it is stronger in summer, and only lasts for several hours in the morning to noon. The study examined the phenomenon in Hongkong, a city with compact high-rise buildings. Another study (Erell and Williamson 2007) analyzed the diurnal and nocturnal pattern of urban heat island in Adelaide, Australia, and found that there is indeed urban cool island phenomenon during daytime in urban street canyon sites, or streets between high-rise buildings that form canyon-like environment. Urban cool island during daytime is weaker than urban heat island during nighttime. The intensity of urban heat island phenomenon was reported to increase after sunset and reached the maximum before

midnight. The finding of that study suggested that, during the day, lower buildings warm up faster than higher buildings, and during the night, lower buildings cool down faster than higher buildings, possibly due to different heat storage capacity of buildings. This causes high-rise buildings to have lower temperature in daytime and higher temperature in nighttime, if compared to low-rise buildings.

Present study only analyzed the cooling phenomenon during daytime before noon and is not capable to consider the impact of different time of the day on the land surface temperature. High-rise buildings may have lower LST during the day, but they may also have higher LST during the night. In addition, only building height is taken into consideration in this study, although other factors, such as building density, building size or volume, etc., can also influence the LST. But the presented results are reasonable, and the study reveals the universal cooling effect of high-rise buildings in cities around the world. In addition, this study shows the applicability of building height data derived from subtracting SRTM from AW3D30 in urban climate study.

5.4.2 Implications of The Findings in Landscape Architecture

Generally, the finding suggests that high-rise buildings have a lower LST compared to low-rise buildings during daytime. Incorporating high-rise buildings into urban planning can help to create cooling effect. Based on the findings, the following points can be considered to alleviate the effect of urban heat island in the city.

1. The data indicate that the land surface temperature decreases as the building height increases, but the temperature decrease becomes insignificant after the building height surpassed certain point (the results show around 30-40 m). It is recommended to have spatially distributed high-rise buildings in an area, but it is not necessary to create very tall buildings that surpassed 40 m. In related to energy

consumption, tall buildings tend to consume larger energy, such as for electricity, etc. High-rise buildings over 20 stories use about two and a half times greater electricity than in buildings of 6 stories or less (UCL 2017). Therefore, it is important not to crowd the area with high-rise buildings as well.

2. The study noted that the LST decrease from low-rise to mixed-height is more significant compared to mixed-height to high-rise, which suggests that a large area of low-rise buildings is not recommended, instead it is better to create a mixed-height building composition in urban setting. Based on the results, in Tokyo, the mean building height in mixed-height class is about 4.1 m, and in Jakarta, the mean building height in mixed-height class is about 8.2 m. Considering the DBHM in this study is about half of the reference height, mean building height of about 8-16 (3-5 stories) m in an area is recommended to create cooling effect.

On another note, from a researcher viewpoint, this study is able to derive urban 3D structure information using a simple method. This method can be applied in urban studies that involve land use / land cover classification analysis. This method can be used as a validation tool of the classification. Classification methods, such as local climate zone (LCZ) (Stewart and Oke 2012), is heavily based on the building height information. However, the method classified the image based on horizontal two-dimensional approach only. For example, LCZ has classes such as “compact high-rise”, “compact mid-rise”, and “compact low-rise”. From a 2D image, we cannot be sure it is categorized as which, but information on 3D structure can support such judgement. The building height model derived from this method can be a useful tool to support the validation of the LCZ classification.

5.5 Chapter Summary

This study investigates the relationship between building height and land surface temperature by utilizing digital building height model (DBHM) obtained from the difference between AW3D30 and SRTM in six areas worldwide. The results show that building height have a negative relationship with LST where high-rise buildings tend to have low LST. The tendency is visible in all investigated areas despite their different spatial distributions and different climate conditions. This study only examines the impact of building height factor on land surface temperature. As discussed, land surface temperature has complex relationship with factors that influence it and cannot be clearly explained by examining building height only, which also beyond the scope of this study. In addition, the observation is limited only during the daytime. The results cannot explain the phenomenon during nighttime, but it raises attention to building height consideration in urban planning and shows the applicability of DBHM for urban climate study, which was barely utilized in existing studies.

CHAPTER 6: Conclusion

6.1 Summary of Findings

Firstly, we analyzed the land cover change and its impact on land surface temperature in Jakarta and its satellite cities. Then, we examined a simpler alternative method to extract building height information from open-sources data. After that, we used the derived building height model to analyze the relationship between building height and land surface temperature in global cities, including Tokyo, Beijing, Jakarta, Los Angeles, New York, and Chicago. A closer observation was also done specifically in Tokyo and Jakarta. Based on the objectives of this study, the findings are summarized as follows.

Objective 1: "Analyzing the land cover change and its impact on land surface temperature"

1) The majority of land cover changed that occurred in Jakarta and its satellite cities are the conversion of vegetated area to built-up area.

   The main cause of land cover conversion is construction for residential purposes and shopping malls. The built-up conversion starts from Jakarta and then spreads to the surrounding satellite cities. According to the built-up expansion proportion of each city's total area, the expansion occurred most extensive in Tangerang, followed by Bekasi, with a slight difference, Depok, and lastly Jakarta.

2) The high LST area is mostly distributed in the built-up area and the land conversion to built-up area highly affected the increase of LST.

   The land cover changes resulted in significantly higher mean LSTs of the analyzed cities. The LST difference ranged from 6.43 ^{o}C to 12.66 ^{o}C. The highest LST difference belongs to Bekasi, meanwhile, the lowest belongs to Depok.

Objective 2: "Examining an alternative method to extract building height information from open-sources data that has lower computational complexity"

3) Open-sources data, AW3D30 and SRTM, can be used to extract building height information with simple calculation → Satellite DCHM = AW3D30 – SRTM

We presented the idea of deriving building height information by simply subtracting SRTM from AW3D30, that we defined as Satellite DCHM. The result showed that there is a good agreement between the Satellite DCHM and the reference height data, LiDAR DCHM. The derived building height from satellite data has lower values than the reference data, roughly about half of the reference data. Although the produced building height model does not present the accurate height values, it is sufficient to show the urban 3D structure information. The produced model can show the existence of mid-rise and high-rise buildings correctly. The data may be used in its original resolution but applying a smoothing filter with window size of 5x5 pixels (150x150 m) is recommended prior to applications in other fields.

Objective 3: "Analyzing the relationship between building height and land surface temperature"

4) Building height has a negative relationship with land surface temperature in all analyzed global cities

We utilized the building height model derived in this study to analyze the relationship between building height and land surface temperature in six global cities with many high-rise buildings, which included area in Tokyo, Beijing, Jakarta, Los Angeles, New York, and Chicago. All these cities exhibit a similar tendency where the high-rise building areas have lower land surface temperature, then the

surrounding low-rise building areas. The result is consistent regardless of different climates and different locations.

5) The decrease of land surface temperature is not linear with the increase of building height

Tokyo and Jakarta were picked to be observed more closely because of their contrasting climate and supporting field knowledge. The land surface temperature difference between low-rise, mixed-height, and high-rise building areas were clearly seen when samples were taken. The decrease of land surface temperature from low-rise to mixed-height area was bigger than from mixed-height to high-rise in both cities. It is also observable from the scatter plots presented in the results where the decrease of land surface temperature is insignificant after surpassing certain height (30-40m) possibly due to the influence of shadow. The increase of shadow area is not significant even if the building height surpasses 30-40 m.

6.2 Contributions and Implications

This study analyzes the factors that affect land surface temperature, such as land cover change and building height. The relationship between land cover change and land surface temperature has been extensively studied, but this study focuses on how a capital city, Jakarta, grows to a larger megaregion. After examining the land cover change impact on land surface temperature, the analysis aims to advance to the vertical aspect such as building height. However, the building height information is still difficult to obtain. Therefore, a method to easily derive building height is examined.

Existing studies derived building height information from open-source data using complex methods. This study offers a simpler method to detect the urban 3D structure information. This method is very simple, and it can easily be applied by anyone,

including individuals who are not experts in the remote sensing field. The produced building height model can detect the existence of mid-rise and high-rise buildings although it does not measure the accurate building height. It is sufficient for the analysis with land surface temperature.

By analyzing the relationship with land surface temperature, this study confirmed the contradicting results where high-rise buildings were said to increase the LST. On the contrary, high-rise buildings could decrease the LST. This study is the first to utilize the building height model calculated from AW3D30 and SRTM for the application in urban climate study.

The findings of this study hopefully will be able to contribute to future studies that previously could not be done due to complex calculation to derive building height. Practically, this study could add some consideration in urban planning sector to create a space where the building height is not uniform because mixed-height area could decrease LST significantly.

6.3 Limitations and Future Research

In Study 1, the land cover and land surface temperature change in Jakarta and its satellite cities are examined. The land surface temperature values are derived from two different sensors that possibly affect the values. Land surface may have great variability at different dates, and it should be considered in multitemporal analysis. Although the results are correct, it may not be representative for the actual condition. Future research should consider calibrating and validating the land surface temperature to produce more accurate results.

The DCHM/DBHM produced in the Study 2 could estimate the building height in urban areas, but it must be used with cautions. First, it is most likely to underestimate

the actual building height due to the resolutions, although roughly, the extracted building height is about half of the actual building height. The data in its present condition cannot be used to obtain the accurate height but is sufficient to observe the tendency. The limitation of this study is that it is only evaluated the results of Satellite DCHM in Tokyo. Obtaining high-precision building height data in other locations is desirable to validate the results with more locations.

The AW3D30 data were acquired in 2006-2011, at one side, buildings that were built after 2011 are not recorded in the dataset, but at the other side, it is advantageous to use the data with other satellites that are launched after that, such as Sentinel-1. Sentinel-1 is also used in an existing study for deriving building height data, and it is launched in 2014. If we derive the building height from AW3D30 and compare it with Sentinel-1, we may observe the building development or expansion during the different period for future study.

The LST data used in Study 1 and Study 3 were acquired during daytime (around 10:00 until 11:00 AM). Therefore, it only captures the phenomenon of daytime without considering the nighttime that possibly exhibit different phenomenon. Daytime and nighttime have different characteristics that were not explored in this research. Future studies should consider adding nighttime temperature observation to the analysis. In addition, Study 3 limits its scope on building height. However, it is rather difficult to distinguish the effect of building height and other factors such as, building density, building materials, vegetation coverage, etc., that may also influence the land surface temperature. Generalizing the findings is still difficult if solely based on current results. Future study that could isolate each factor's effect and also analyze the interaction between each factor would be beneficial.

REFERENCES

Alexander, Cici. 2021. “Influence of the Proportion, Height and Proximity of Vegetation and Buildings on Urban Land Surface Temperature.” *International Journal of Applied Earth Observation and Geoinformation* 95: 102265. https://doi.org/10.1016/j.jag.2020.102265.

Alobeid, Abdalla, Karsten Jacobsen, and Christian Heipke. 2010. “Comparison of Matching Algorithms for DSM Generation in Urban Areas from Ikonos Imagery.” *Photogrammetric Engineering and Remote Sensing* 76 (9): 1041–50. https://doi.org/10.14358/PERS.76.9.1041.

Berger, C., J. Rosentreter, M. Voltersen, C. Baumgart, C. Schmullius, and S. Hese. 2017. “Spatio-Temporal Analysis of the Relationship between 2D/3D Urban Site Characteristics and Land Surface Temperature.” *Remote Sensing of Environment* 193 (May): 225–43. https://doi.org/10.1016/J.RSE.2017.02.020.

Bhatta, Niraj Prasad, and M Geethapriya. 2017. “RADAR and Its Applications” 10 (03): 1–9.

Bi, Shusheng, Chang Yuan, Chang Liu, Jun Cheng, Wei Wang, and Yueri Cai. 2021. “A Survey of Low-cost 3D Laser Scanning Technology.” *Applied Sciences (Switzerland)* 11 (9). https://doi.org/10.3390/app11093938.

Borck, Rainald. 2016. “Will Skyscrapers Save the Planet? Building Height Limits and Urban Greenhouse Gas Emissions.” *Regional Science and Urban Economics* 58 (May): 13–25. https://doi.org/10.1016/J.REGSCIURBECO.2016.01.004.

BPS - Statistics of DKI Jakarta Province. 2017. *Jakarta in Figures 2017*. Edited by Yayat Rochadiyat. Jakarta: BPS - Statistics of DKI Jakarta Province. http://jakarta.bps.go.id.

Cai, Meng, Chao Ren, Yong Xu, Kevin Ka Lun Lau, and Ran Wang. 2018. "Investigating the Relationship between Local Climate Zone and Land Surface Temperature Using an Improved WUDAPT Methodology – A Case Study of Yangtze River Delta, China." *Urban Climate* 24: 485–502. https://doi.org/10.1016/j.uclim.2017.05.010.

Căţeanu, Mihnea, and Arcadie Ciubotaru. 2020. "Accuracy of Ground Surface Interpolation from Airborne Laser Scanning (ALS) Data in Dense Forest Cover." *ISPRS International Journal of Geo-Information* 9 (4). https://doi.org/10.3390/ijgi9040224.

Chen, Ran. 2011. "The Development of 3D City Model and Its Applications in Urban Planning." *Proceedings - 2011 19th International Conference on Geoinformatics, Geoinformatics 2011*, 1–5. https://doi.org/10.1109/GeoInformatics.2011.5981007.

Chen, Wei, Jianjun Zhang, Xuelian Shi, and Shidong Liu. 2020. "Impacts of Building Features on the Cooling Effect of Vegetation in Community-Based Microclimate: Recognition, Measurement and Simulation from a Case Study of Beijing." *International Journal of Environmental Research and Public Health* 17 (23): 1–23. https://doi.org/10.3390/ijerph17238915.

Danniswari, Dibyanti, Tsuyoshi Honjo, Akira Kato, and Katsunori Furuya. 2021. "Utilizing Open-Source Satellite Data for the Relationship between Building Height and Land Surface Temperature." *Journal of Environmental Information Science* 2021: 1–10. https://doi.org/10.11492/ceispapersen.2021.2_1.

Demuzere, Matthias, Jonas Kittner, and Benjamin Bechtel. 2021. "LCZ Generator: A Web Application to Create Local Climate Zone Maps." *Frontiers in Environmental Science* 9 (April). https://doi.org/10.3389/fenvs.2021.637455.

Douglass, Michael. 2010. "Globalization, Mega-Projects and the Environment: Urban

Form and Water in Jakarta." *Environment and Urbanization ASIA* 1 (1): 45–65. https://doi.org/10.1177/097542530900100105.

El-Hattab, Mamdouh M. 2016. "Applying Post Classification Change Detection Technique to Monitor an Egyptian Coastal Zone (Abu Qir Bay)." *Egyptian Journal of Remote Sensing and Space Science* 19 (1): 23–36. https://doi.org/10.1016/j.ejrs.2016.02.002.

Emahlia, and M. Baiquni. 2017. "Distribusi Dan Pola Pusat Perbelanjaan Skala Besar Secara Spasial Di Kota Bekasi." *Geografi UGM* 6 (3): 1–15.

EPA. 2021. "Land Use." 2021. https://www.epa.gov/report-environment/land-use.

———. 2022. "Land Cover." 2022. https://www.epa.gov/report-environment/land-cover.

Erell, E., and T. Williamson. 2007. "Intra-Urban Differences in Canopy Layer Air Temperature at a Mid-Latitude City." *International Journal of Climatology* 27 (9): 1243–55. https://doi.org/10.1002/joc.1469.

Estoque, Ronald C., Yuji Murayama, and Soe W. Myint. 2017. "Effects of Landscape Composition and Pattern on Land Surface Temperature: An Urban Heat Island Study in the Megacities of Southeast Asia." *Science of the Total Environment* 577: 349–59. https://doi.org/10.1016/j.scitotenv.2016.10.195.

Farr, Tom G., Paul A. Rosen, Edward Caro, Robert Crippen, Riley Duren, Scott Hensley, Michael Kobrick, et al. 2007. "The Shuttle Radar Topography Mission." *Reviews of Geophysics* 45 (2): RG2004. https://doi.org/10.1029/2005RG000183.

Ferreira, Luciana Schwandner, and Denise Helena Silva Duarte. 2019. "Exploring the Relationship between Urban Form, Land Surface Temperature and Vegetation Indices in a Subtropical Megacity." *Urban Climate* 27 (November 2018): 105–23. https://doi.org/10.1016/j.uclim.2018.11.002.

Fitriani, Rahma, and Michael Harris. 2011. “The Extent of Sprawl in the Fringe of Jakarta Metropolitan Area From the Perspective of Externalities.” *Australian Agricultural and Resource Economics Society*, no. February. https://ageconsearch.umn.edu/bitstream/100700/2/Rahma.pdf.

Gamba, Paolo, Bijan Houshmand, and Matteo Saccani. 2000. “Detection and Extraction of Buildings from Interferometric SAR Data.” *IEEE Transactions on Geoscience and Remote Sensing* 38 (1 II): 611–18. https://doi.org/10.1109/36.823956.

Good, Elizabeth J., Darren J. Ghent, Claire E. Bulgin, and John J. Remedios. 2017. “A Spatiotemporal Analysis of the Relationship between Near-Surface Air Temperature and Satellite Land Surface Temperatures Using 17 Years of Data from the ATSR Series.” *Journal of Geophysical Research: Atmospheres* 122 (17): 9185–9210. https://doi.org/10.1002/2017JD026880.

Gorelick, Noel, Matt Hancher, Mike Dixon, Simon Ilyushchenko, David Thau, and Rebecca Moore. 2017. “Google Earth Engine: Planetary-Scale Geospatial Analysis for Everyone.” *Remote Sensing of Environment* 202: 18–27. https://doi.org/10.1016/j.rse.2017.06.031.

Güneralp, Burak, Yuyu Zhou, Diana Ürge-Vorsatz, Mukesh Gupta, Sha Yu, Pralit L. Patel, Michail Fragkias, Xiaoma Li, and Karen C. Seto. 2017. “Global Scenarios of Urban Density and Its Impacts on Building Energy Use through 2050.” *Proceedings of the National Academy of Sciences of the United States of America* 114 (34): 8945–50. https://doi.org/10.1073/pnas.1606035114.

Guo, Guanhua, Xiaoqing Zhou, Zhifeng Wu, Rongbo Xiao, and Yingbiao Chen. 2016. “Characterizing the Impact of Urban Morphology Heterogeneity on Land Surface Temperature in Guangzhou, China.” *Environmental Modelling and Software* 84: 427–39. https://doi.org/10.1016/j.envsoft.2016.06.021.

Guth, Peter L., Adriaan Van Niekerk, Carlos H. Grohmann, Jan Peter Muller, Laurence Hawker, Igor V. Florinsky, Dean Gesch, et al. 2021. “Digital Elevation Models: Terminology and Definitions.” *Remote Sensing* 13 (18): 1–19. https://doi.org/10.3390/rs13183581.

Honjo, Tsuyoshi, Dibyanti Danniswari, Yuhwan Seo, Nobumitsu Tsunematsu, and Hitoshi Yokoyama. 2022. “Simple Method for Detecting Urban 3D Structure Using Open-Source Satellite Data. [Manuscript Submitted for Publication].”

Honjo, Tsuyoshi, Nobumitsu Tsunematsu, Hitoshi Yokoyama, Yudai Yamasaki, and Kiyoshi Umeki. 2017. “Analysis of Urban Surface Temperature Change Using Structure-from-Motion Thermal Mosaicing.” *Urban Climate* 20: 135–47. https://doi.org/10.1016/j.uclim.2017.04.004.

Hummel, Susan, A. T. Hudak, E. H. Uebler, M. J. Falkowski, and K. A. Megown. 2011. “A Comparison of Accuracy and Cost of LiDAR versus Stand Exam Data for Landscape Management on the Malheur National Forest.” *Journal of Forestry* 109 (5): 267–73.

Hussain, Masroor, Dongmei Chen, Angela Cheng, Hui Wei, and David Stanley. 2013. “Change Detection from Remotely Sensed Images: From Pixel-Based to Object-Based Approaches.” *ISPRS Journal of Photogrammetry and Remote Sensing* 80: 91–106. https://doi.org/10.1016/j.isprsjprs.2013.03.006.

Ibrahim, Eldemery. 2007. “High-Rise Buildings – Needs & Impacts.” *CIB World Building Congress 2017* CIB2007 (269): 1998–2008. http://www.irbnet.de/daten/iconda/CIB5047.pdf.

Jeevalakshmi, D., S. Narayana Reddy, and B. Manikiam. 2017. “Land Surface Temperature Retrieval from LANDSAT Data Using Emissivity Estimation.” *International Journal of Applied Engineering Research* 12 (20): 9679–87.

Jia, Zhuanhong, Qinglin Zhu, and Faliang Ao. 2006. “Atmospheric Attenuation Analysis in the FSO Link.” *International Conference on Communication Technology Proceedings, ICCT*. https://doi.org/10.1109/ICCT.2006.341919.

Jiang, Yingjie, Changguang Wu, and Mingjun Teng. 2020. “Impact of Residential Building Layouts on Microclimate in a High Temperature and High Humidity Region.” *Sustainability (Switzerland)* 12 (3). https://doi.org/10.3390/su12031046.

Kim, Isaac I., Bruce McArthur, and Eric J. Korevaar. 2001. “Comparison of Laser Beam Propagation at 785 Nm and 1550 Nm in Fog and Haze for Optical Wireless Communications.” *Optical Wireless Communications III* 4214: 26–37. https://doi.org/10.1117/12.417512.

Kottek, Markus, Jürgen Grieser, Christoph Beck, Bruno Rudolf, and Franz Rubel. 2006. “World Map of the Köppen-Geiger Climate Classification Updated.” *Meteorologische Zeitschrift* 15 (3): 259–63. https://doi.org/10.1127/0941-2948/2006/0130.

Kouklis, Georgios-Rafail, and Athena Yiannakou. 2021. “The Contribution of Urban Morphology to the Formation of the Microclimate in Compact Urban Cores: A Study in the City Center of Thessaloniki.” *Urban Science* 5 (2): 37. https://doi.org/10.3390/urbansci5020037.

Larondelle, Neele, Zoé A. Hamstead, Peleg Kremer, Dagmar Haase, and Timon McPhearson. 2014. “Applying a Novel Urban Structure Classification to Compare the Relationships of Urban Structure and Surface Temperature in Berlin and New York City.” *Applied Geography* 53: 427–37. https://doi.org/10.1016/j.apgeog.2014.07.004.

Li, Xuecao, Yuyu Zhou, Peng Gong, Karen C. Seto, and Nicholas Clinton. 2020. “Developing a Method to Estimate Building Height from Sentinel-1 Data.” *Remote*

Sensing of Environment 240 (January): 111705. https://doi.org/10.1016/j.rse.2020.111705.

Lu, Linlin, Qihao Weng, Da Xiao, Huadong Guo, Qingting Li, and Wenhua Hui. 2020. "Spatiotemporal Variation of Surface Urban Heat Islands in Relation to Land Cover Composition and Configuration: A Multi-Scale Case Study of Xi'an, China." *Remote Sensing* 12 (17). https://doi.org/10.3390/RS12172713.

McFeeters, S. K. 1996. "The Use of the Normalized Difference Water Index (NDWI) in the Delineation of Open Water Features." *International Journal of Remote Sensing* 17 (7): 1425–32. https://doi.org/10.1080/01431169608948714.

Mcgranahan, Gordon, and David Satterthwaite. 2014. "Urbanisation Concepts and Trends." *International Institute for Environment and Development*, no. June: 1–27.

Md Din, Mohd Fadhil. 2012. "Investigation of Heat Impact Behavior on Exterior Wall Surface of Building Material at Urban City Area." *Journal of Civil & Environmental Engineering* 02 (02). https://doi.org/10.4172/2165-784x.1000110.

Melin, Markus, C. Aurélie Shapiro, and Paul Glover-Kapfer. 2017. "Remote Sensing: Lidar." *WWF Conservation Technology Series 1(3)*, 40.

Misra, Prakhar, Ram Avtar, and Wataru Takeuchi. 2018. "Comparison of Digital Building Height Models Extracted from AW3D, TanDEM-X, ASTER, and SRTM Digital Surface Models over Yangon City." *Remote Sensing* 10 (12). https://doi.org/10.3390/rs10122008.

Mukul, Manas, Vinee Srivastava, Sridevi Jade, and Malay Mukul. 2017. "Uncertainties in the Shuttle Radar Topography Mission (SRTM) Heights: Insights from the Indian Himalaya and Peninsula." *Scientific Reports* 7 (February 2016): 1–10. https://doi.org/10.1038/srep41672.

Murdoch, Duncan, and Daniel Adler. 2022. "Rgl: 3D Visualization Using OpenGL."

https://cran.r-project.org/package=rgl. https://github.com/dmurdoch/rgl, https://dmurdoch.github.io/rgl/.

Nichol, Janet E. 1996. “High-Resolution Surface Temperature Patterns Related to Urban Morphology in a Tropical City: A Satellite-Based Study.” *Journal of Applied Meteorology*. https://doi.org/10.1175/1520-0450(1996)035<0135:HRSTPR>2.0.CO;2.

NOAA Coastal Services Center. 2012. “Lidar 101 : An Introduction to Lidar Technology , Data , and Applications.” *NOAA Coastal Services Center*, no. November: 76.

Nurwanda, Atik, and Tsuyoshi Honjo. 2018. “Analysis of Land Use Change and Expansion of Surface Urban Heat Island in Bogor City by Remote Sensing.” *ISPRS International Journal of Geo-Information* 7 (5): 165. https://doi.org/10.3390/ijgi7050165.

Peng, Shushi, Shilong Piao, Philippe Ciais, Pierre Friedlingstein, Catherine Ottle, François Marie Bréon, Huijuan Nan, Liming Zhou, and Ranga B. Myneni. 2012. “Surface Urban Heat Island across 419 Global Big Cities.” *Environmental Science and Technology* 46 (2): 696–703. https://doi.org/10.1021/es301811b.

R Core Team. 2020. “R: A Language and Environment for Statistical Computing.” R Foundation for Statistical Computing, Vienna, Austria. URL https://www.R-project.org/. https://www.r-project.org/.

Rad, H Rezaei, M Rafieian, and H Sozer. 2017. “Evaluating the Effects of Increasing of Building Height on Land Surface Temperature.” *Int. J. Urban Manage Energy Sustainability* 1 (1): 11–16.

Rahimi, Ehsan, Shahindokht Barghjelveh, and Pinliang Dong. 2021. “Quantifying How Urban Landscape Heterogeneity Affects Land Surface Temperature at Multiple

Scales." *Journal of Ecology and Environment* 45: 1–13.

Rahman, Md Mustafizur, Ram Avtar, Ali P. Yunus, Jie Dou, Prakhar Misra, Wataru Takeuchi, Netrananda Sahu, et al. 2020. "Monitoring Effect of Spatial Growth on Land Surface Temperature in Dhaka." *Remote Sensing* 12 (7). https://doi.org/10.3390/rs12071191.

Reinartz D'Angelo, P., Krauss, T., Chaabouni-Chouayakh, H., P. 2010. "DMS Generation and Filtering from High Resolution Optical Stereo Satellite Data." *30th EARSeL Symposium Remote Sensing for Science, Education and Cultural Heritage*, no. November 2014: 527–35.

Ren, Chao, Meng Cai, Xinwei Li, Yuan Shi, and Linda See. 2020. "Developing a Rapid Method for 3-Dimensional Urban Morphology Extraction Using Open-Source Data." *Sustainable Cities and Society* 53 (November 2019): 101962. https://doi.org/10.1016/j.scs.2019.101962.

Richards, Daniel, Mahyar Masoudi, Rachel R.Y. Oh, Erik S. Yando, Jingyuan Zhang, Daniel A. Friess, Adrienne Grêt-Regamey, Puay Yok Tan, and Peter J. Edwards. 2019. "Global Variation in Climate, Human Development, and Population Density Has Implications for Urban Ecosystem Services." *Sustainability (Switzerland)* 11 (22). https://doi.org/10.3390/su11226200.

RStudio Team. 2020. "RStudio: Integrated Development for R." RStudio, PBC, Boston, MA URL http://www.rstudio.com/.

Santillan, J. R., and M. Makinano-Santillan. 2016. "Vertical Accuracy Assessment of 30-M Resolution ALOS, ASTER, and SRTM Global DEMS over Northeastern Mindanao, Philippines." *International Archives of the Photogrammetry, Remote Sensing and Spatial Information Sciences - ISPRS Archives* 41 (June): 149–56. https://doi.org/10.5194/isprsarchives-XLI-B4-149-2016.

Santillan, Jojene R., Meriam Makinano-Santillan, Linbert C. Cutamora, and Jesiree L. Serviano. 2015. “3D Building Gis Database Generation from LiDAR Data and Free Online Web Maps and Its Application for Flood Hazard Exposure Assessment.” *ACRS 2015 - 36th Asian Conference on Remote Sensing: Fostering Resilient Growth in Asia, Proceedings*, no. May 2016.

Sekertekin, Aliihsan, and Stefania Bonafoni. 2020. “Land Surface Temperature Retrieval from Landsat 5, 7, and 8 over Rural Areas: Assessment of Different Retrieval Algorithms and Emissivity Models and Toolbox Implementation.” *Remote Sensing* 12 (2). https://doi.org/10.3390/rs12020294.

Shi, Ge, Jie Shan, Liang Ding, Peng Ye, Yang Li, and Nan Jiang. 2019. “Urban Road Network Expansion and Its Driving Variables: A Case Study of Nanjing City.” *International Journal of Environmental Research and Public Health* 16 (13): 2318. https://doi.org/10.3390/ijerph16132318.

Song, Juer, Shihong Du, Xin Feng, and Luo Guo. 2014. “The Relationships between Landscape Compositions and Land Surface Temperature: Quantifying Their Resolution Sensitivity with Spatial Regression Models.” *Landscape and Urban Planning* 123: 145–57. https://doi.org/10.1016/j.landurbplan.2013.11.014.

Stewart, I. D., and T. R. Oke. 2012. “Local Climate Zones for Urban Temperature Studies.” *Bulletin of the American Meteorological Society* 93 (12): 1879–1900. https://doi.org/10.1175/BAMS-D-11-00019.1.

Sun, Jing, and Suwit Ongsomwang. 2021. “Impact of Multitemporal Land Use and Land Cover Change on Land Surface Temperature Due to Urbanization in Hefei City, China.” *ISPRS International Journal of Geo-Information* 10 (12). https://doi.org/10.3390/ijgi10120809.

Sun, Tao, Ranhao Sun, and Liding Chen. 2020. “The Trend Inconsistency between Land

Surface Temperature and near Surface Air Temperature in Assessing Urban Heat Island Effects." *Remote Sensing* 12 (8). https://doi.org/10.3390/RS12081271.

Tadono, T., H. Nagai, H. Ishida, F. Oda, S. Naito, K. Minakawa, and H. Iwamoto. 2016. "Generation of the 30 M-MESH Global Digital Surface Model by Alos Prism." *International Archives of the Photogrammetry, Remote Sensing and Spatial Information Sciences - ISPRS Archives* 41 (July): 157–62. https://doi.org/10.5194/isprsarchives-XLI-B4-157-2016.

Takaku, Junichi, Takeo Tadono, and Ken Tsutsui. 2014. "Generation of High Resolution Global DSM from ALOS PRISM." *International Archives of the Photogrammetry, Remote Sensing and Spatial Information Sciences - ISPRS Archives* 40 (4): 243–48. https://doi.org/10.5194/isprsarchives-XL-4-243-2014.

The World Bank. 2016a. "Indonesia's Urban Story." *June 14, 2016*, 2016–18. http://www.worldbank.org/en/news/feature/2016/06/14/indonesia-urban-story.

———. 2016b. "Indonesia's Urban Story." *The World Bank*. Jakarta.

Thomlinson, John R., Paul V. Bolstad, and Warren B. Cohen. 1999. "Coordinating Methodologies for Scaling Landcover Classifications from Site-Specific to Global: Steps toward Validating Global Map Products." *Remote Sensing of Environment* 70 (1): 16–28. https://doi.org/10.1016/S0034-4257(99)00055-3.

Tian, Jiaojiao, Shiyong Cui, and Peter Reinartz. 2014. "Building Change Detection Based on Satellite Stereo Imagery and Digital Surface Models." *IEEE Transactions on Geoscience and Remote Sensing* 52 (1): 406–17. https://doi.org/10.1109/TGRS.2013.2240692.

Tomljenovic, Ivan, Bernhard Höfle, Dirk Tiede, and Thomas Blaschke. 2015. "Building Extraction from Airborne Laser Scanning Data: An Analysis of the State of the Art." *Remote Sensing* 7 (4): 3826–62. https://doi.org/10.3390/rs70403826.

U.S. Geological Survey. 2019. “Landsat 8 Data Users Handbook.” *Nasa* 8 (November): 114. https://landsat.usgs.gov/documents/Landsat8DataUsersHandbook.pdf.

UCL. 2017. “High-Rise Buildings Much More Energy-Intensive than Low-Rise | UCL News - UCL – University College London.” https://www.ucl.ac.uk/news/2017/jun/high-rise-buildings-much-more-energy-intensive-low-rise.

United Nations, Department of Economic and Social Affairs, Population Division. 2018. “The World ’s Cities in 2018.” *The World’s Cities in 2018 - Data Booklet (ST/ESA/ SER.A/417),* 34.

USGS. 2016. *Landsat 8 (L8) Data Users Handbook Version 2.0*. *USGS Landsat User Service*. https://doi.org/http://www.webcitation.org/6mu9r7riR.

———. 2020. “USGS EROS Archive - Digital Elevation - Shuttle Radar Topography Mission (SRTM) Void Filled.” Earth Resources Observation and Science (EROS) Center. 2020. https://doi.org/10.5066/F7PR7TFT.

Vermote, Eric, Chris Justice, Martin Claverie, and Belen Franch. 2016. “Preliminary Analysis of the Performance of the Landsat 8/OLI Land Surface Reflectance Product.” *Remote Sensing of Environment* 185: 46–56. https://doi.org/10.1016/j.rse.2016.04.008.

Voogt, J. A., and T. R. Oke. 2003. “Thermal Remote Sensing of Urban Climates.” *Remote Sensing of Environment* 86 (3): 370–84. https://doi.org/10.1016/S0034-4257(03)00079-8.

Wandira, Puspitasari Ayu, and Kwon Jongwook. 2017. “The Influence of Tall Buildings to the Modern Urban Landscape of Jakarta City.” *UIA 2017 Seoul World Architects Congress,* no. October: 0–6.

Wang, Meiya, and Hanqiu Xu. 2021. “The Impact of Building Height on Urban Thermal

Environment in Summer: A Case Study of Chinese Megacities." *PLoS ONE* 16 (4 April): 1–15. https://doi.org/10.1371/journal.pone.0247786.

Wong, K. M.Grace. 2004. "Vertical Cities as a Solution for Land Scarcity: The Tallest Public Housing Development in Singapore." *Urban Design International* 9 (1): 17–30. https://doi.org/10.1057/palgrave.udi.9000108.

Yang, Xinyan, and Yuguo Li. 2015. "The Impact of Building Density and Building Height Heterogeneity on Average Urban Albedo and Street Surface Temperature." *Building and Environment* 90: 146–56. https://doi.org/10.1016/j.buildenv.2015.03.037.

Yang, Xinyan, Yuguo Li, Zhiwen Luo, and Pak Wai Chan. 2017. "The Urban Cool Island Phenomenon in a High-Rise High-Density City and Its Mechanisms." *International Journal of Climatology* 37 (2): 890–904. https://doi.org/10.1002/joc.4747.

Zhang, Keqi, Jianhua Yan, and Shu Ching Chen. 2006. "Automatic Construction of Building Footprints from Airborne LIDAR Data." *IEEE Transactions on Geoscience and Remote Sensing* 44 (9): 2523–33. https://doi.org/10.1109/TGRS.2006.874137.

Zhao, Chunhong, Qihao Weng, and Anna M. Hersperger. 2020. "Characterizing the 3-D Urban Morphology Transformation to Understand Urban-Form Dynamics: A Case Study of Austin, Texas, USA." *Landscape and Urban Planning* 203 (October 2019): 103881. https://doi.org/10.1016/j.landurbplan.2020.103881.

Zheng, Zhong, Weiqi Zhou, Jingli Yan, Yuguo Qian, Jia Wang, and Weifeng Li. 2019. "The Higher, the Cooler? Effects of Building Height on Land Surface Temperatures in Residential Areas of Beijing." *Physics and Chemistry of the Earth* 110 (November 2018): 149–56. https://doi.org/10.1016/j.pce.2019.01.008.

Zhu, Zhe, and Curtis E Woodcock. 2012. “Remote Sensing of Environment Object-Based Cloud and Cloud Shadow Detection in Landsat Imagery.” *Remote Sensing of Environment* 118: 83–94. https://doi.org/10.1016/j.rse.2011.10.028.

APPENDIX

Thesis Review PowerPoint Handout (Presented on 22nd July 2022)

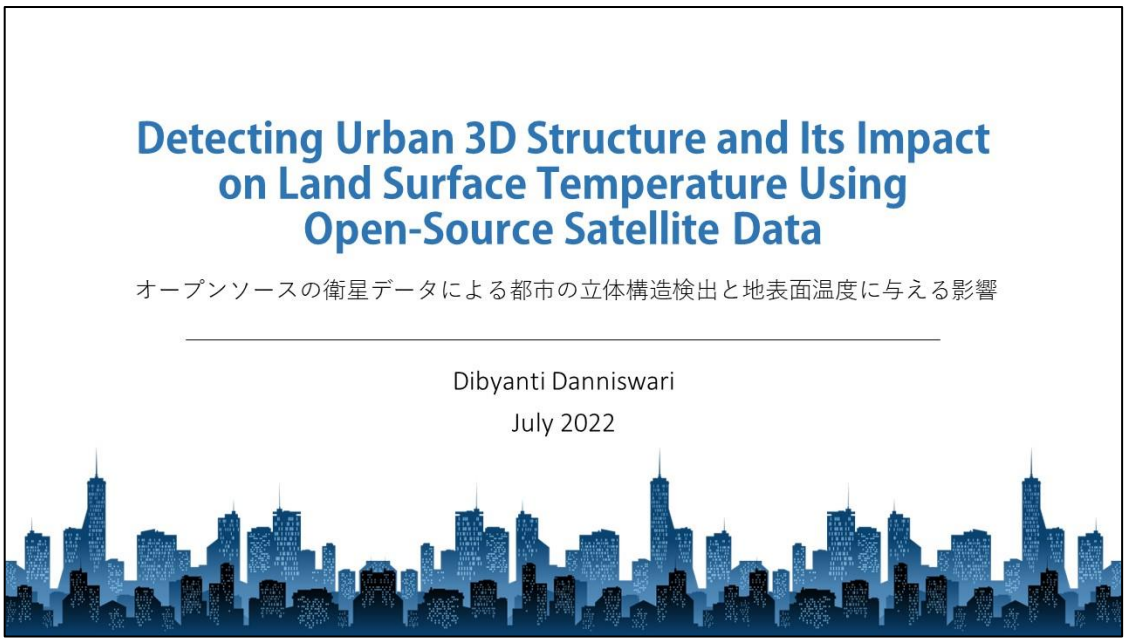

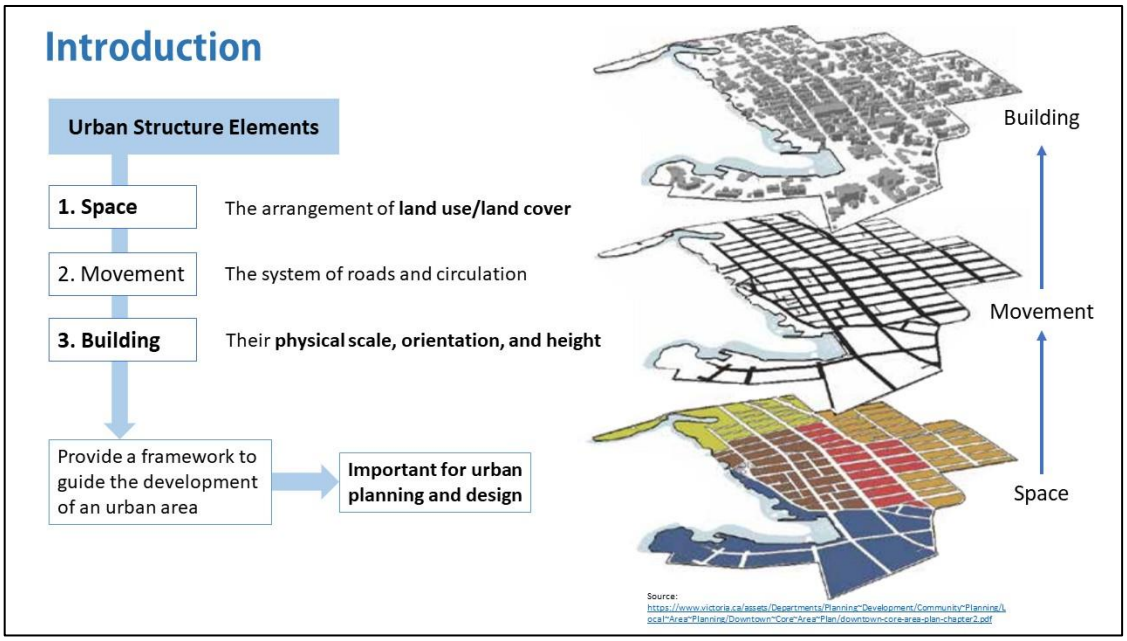

Introduction

Space
(Land use/land cover)

Building
(Height)

Known to affect land surface temperature

Urban Heat Island

General study objective:
To analyze how land use/land cover and building height affecting the land surface temperature

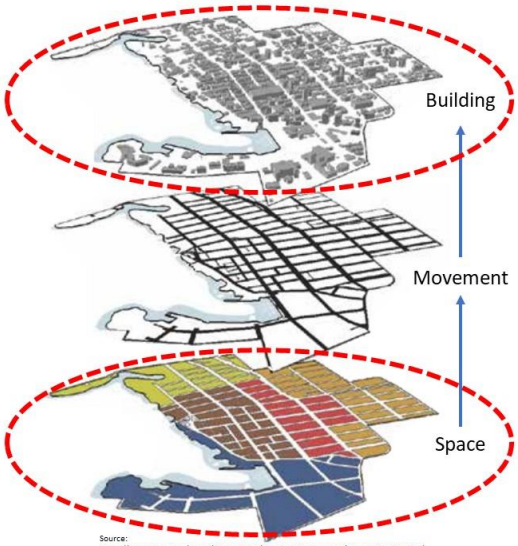

Source:
https://www.victoria.ca/assets/Departments/Planning~Development/Community~Planning/Local~Area~Planning/Downtown~Core~Area~Plan/downtown-core-area-plan-chapter2.pdf

Introduction

Urban Structure and Land Surface Temperature

Focus of Study 1	Focus of Study 2	Focus of Study 3
To analyze the impact of **land cover change** on land surface temperature	**To obtain building height** data with a simple method from open-source data	To analyze the impact of **building height** on land surface temperature
Open-source input data are relatively **easy** to obtain	Bridge the studies	Open-source input data are **difficult** to obtain

Overview of The Study

	Study 1	Study 2	Study 3	
			Study case: 6 cities	Study case: 2 cities
Objective	Analyzing the impact of land cover change on LST in Jakarta and its satellite cities	Deriving building height with a simple method (AW3D30 - SRTM)	Analyzing relationship between building height and land surface temperature (closer observation in Tokyo and Jakarta)	
Study area	Jakarta, Bogor, Depok, Tangerang, Bekasi	Tokyo	Tokyo, Beijing, Jakarta, New York, Chicago, Los Angeles	Tokyo, Jakarta
Data collection	Land cover: 1. Landsat 5 visual band 2. Landsat 8 visual band Surface temperature: Landsat 5 thermal band Landsat 8 thermal band	Satellite DCHM: 1. AW3D30 2. SRTM LiDAR DCHM: 1. LiDAR DSM 2. LiDAR DTM	Building height: 1. AW3D30 2. SRTM Surface temperature: 1. Landsat 8 LST Veg. & water mask: 1. Landsat 8 NDVI 2. Landsat 8 NDWI	Building height: 1. AW3D30 2. SRTM Surface temperature: Landsat 5 LST Veg. & water mask: 1. Landsat 5 NDVI 2. Landsat 5 NDWI
Data analysis	1. Land cover classification 2. Accuracy assessment 3. Comparison between LST of different land covers	1. 2D and 3D visualization 2. Smoothing filter 3. Correlation and regression between Satellite DCHM and LiDAR DCHM	1. 2D and 3D visualization 2. Correlation and regression between Satellite DCHM and LST	1. 2D and 3D visualization 2. Smoothing filter 3. Correlation and regression between Satellite DCHM and LST
Tools	QGIS and ArcGIS	Data collection: Google Earth Engine (GEE) Data analysis: R		

5

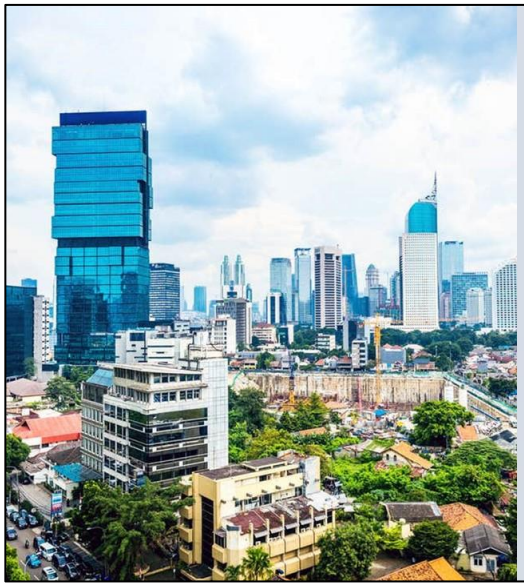

Study 1:

Land Cover Change Impacts on Land Surface Temperature

(Case of Jakarta and Its Satellite Cities)

6

Background

Land cover change ← **Jakarta is a rapidly growing city**

Affecting Land Surface Temperature

Urban development spreads to the surrounding cities

The relationship has been widely observed

Urban development causes urban heat island?

Lack of studies in Jakarta and its surrounding/satellite cities

Question: **How does land cover change affect the land surface temperature in rapidly-growing cities such as Jakarta and its satellite cities?**

7

Objective

Analyzing the impact of land cover change on land surface temperature in Jakarta and its satellite cities

8

Methods Framework

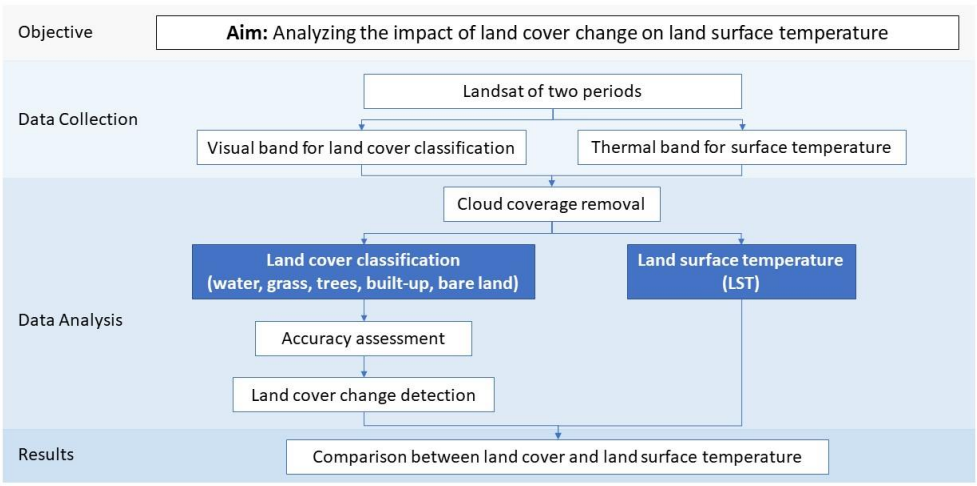

Methods

Study area and materials

- The study area includes **Jakarta** and its 3 directly connected satellite cities: **Tangerang, Bekasi, and Depok**
- We used Landsat satellite imagery. Patching was needed when the main image is cloudy
- **Two datasets each city:** year **1989**/1990; **2015**/2018

City	Image Acquisition Date				Sensor	Bands
	Main Imagery		Patch			
	Year	Date	Year	Date		
Jakarta	1990	9 Jul	1990	6 Jun	Landsat-5	1-5 & 7
	2015	31 Aug	2014	13 Sep	Landsat-8	2-7
Depok	1989	6 Jul	No cloud		Landsat-5	1-5 & 7
	2018	1 Apr	No cloud		Landsat-8	2-7
Tangerang	1989	6 Jul	1989	12 Jun	Landsat-5	1-5 & 7
	2015	31 Aug	2014	13 Sep	Landsat-8	2-7
Bekasi	1989	6 Jul	No cloud		Landsat-5	1-5 & 7
	2015	31 Aug	No cloud		Landsat-8	2-7

10

Methods

1. Cloud Patching

- The cloudy parts were removed using ***Fmask* function**
- After that, the cloud coverage is patched with the nearest date clear satellite image

2. Land Cover Classification

- We classified the land cover into **five** categories:
  1. **Water**
  2. **Grass (low vegetation)**
  3. **Trees (high vegetation)**
  4. **Built-up**
  5. **Bare land**
- **Supervised classification** in **QGIS**, Semi-Automatic Classification plug-in, **maximum likelihood** algorithm

3. Accuracy assessment

- For every city's land cover map, we created a layer of **50 to 70 random points** in Arc GIS, then the value is compared to Google Earth historical imagery

4. Land Cover Change Detection

- The change was detected by a **post-classification comparison**, a pixel-based technique
- We **reclassified** the raster value of the maps and then multiplied the maps to generate unique number so each change can be detected

11

Results - Land Cover Change

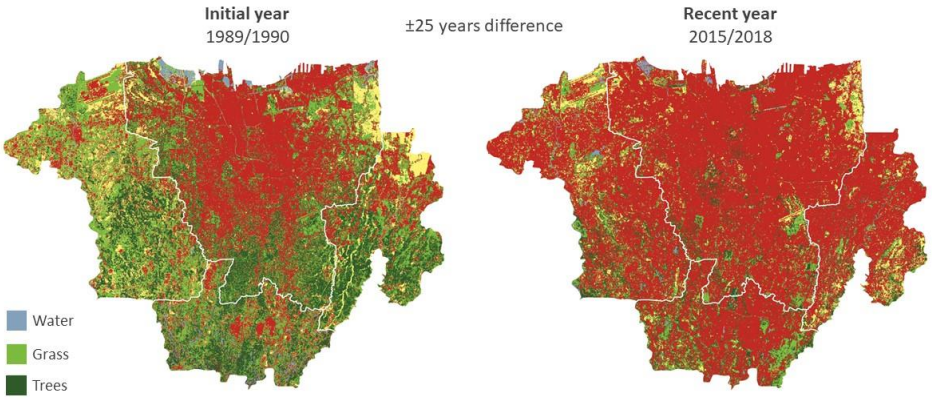

- Results exceed the target overall accuracy of 85% with no class under 70% accurate
- Overall Kappa Statistics > 0.8

Results - Land Cover Change

Land cover proportions of each city in different periods

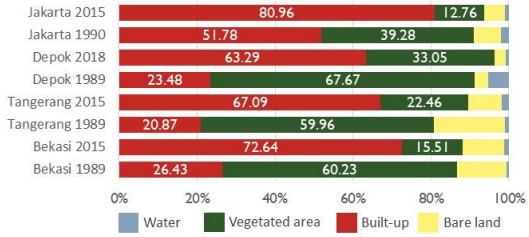

City	Total Area (ha)	Built-up Expansion Past to Recent (ha)	Expansion Proportion* (100%-total area each city	Average expansion per year (ha/year)
Jakarta	65,265.30	19,042.56	29.18%	761.70
Depok	20,104.20	8,003.34	39.81%	275.98
Tangerang	34,813.44	16,092.81	46.23%	618.95
Bekasi	21,442.68	9,910.17	46.22%	381.16

*100% = the total area of each city

- In terms of total area and average expansion per year, **Jakarta had the highest** expansion
- In terms of proportion, **Tangerang had the highest** expansion

Results - Land Cover Change

Total area and proportion of each land cover type that is converted to the built-up area

Land cover	Built-up Jakarta (2015)		Built-up Depok (2018)		Built-up Tangerang (2015)		Built-up Bekasi (2015)	
	Hectares	%	Hectares	%	Hectares	%	Hectares	%
Water	836.19	1.28	452.88	2.25	73.80	0.21	63.90	0.30
Grass	8,950.32	13.71	4,394.79	21.86	8,703.99	25.00	4,253.76	19.84
Trees	8,595.90	13.17	4,069.26	20.24	4,736.52	13.61	4,366.08	20.36
Bare land	2,909.70	4.46	458.55	2.28	3,868.56	11.11	1,894.23	8.83

*100% = the total area of each city

The expansion of the built-up area seemed to happen mostly at the expense of the vegetated area in every city

Results - Land Surface Temperature (LST)

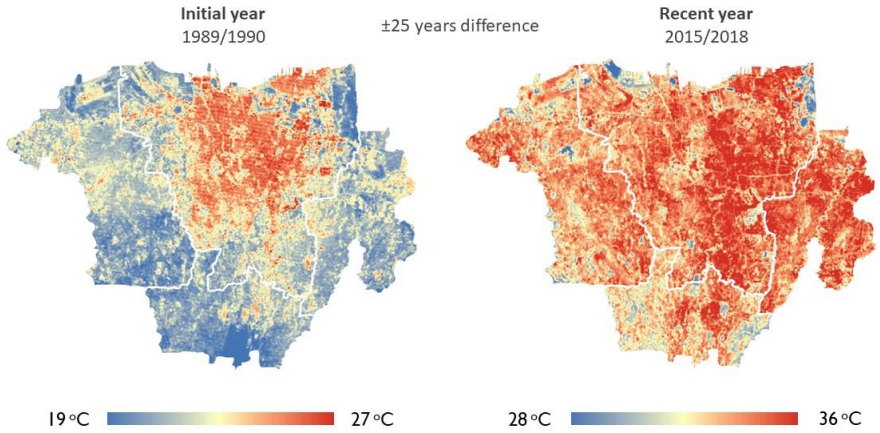

15

Results - The impact of land cover change on LST

Mean land surface temperature (LST) of each city for each land cover type

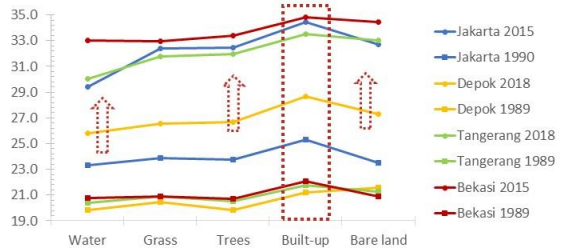

- The LST increased significantly
- The **temperature of the built-up** area was the **highest** among the land cover types

Mean LST of each land cover type

Land cover	Jakarta (°C)		Depok (°C)		Tangerang (°C)		Bekasi (°C)	
	1990	2015	1989	2018	1989	2015	1989	2015
Water	23.29	29.44	19.86	25.81	20.40	30.03	20.79	33.00
Grass	23.85	32.41	20.44	26.55	20.89	31.76	20.91	32.98
Trees	23.76	32.43	19.85	26.70	20.49	31.96	20.68	33.38
Built-up	25.29	34.45	21.21	28.69	21.73	33.52	22.09	34.82
Bare land	23.53	32.72	21.55	27.27	21.27	33.01	20.88	34.46
Mean	23.95	32.29	20.58	27.01	20.96	32.05	21.07	33.73

- In the **initial year, Jakarta had the highest** mean LST
- In the **recent year, Bekasi had the highest** mean LST

16

Summary

1. Built-up area expanded from Jakarta to the surrounding cities
2. The increase of LST is highly affected by the land conversion to the built-up area
3. Jakarta had the largest built-up expansion, but the highest LST increase is found in Bekasi.

17

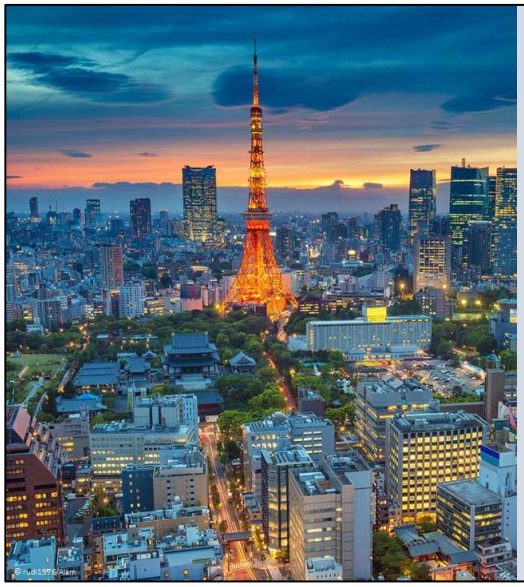

Study 2:

Extracting Building Height from Open Global Datasets

18

Important Definitions

Digital Surface Model (DSM)

subtract

Digital Terrain Model (DTM)

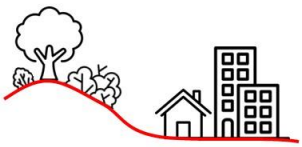

Digital Canopy Height Model (DCHM)

Digital Building Height Model (DBHM)

19

Background

Building Height

- Known to affect general environmental quality, including urban heat island and land surface temperature
- Obtained from airborne vehicle or satellite data → **Difficult to obtain**

Why?

1. Obtaining the accurate data is **expensive**
2. Extracting from open-source data requires **complex calculations**
3. Some countries' data are restricted for **government-use only**

Question:

Is there any simpler method to obtain building height from open-source data?

20

Background

Open global datasets

AW3D30

ALOS World 3D 30m, JAXA

Made from stereo image of visible band

SRTM

Shuttle Radar Topography Mission, NASA

Made from radar data

AW3D30 - SRTM = DCHM ?

If Yes → Almost no study that examines the possibility

Simple and useful

DCHM: Digital Canopy Height Model

21

Objective

To examine whether building height can be extracted from AW3D30 and SRTM

22

Methods Framework

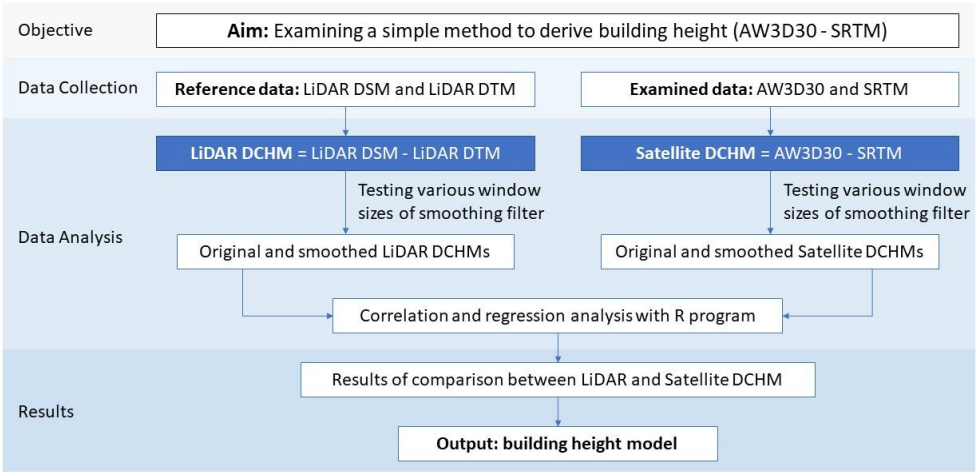

Methods

Study area

- Center part of Tokyo
- 20 km x 18 km

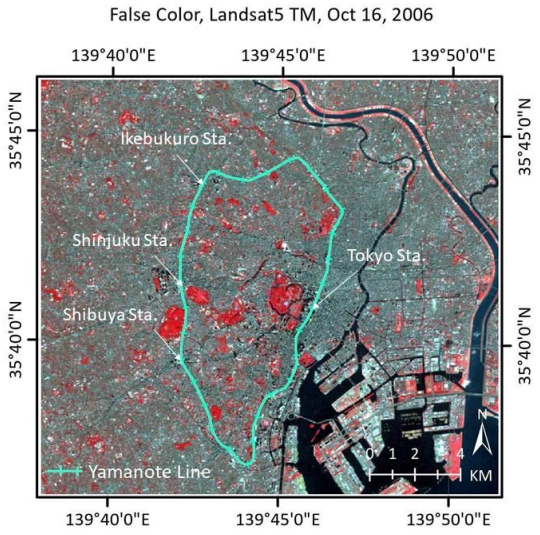

24

Methods

Data

Reference data:
1. LiDAR DSM
2. LiDAR DTM

Examined satellite data:
1. AW3D30
2. SRTM

- Airborne LiDAR data are provided by Kanto Regional Dev. Bureau
- Satellite data are downloaded from Google Earth Engine

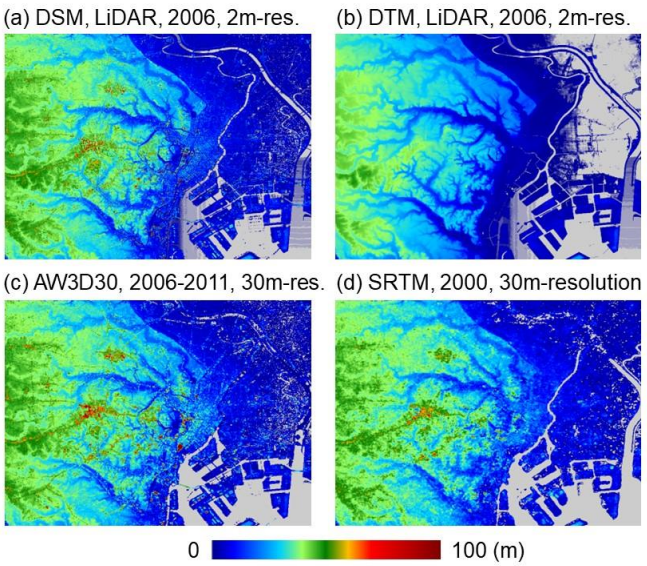

DCHM: Digital Canopy Height Model
DSM: Digital Surface Model
DTM: Digital Terrain Model

25

Methods

LiDAR DCHM =
DSM – DTM

Satellite DCHM =
AW3D30 – SRTM

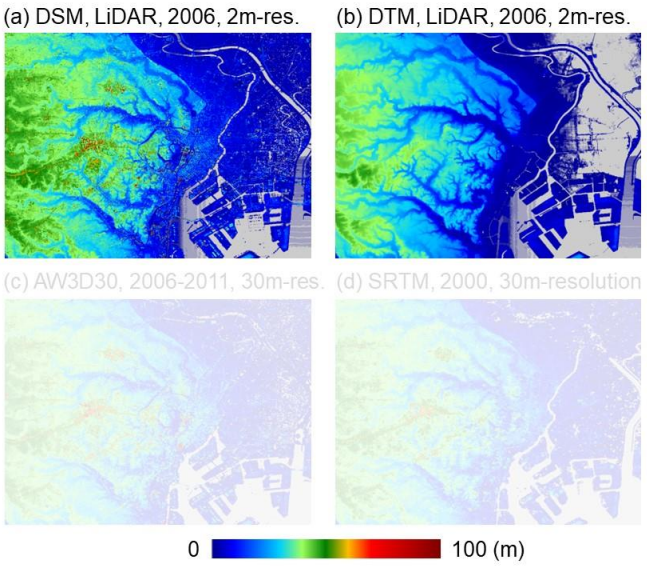

DCHM: Digital Canopy Height Model
DSM: Digital Surface Model
DTM: Digital Terrain Model

26

Methods

LiDAR DCHM = DSM – DTM

(a) DSM, LiDAR, 2006, 2m-res.

(b) DTM, LiDAR, 2006, 2m-res.

(c) AW3D30, 2006-2011, 30m-res.

(d) SRTM, 2000, 30m-resolution

Satellite DCHM = AW3D30 – SRTM

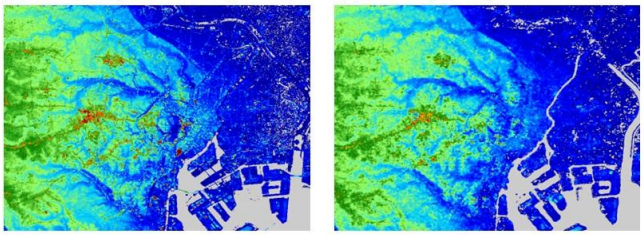

0 100 (m)

DCHM: Digital Canopy Height Model
DSM: Digital Surface Model
DTM: Digital Terrain Model

27

Methods

Cross-section images

(a) DSM

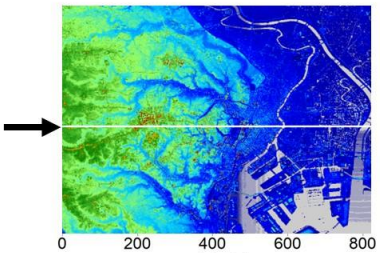

0 100 (m)

DCHM: Digital Canopy Height Model
DSM: Digital Surface Model
DTM: Digital Terrain Model

(b) Digital Surface Model and Digital Terrain Model

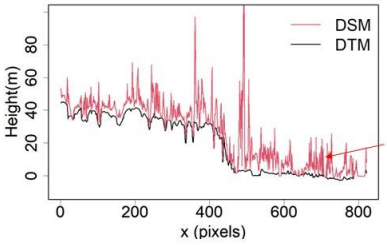

DSM higher than DTM

(c) AW3D30 and SRTM

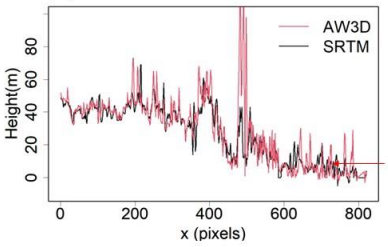

Overlapping

28

Methods

Smoothing

- The images are smoothed to avoid large error during the pixel-by-pixel analysis and to improve the spatial alignment between LiDAR DCHM and Satellite DCHM
- Smoothing window size is (2n+1) x (2n+1)
- Window size from n=0 to n=10 were tested

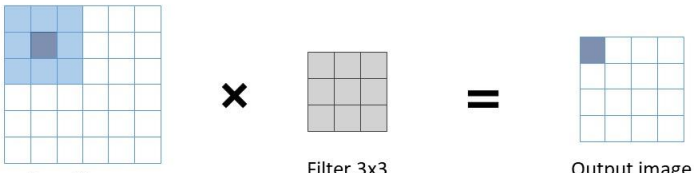

Input image × Filter 3x3 (n=1) = Output image (1 pixel value = average of 9 pixel)

29

Results - Detected Information in LiDAR and Satellite DCHM

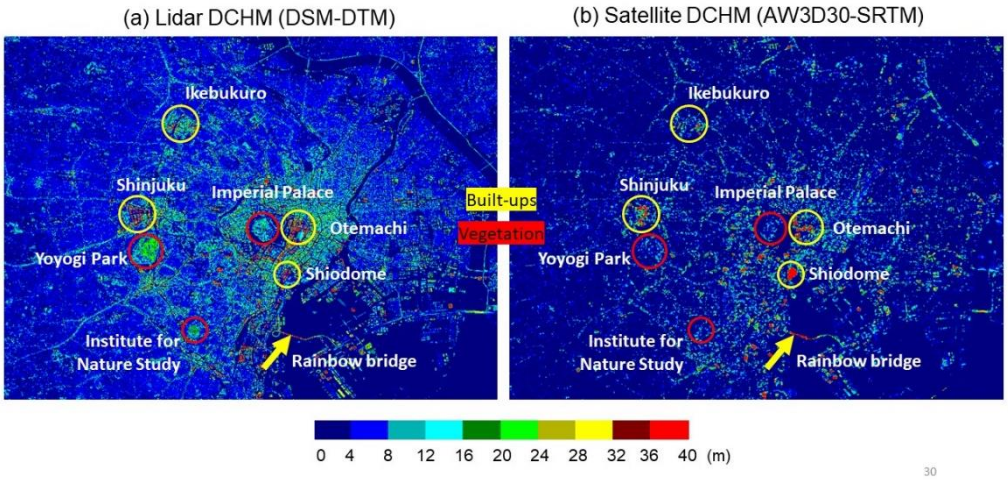

30

Results - Detected Information in LiDAR and Satellite DCHM

Cross-section images

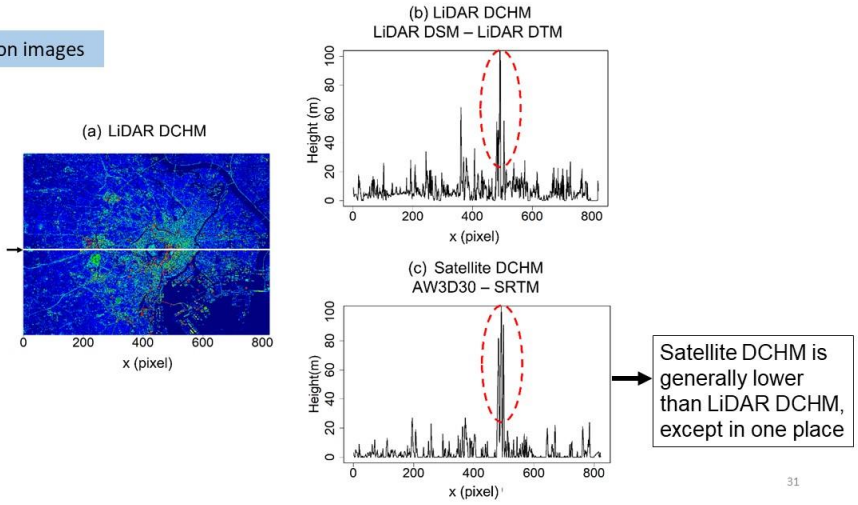

Satellite DCHM is generally lower than LiDAR DCHM, except in one place

31

Results - 3D Visualization

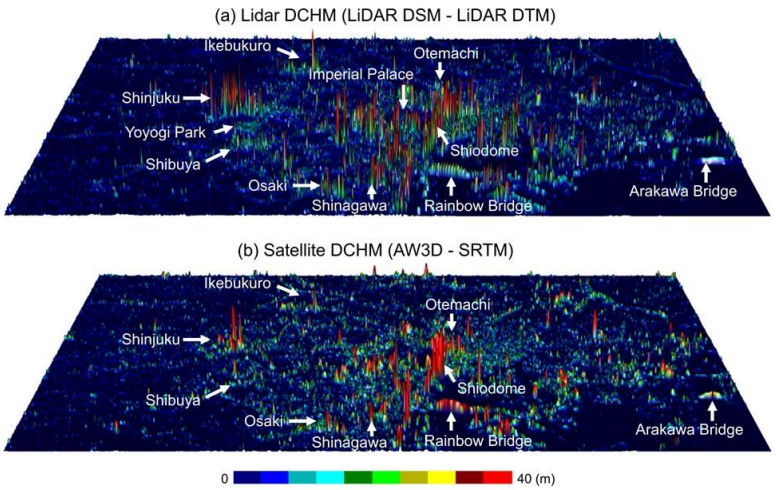

32

Results - Comparison between LiDAR and Satellite DCHM

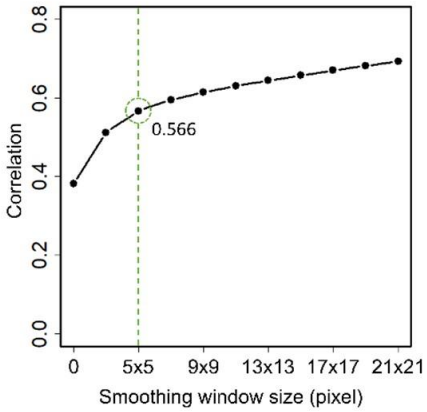

The correlation increase is slower and nearly become constant as the window size becomes bigger

Optimal value at window 5x5 pixel or 150x150 m

33

Results - Comparison between LiDAR and Satellite DCHM

Smoothing window size = 5 x 5 pixel (n = 2)

(a) Lidar DCHM (DSM-DTM)

(b) Satellite DCHM (AW3D-SRTM)

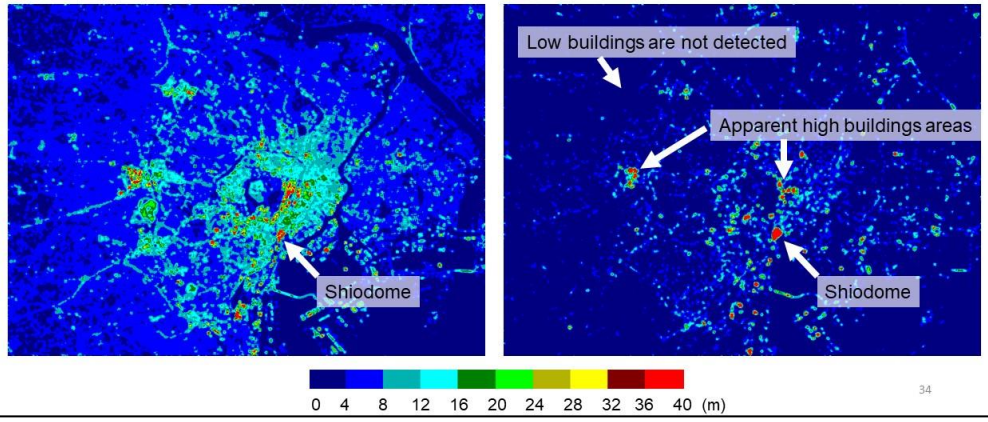

34

Results - Comparison between LiDAR and Satellite DCHM

Original resolution

Scattering, no strong correlation

Satellite DCHM < LiDAR DCHM

The values of Satellite DCHM are about half of LiDAR DCHM

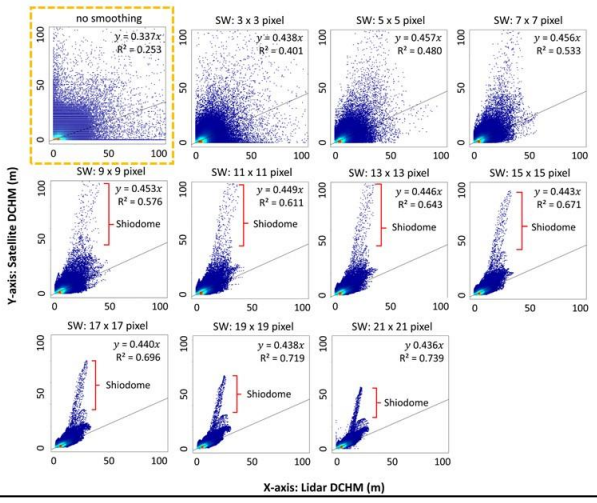

There are uncertainties in Shiodome area

Correlation increases as the smoothing window size becomes bigger

35

Summary

1	Satellite DCHM (AW3D30 – SRTM) and LiDAR DCHM (LiDAR DSM – DTM) shows a good similarity
2	Satellite DCHM does not detect vegetation well
3	Correlation between LiDAR and Satellite DCHM increases as smoothing window becomes bigger. Smoothing window of 5 x 5 pixel or 150 x 150 m shows optimal correlation value

Although Satellite DCHM has a limitation, it gives valuable height information when LiDAR DCHM is not available due to economic or technical reasons

36

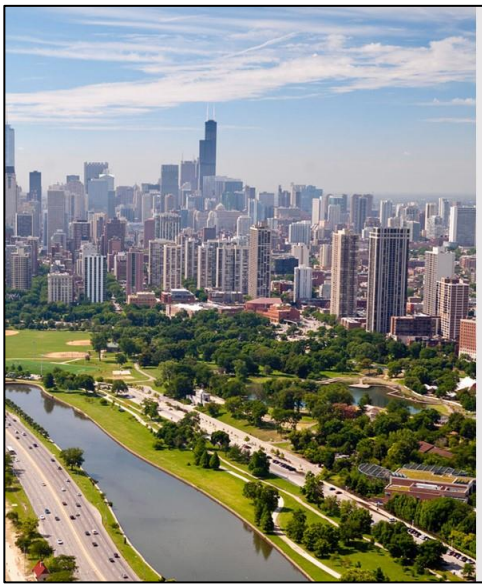

Study 3:

Analyzing the Relationship between Building Height and Land Surface Temperature

37

Background

Building height

Existing studies show mixed results on how building height affect the temperature

Increase land surface temperature (LST)?
- High anthropogenic heat
- Extensive impervious surface

Decrease land surface temperature (LST)?
- Large building shadow
- Reflective material
- Vegetation near the building

Question: **Does building height increase or decrease the temperature?**

Existing studies mostly only analyze a small region due to the limitation of available building height data → By using the previously presented building height extraction method → can analyze global cities → **advancement** from existing studies

38

Objective

To analyze the relationship between land surface temperature and building height, and to clarify whether high-rise buildings tend to increase or decrease land surface temperature

39

Methods Framework

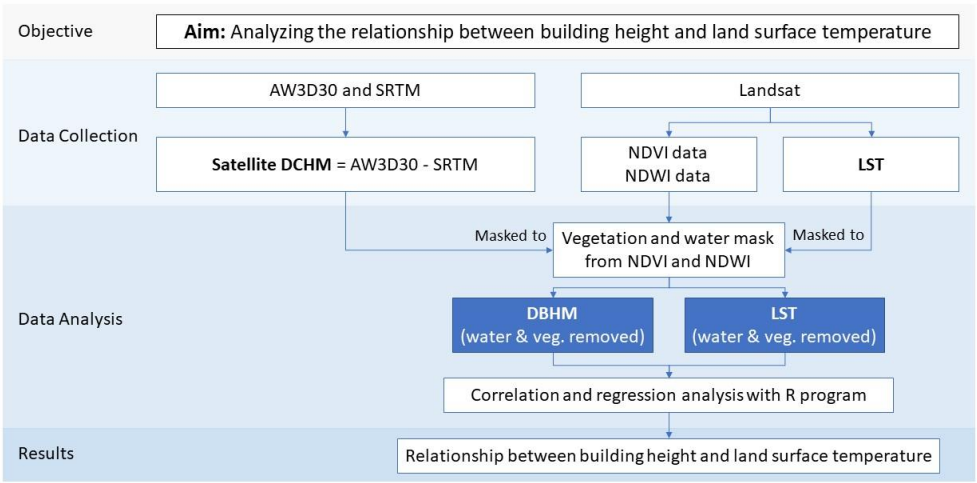

Methods - Study Area

Six urban areas in Tokyo, Beijing, Jakarta, Los Angeles, New York, Chicago

The size is 0.1 × 0.1 degrees in longitude and latitude each

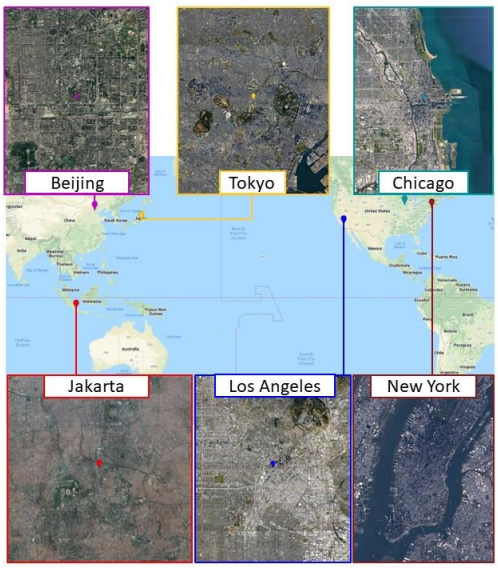

Methods - Data

Table of used Land Surface Temperature data (Landsat 8)

Area / Time*	Dates used (March –Oct)
Tokyo 10:15	2013/09/17, 2014/05/31, 2015/03/31, 2015/10/09, 2017/03/20, 2018/10/01
Beijing 10:55	2013/10/03, 2014/09/04, 2017/05/07, 2017/07/10, 2017/09/12, 2017/09/28
Jakarta 10:00	2019/09/11, 2018/07/06, 2019/07/25, 2014/09/13, 2020/04/22, 2015/08/31
Los Angeles 10:30	2016/09/26, 2018/08/31, 2019/07/01, 2014/06/01, 2018/09/16, 2015/06/20,
New York 10:40	2017/07/30, 2013/06/01, 2016/06/09, 2015/06/07, 2017/06/12, 2014/07/06
Chicago 10:30	2014/09/23, 2014/07/21, 2017/09/15, 2020/07/05, 2014/05/18, 2016/05/23

Warm season

Temperature difference is more apparent

Composited

Each city is composited to avoid single data error

42

Methods - Vegetation and Water Mask

Vegetation and water coverages were removed using masks to minimize the bias

- Vegetation mask → binarized Normalized Difference Vegetation Index (NDVI)
- Water mask → binarized Normalized Difference Water Index (NDWI)
- Thresholds were decided after comparing the binarized NDVI and NDWI images with Google Earth image

Vegetation mask (NDVI threshold 0.4)

Water mask (NDWI threshold 0.1)

Vegetation and Water Mask (**White color: removed area**)

43

Results - LST and DBHM Comparison

Tokyo → Low LST area corresponds well with high buildings area

Land surface temperature

Digital building height model

Landsat true color

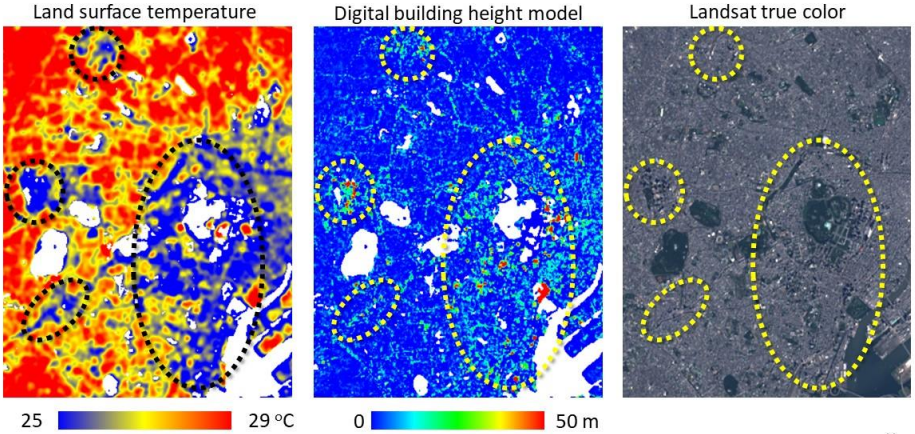

25 29 °C

0 50 m

44

Results - LST and DBHM Comparison

Tokyo

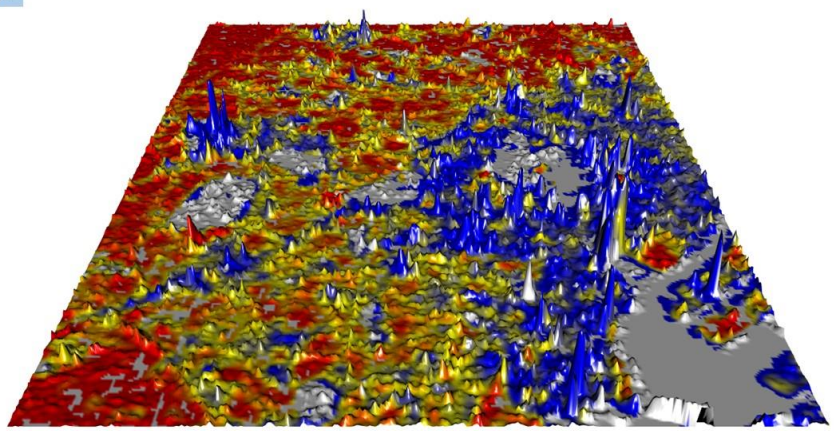

25 29 °C

45

Results - LST and DBHM Comparison

Beijing → Low LST area corresponds well with high buildings area

Land surface temperature

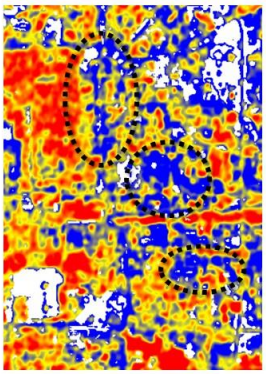

28 32 °C

Digital building height model

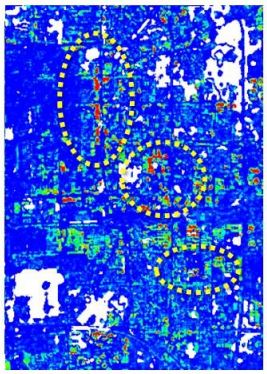

0 50 m

Landsat true color

46

Results - LST and DBHM Comparison

Beijing

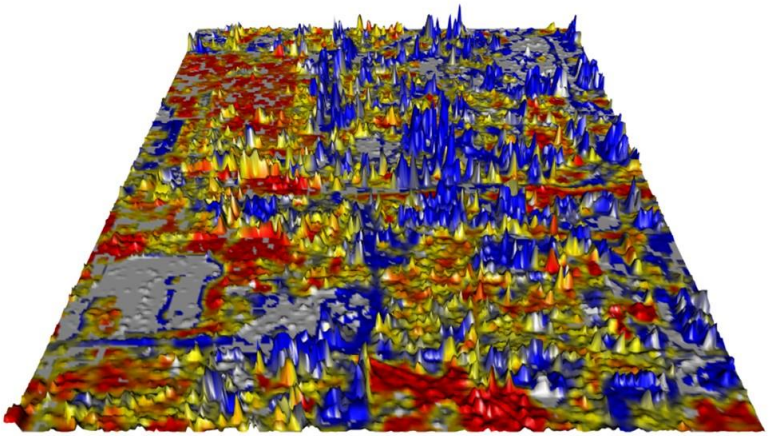

28 32 °C

47

Results - LST and DBHM Comparison

Jakarta → Low LST area corresponds well with high buildings area

Land surface temperature | Digital building height model | Landsat true color

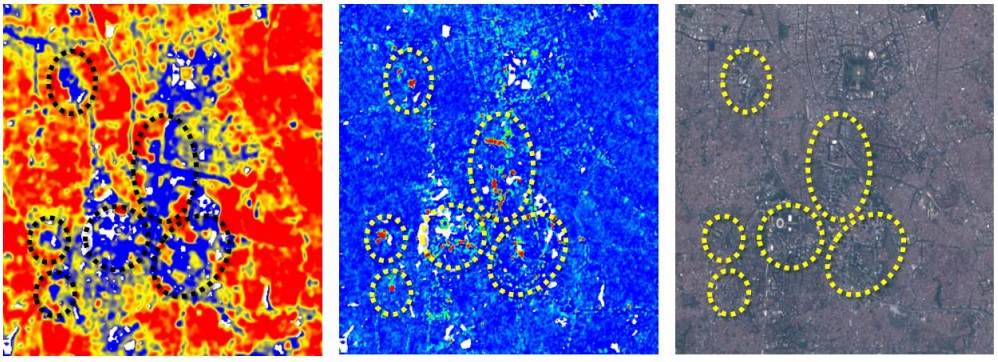

25 29 °C 0 50 m

48

Results - LST and DBHM Comparison

Jakarta

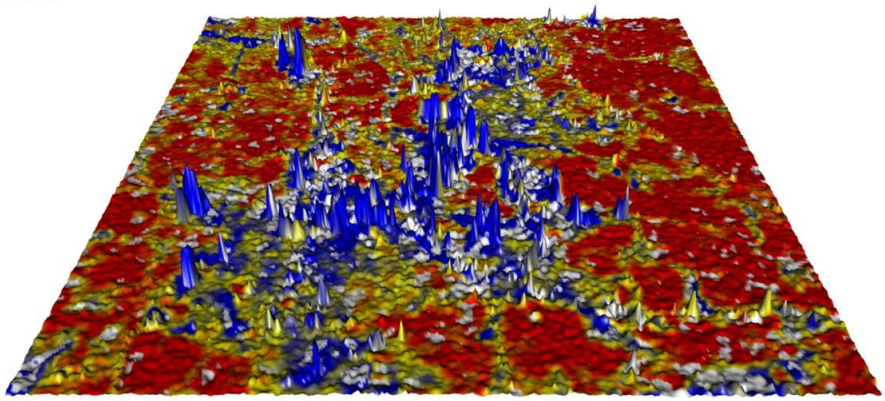

25 29 °C

49

Results - LST and DBHM Comparison

- Other cities show similar tendency
- Only the 3D visualization is presented

Los Angeles

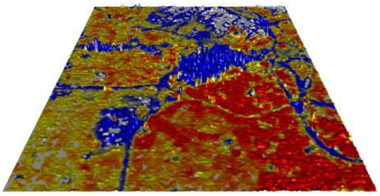

Chicago

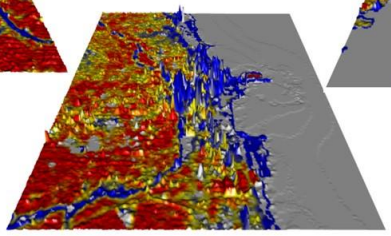

New York

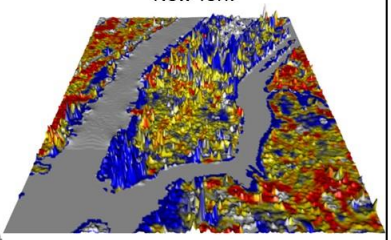

50

Results - Relationship between LST and DBHM

Pearson's correlation analysis results

Area	Pearson's Correlation Coefficient	Number of analyzed pixels
Tokyo	-0.2474	114,818
Beijing	-0.2282	107,797
Jakarta	-0.2973	137,641
Los Angeles	-0.1535	117,750
New York	-0.0885	106,964
Chicago	-0.1667	104,813

Regression analysis results

Area	Regression Equation
Tokyo	LST = 27.2938 - 0.0456 × DBHM
Beijing	LST = 29.8596 - 0.0331 × DBHM
Jakarta	LST = 33.1949 - 0.0489 × DBHM
Los Angeles	LST = 41.1800 - 0.0654 × DBHM
New York	LST = 29.4429 - 0.0143 × DBHM
Chicago	LST = 28.3656 - 0.0314 × DBHM

Negative relationship → Land surface temperature ↓ when building height ↑

These results are statistically significant at the 0.05 level

LST: Land Surface Temperature
DBHM: Digital Building Height Model

51

Results - Relationship between LST and DBHM

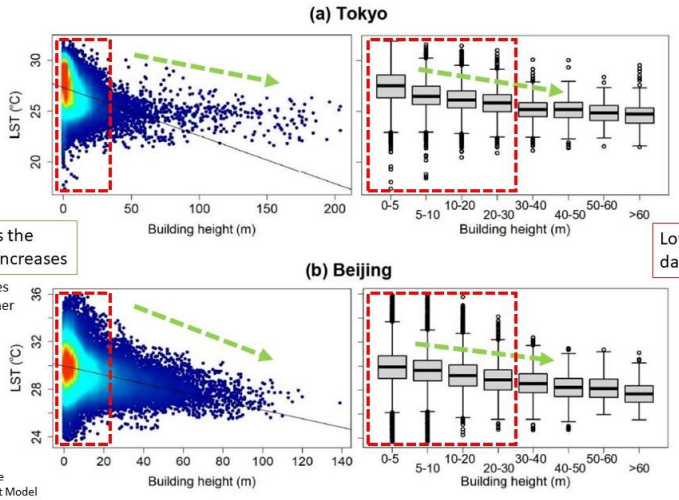

LST decreases as the building height increases

The decrease becomes less significant in higher classes

Lower building height data is more deviated

LST: Land Surface Temperature
DBHM: Digital Building Height Model

52

Results - Relationship between LST and DBHM

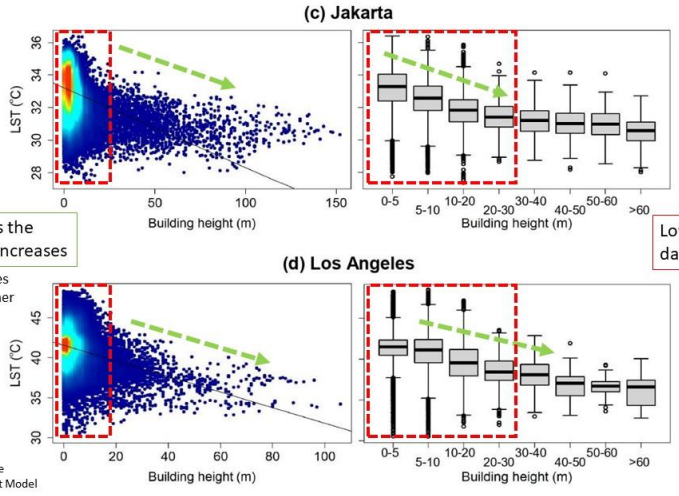

LST decreases as the building height increases

The decrease becomes less significant in higher classes

Lower building height data is more deviated

LST: Land Surface Temperature
DBHM: Digital Building Height Model

53

Results - Relationship between LST and DBHM

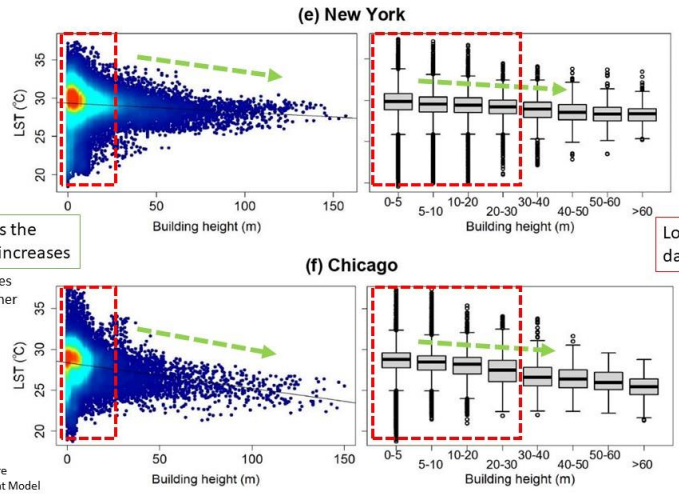

LST decreases as the building height increases

The decrease becomes less significant in higher classes

Lower building height data is more deviated

LST: Land Surface Temperature
DBHM: Digital Building Height Model

54

Results - Sampling of Smaller Areas

→ To observe the effect more clearly

Three sample areas in Tokyo and Jakarta
→ Cities with contrasting climate

1. Low-rise buildings
2. Mixed-height buildings
3. High-rise buildings

Size: 600 x 600 m

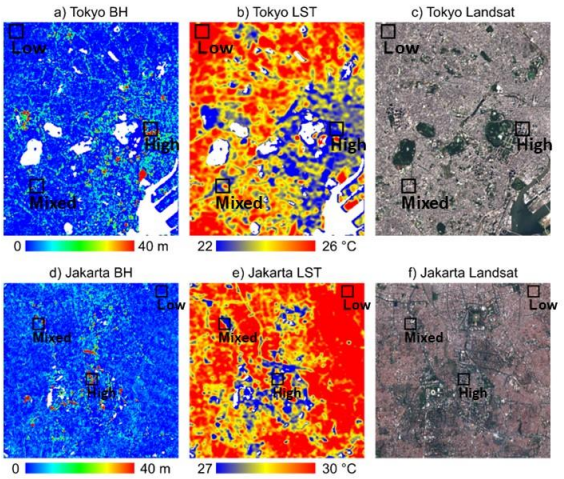

55

Results - Sampling of Smaller Areas

The LST decrease is steeper from low-rise to mixed-height, compared to mixed-height to high-rise

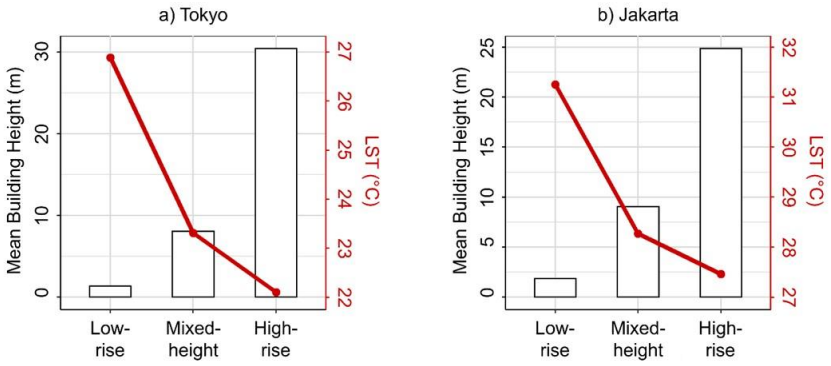

56

Summary

1	Land surface temperature consistently tends to decrease as building height increases
2	The decrease of land surface temperature in higher height class is not as significant as in the lower classes
3	A relatively small increase in building height could significantly decrease the LST

57

Discussion and Conclusion

58

Discussions - Land Cover vs Land Surface Temperature

Built-up expansion increases LST

Highest built-up expansion ≠ highest LST increase

- Highest LST increase → Bekasi
- Highest built-up expansion → Jakarta
- This is suspected due to the different development type of the city
- Industrial zone produces more heat than residential, offices, and shopping malls

Industrial zone in Bekasi

Office area in Jakarta

Residential area in Tangerang

59

Discussions - Satellite DBHM

Satellite DBHM overall show a good agreement with the reference data

Possibly because building surface is detected well in AW3D30, but not in SRTM

Vegetation area is not detected well in Satellite DCHM

Possibly because both AW3D30 and SRTM can detect vegetation well

Overlayed DBHM map on 3D building in Shinjuku

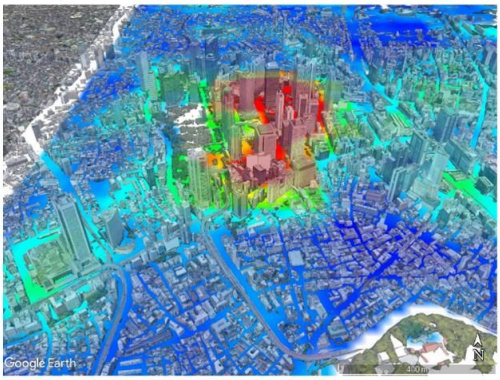

0 20 m

60

Discussions - The Causes of Low LST in High-Rise Area

High-rise buildings consistently have lower LST

Some possible factors that caused it are:
1. Buildings' shadow
2. The ratio between street surfaces versus wall surface
3. The building's surface material
4. The formation of wind corridor

The decrease of LST is not linear with the increase of building height

LST does not keep decreasing when building height keep increasing
→ Possibly due to the insignificant increase of building's shadow / wall surface size in higher buildings that satellite cannot "see"
→ The narrow angle of sun that creates the shadow

Overlayed LST map on 3D building in Shinjuku

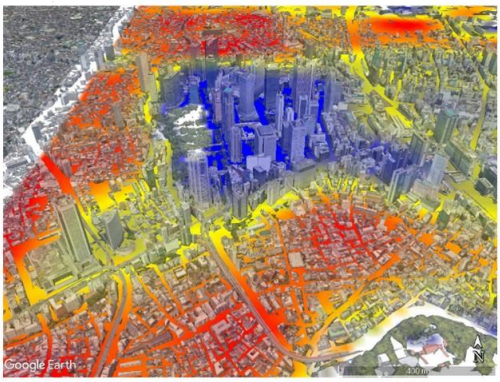

22 26 °C

61

Discussions - Implications in Landscape Architecture

- According to the study results, to decrease land surface temperature, it is recommended to:

1. Have spatially distributed high-rise buildings in an area

But it is not necessary to create very tall buildings (that surpassed 80 m)

2. Avoid a large area of low-rise buildings

Large low-rise areas have high surface temperature. Creating mixed-height building area is more recommended.

Considering the DBHM in this study is about half of the reference height, mean building height of about 8-16 m (3-5 stories) in an area can create cooling effect.

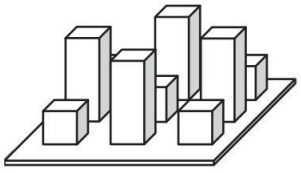

(illustration from Yang and Li 2015)

62

Conclusions of Presented Works

Study 1	Study 2	Study 3
• The majority of land cover change in Jakarta and its satellite cities is from vegetation to built-up area • The conversion of vegetation to built-up area increases the land surface temperature	• Building height data can be obtained from open-source data with a simple method. • The results is similar with the reference data	• Building height has a negative relationship with land surface temperature in many cities in the world • The decrease of land surface temperature is not linear with the increase of building height

Overall	• When built-up area expands horizontally, the land surface temperature increases compared to other types of land cover. • However, inside the built-up area, when the buildings expands vertically, the land surface temperature of high-rise buildings is cooler compared to low-rise buildings.

63

Contributions and Limitations of This Study

Contributions

1. This study analyzed the **land cover change impacts on land surface temperature** in Jakarta and its satellite cities which was lacking in existing studies
2. This study presented **a simpler method to extract building height** from two global satellite data, AW3D30 and SRTM, which is not explored enough in existing studies.
3. This study **introduced the applicability** of the extracted satellite building height data to examine its relationship with land surface temperature.
4. This study **confirmed the contradicting results** where high-rise buildings were said to increase the land surface temperature. On the contrary, **high-rise buildings could decrease land surface temperature**.

Limitations

1. The building height extracted from this study is not validated with precise LiDAR data in other cities
2. The building height data in its present condition cannot be used to obtain the accurate height, it is only sufficient to observe the tendency

64

Thank you for your attention